Chapter – 4

Synthesis, Characterization and adsorption performance of Biocomposites of clay

Equilibrium, Kinetics and Thermodynamic study on Adsorption of individual dyes and binary mixture of dyes by Chitosan-Organically modified Nanoclay (Cloisite 30B) nano-bio composite

4.1 Introduction

The most efficient method for the removal of dyes from aqueous effluents is adsorption [1], where one of the most widely used adsorbents, due to its high adsorption capacity is activated carbon as mentioned in Chapter 1 [2-4]. However, it is expensive and difficult to regenerate. Much attention has thus recently been focused on biosorbent materials [5-8] than those that are not expensive, can be obtained from renewable resources, and are harmless to nature. Special attention has been given to polysaccharides such as chitosan–the deacetylated form of chitin, which is a linear polymer of acetylamino-d-glucose. Chitosan has excellent properties for adsorption of anionic dyes, principally due to the presence of protonated amino groups ($–NH^{3+}$) in the polymer matrix, which interact with dyes in solution by ion exchange at an appropriate pH [9-11]. Removal of dyes using chitosan has its drawbacks as its adsorption potential is strongly pH dependent, so the pH of the wastewater has to be adjusted before treatment. The other attractive adsorbents are layered silicates clays, due to their low cost and their abundance across the globe [12-18]. Clays themselves have adsorption potential, so combining clays with chitosan can produce a very good sorbent, at the same time decreasing the chitosan drawbacks. Since each chitosan unit possesses one amino and two hydroxylic groups, these functional groups can form hydrogen bonds with the silicate hydroxylated end groups of clay, leading to strong interaction between chitosan and clay. Dissolution of chitosan in acetic acid resulted in reaction between amine group from chitosan and acetic acid residue ($NH^{3+}Ac^{–}$). Chitosan hydroxyl group form H-bonds with Si-O-Si groups of silicate multilayer of montmorillonite (MMT). Nanocomposites of chitosan and MMT have been already tested as electrochemical sensors, as adsorbents for tannic acid [19, 20], and for controlled release of ofloxacin [21]. The beads of chitosan/MMT were studied for removal of Reactive Red 120 [22] Basic Blue 9, Basic Blue 66 and Basic Yellow 1 [23]

Thus clay-based nanocomposites and bionanocomposites have become materials of increasing interest due to their nanosized structural and functional properties. This has thus become an attractive way to develop organic–inorganic nanohybrid materials with properties that are inherent to both types of components [24].

Darder et al. [25] showed that chitosan can be intercalated into Na+-saturated montmorillonite providing compact and robust three-dimensional nanocomposites with interesting functional properties. Chitosan chains formed mono- or bilayer structures within the clay mineral interlayer depending on the relative amount of chitosan with respect to the cationic exchange capacity (CEC) of the clay. Subsequent studies have shown that a number of factors, such as pH and temperature, can affect the extent and mode of chitosan adsorption on montmorillonite [26]. For instance, since the pKa of the primary amine groups in the chitosan structure is 6.3, an increase in pH leads to a decrease in the degree of protonation of the biopolymer, which increases the amount adsorbed on montmorillonite [26]. Adsorption of chitosan on montmorillonite, particularly when in excess of the CEC of the clay mineral, results in structures with good adsorption properties for anions because the $–NH^{3+}$ groups not directly involved in the interaction with the clay surfaces can act as anionic exchange sites [25]. Accordingly, montmorillonite–chitosan bionanocomposites have recently been proposed for anion-adsorption related applications, such as the development of potentiometric sensors for anions or the removal of selenate and tannic acid from water [27-29]. Clay minerals are good adsorbents for cationic and very polar pesticides [30-41]. However, they usually display limited affinity for anionic pesticides, as a result of repulsions between the anionic pesticide species and the negatively charged clay surfaces [42]. The interaction of organic cations with clay minerals can reduce such repulsions, changing the nature of the clay mineral surfaces from hydrophilic to hydrophobic or if adsorbed in excess of the CEC of the clay, even producing charge reversal. Thus, modification with organic cations is a potentially useful strategy to enhance the affinity of clay minerals for anionic pesticides [35, 38, 42–46]. Efforts in this direction have led us to the development of chitosan clay nanocomposites. In this work, the adsorption potential of chitosan (C), nanoclay (NC) as well as chitosan-clay nanocomposite (CC) for the individual dyes (Reactive blue-21 (R-21), Reactive red-141(RR-141), Rhodamine (Rh-6G) and binary mixture of

dyes (RB+RH, RB+RR, and RR+RH) was investigated. The influence of several parameter such as initial dye concentration, pH, adsorbent dosage and temperature on the adsorbents under kinetic and equilibrium conditions were explored. The rate limiting step of the dye onto the adsorbents was determined from the adsorption kinetic results. Adsorption isotherm equations were used to treat the equilibrium data and thermodynamic parameters were calculated. Furthermore since luminescent and photoactive low cost hybrid materials or composites present significant potential utility in modern industrial applications, it was felt that Rh6G loaded adsorbents could prove to be potential materials with interesting optical properties. We thus studied the photophysical properties of the dye loaded adsorbents. Literature search has shown that, there are limited reports on the removal of reactive red 141 (RR-141) and Rhodamine 6G (Rh-6G), an azo dye and no reports on the removal of reactive blue 21 (RB-21) a copper containing phthalocyanine dye using chitosan composites. Furthermore, there are no reports on the use of chitosan/nano clay composites especially organoclay for the removal of dyes. B. H. Hameed et al prepared modified ball clay chitosan composite adsorbent for adsorption of methylene blue [47].

Therefore the aim of the present work was to explore the feasibility of utilizing chitosan/Organically modified Nanoclay-Cloisite 30B nano biocomposite (CC) for the removal of dyes and to apply various isotherm and kinetic models to understand the adsorption mechanism.

4.1.1 Materials and methods

Chitosan flakes (87.6% deacetylated and molecular weight 5.5 x 105 g/mol) procured from Sigma was used directly for experimental studies as adsorbent (C). Commercial grade Reactive blue (RB-21), Reactive red (RR-141) and Rhodamine 6G (Rh-6G) were used without further purification. Vinyl pyrrolidone (VP) used in this study were purchased from Sigma-Aldrich. Methylene bisacrylamide (MBA) was purchased from National chemicals and Ammonium persulphate from SISCO Research Pvt Ltd. Organically modified Nanoclay (NC) (montmorillonite modified with 25-30 wt% methyl dihydroxyethyl hydrogenated tallow ammonium) was procured from Sigma Aldrich and was directly used for the synthesis of nanocomposite (CC). Hydrotalcite (HT) was a gift sample from Heubach Colour Private Limited, Ankleshwar, Gujarat, India.

4.1.2 Synthesis of Chitosan clay nanocomposite (CC)

A 1% aqueous clay suspension was added to 1% Chitosan solution in acetic acid whose pH was adjusted to 5. The mixture was then stirred for 8 h at 323K. The Chitosan-clay nanocomposite (CC) was then centrifuged washed and dried at 323 K. The surface areas of C, NC and CC as measured by BET analysis were found to be 7.336, 157.404 and 209.121 m^2/g respectively.

4.1.3 Characterization

FTIR was used to determine the changes in vibrational frequencies of the functional groups in the adsorbents under study and dye loaded adsorbents. The spectra were collected by a Perkin Elmer RX1 model within the wave number range of 400-4000 cm^{-1}. Topography of the adsorbents was visualized using a SEM microscope (JEOL, Model JSM-5610LV).TEM images were recorded using Philips (Model CM200) transmission electron microscope. Confocal images were visualized using ISM-710CARLZEISS GERMANY. Optical images were visualized using Leica DM 2000 optical instrument. Thermogravimetric analysis was done using EXSTAR6000 TG/DTA 6300 model instrument. X-ray diffraction patterns were measured by a Rigaku ultima-3 diffractometer Cu Kα radiation of wavelength 1.54184 A^0.

4.1.4 Preparation of dye solutions and batch sorption Experiments for single and binary mixture of dyes

Preparation of dye solutions

Stock solutions of dyes (1g/L) were prepared by dissolving accurately weighed amount of Reactive blue -21(RB-21), Reactive red 141 (RR-141) and Rhodamine 6G (RH-6G) in double distilled water and subsequently diluting to the required concentration.

Batch sorption Experiments

Experiments were conducted to study the effect of various parameters for the removal of RB-21, RR-141 and RH-6G onto Chitosan (C) Nanoclay (NC) and Chitosan clay nanocomposite (CC). For each experiment 25 mL of dye solution of known initial concentration and pH were taken in a 100 mL stoppered conical flask. A suitable adsorbent dose is added to the solution and the mixture was shaken at a

constant speed. The supernatant was separated from the adsorbent by filtration and analyzed for the presence of unadsorbed dye by using SYSTRONICS Digital 166 model visible spectrophotometer at maximum wavelength (RB-21=610 nm, RR-141=540, RH-6G=525 nm). The percentage removal of the dye and the amount adsorbed (mg/g) were calculated by the following relationship:

$$q_e = \frac{C_i - C_e}{m} \quad \text{.... eq. (1)}$$

Where, C_i-initial concentration of dye in mg/L; C_e – Equilibrium concentration of dye in mg/L; m – Mass of adsorbent g/L; q_e – Amount of dye adsorbed per gram of adsorbent.

Experiments were done to determine the pH range at which the maximum uptake of dyes would take place on the adsorbents under study by varying the initial pH of the solution in the range 1to 11using 0.1 N NaOH and/or HCl. The effect of the initial concentration (100to1000mg/L) was also studied in order to determine the effect of the parameter on the adsorption of dye from the solution. The optimum equilibrium time was determined as the contact time required for the concentration of dye in the solution to reach equilibrium and was obtained by varying the contact time in the range 30 to 300 minutes. The effect of dose was determined by varying the dose from 0.01 g to 0.1 gm. At the end of the predetermined time intervals, the suspensions were filtered and the dye content in the filtrate was analysed by using absorption spectrophotometer. The uptake of dye by the adsorbents under study (q_e) was calculated from the difference between the initial and final concentration as follows:

$$\mathbf{q_e = (C_i - C_e)/m} \text{.... eq. (2)}$$

Where,C_i-initial concentration of dye mg/L; C_e–Equilibrium concentration of dye in mg/L; m–Mass of adsorbent g/L; q_e –Amount of dye adsorbed per gram of adsorbent. Each experimental result was obtained by averaging the data from three parallel experiments.

Adsorption isotherm experiments were also performed by agitating 0.05g of the adsorbent under study with a series of 25mL solutions at optimum pH, containing different initial concentrations of (100 to 1000 mg/L) at 30 °C. After the established contact time was attained, the suspension was filtered, and supernatant was analysed for the dye concentration. The adherence of the equilibrium isotherm and data obtained to different adsorption isotherms models as given in Table 3.1 was tested.

For binary system, all the dye solutions were prepared with equal concentrations and the batch experiment was done in a similar method as described for single component system. Analysis was done using SYSTRONICS Digital 166 model visible spectrophotometer by measuring the maximum absorbance of the individual components in the mixture at its particular maximum wavelength. Calibration for cross interference was carried out by a previously described method as described by Al Duri and McKay [43]. The dye concentrations were calculated as follows. For a binary system of components A and B measured at λ_1 and λ_2 respectively, to give optical densities of d_1 and d_2,

$$C_A = \frac{k_{B2}d_1 - k_{B1}d_2}{k_{A1}k_{B2} - k_{A2}k_{B1}} \quad \text{.... eq. (3)}$$

$$C_B = \frac{k_{A1}d_2 - k_{A2}d_1}{k_{A1}k_{B2} - k_{A2}k_{B1}} \quad \text{.... eq. (4)}$$

Where, K_{A1}, $K_{B1,}$ K_{A2} andK_{B2} are the calibration constants for components A and B at the two wavelengths respectively.

4.1.5 Equilibrium Sorption Studies

Adsorption isotherms were determined by the treatment of 0.05 g of adsorbent under study with dye solution having an initial concentration varied from 100 to 1000 mg/L in a thermostated rotary mechanical shaker. After agitation the contents of the flasks were filtered. The concentration of dye remaining in the solution was determined by Spectrophotometer. The results of experimental measurements were in the form of adsorption isotherms. Attempts were made to fit the equilibrium dye sorption isotherm data to a number of well-known models (Table 1) like Freundlich, Langmuir, Temkin, and Halsey for the better understanding of the processes governing adsorption of dye on to the adsorbents under study.

Table 4.1 Isotherm and Kinetic models

Models	Equation	Assumptions
Isotherm models		
Freundlich	$q_e = K_f C_e^{1/n}$	Freundlich isotherm [48] describes the non-ideal and reversible adsorption. This empirical model can be applied to multilayer adsorption, with non-uniform distribution of adsorption heat and affinities over the heterogeneous surface. Freundlich isotherm is widely applied in heterogeneous systems especially for organic compounds or highly interactive species on activated carbon and molecular sieves. The slope ranges between 0 and 1 is a measure of adsorption intensity or surface heterogeneity, becoming more heterogeneous as its value gets closer to zero. Whereas, a value below unity implies the process to be chemisorption. High values for K_f shows high adsorption capacity; The constant n is the empirical parameter related to the intensity of adsorption, which varies with the heterogeneity of the material. To describe heterogeneous systems 1/n values indicate the type of isotherm to be irreversible (1/n = 0), favorable (0 <1/n < 1) and unfavorable (1/n>1) shows the adsorption capacity of an adsorbent.
Langmuir	$\frac{q_e}{q_m} = \frac{K_L C_e}{1 + K_L C_e}$	Langmuir isotherm [49] refers to homogeneous adsorption, which each

		molecule possess constant enthalpies and sorption activation energy. The Langmuir theory is valid for monolayer adsorption onto a surface containing a finite number of identical sites. Langmuir model for isotherm modeling were unsuccessful in the low concentration. q_m and K_l represent maximum adsorption capacity and energy of adsorption. Separation factor (R_L) defined by Webber and Chakkravorti [50]. 0<RL<1implies favorable adsorption; RL values indicate the type of isotherm to be irreversible (RL = 0), favorable (0 < R< 1), linear (RL = 1) or unfavorable (R>1).
Temkin	$\frac{q_e}{q_m} = \frac{R_T}{\Delta Q}\mathrm{Ln}(K_T C_e)$	Temkin isotherm model [51] describes the adsorption of hydrogen onto platinum electrodes within the acidic solutions. This isotherm contains a factor that accounts the interaction of adsorbent–adsorbate. By ignoring the extremely low and large value of concentrations, the model assumes that heat of adsorption (function of temperature) of all molecules in the layer would decrease linearly rather than logarithmic with coverage. Parameters from Temkin model describes The heat of adsorption of all the molecules in the layer decreases linearly with coverage due to adsorbent–adsorbate interactions, and that the adsorption is characterized by a uniform distribution of binding

		energies, up to some maximum binding energy; K_T equilibrium constant corresponds to maximum binding energy and B_T is related to heat of adsorption.
Halsey	$q_e = K_H/C_e^{1/n_H}$	Halsey proposed [52] an expression for condensation of a multilayer at a relatively large distance from the surface.
Kinetic models		
Pseudo first order	$\frac{dq}{dt} = K_i'(q_e - q_t)$	Lagergren (1898) [53] presented a first-order rate equation to describe the kinetic process of liquid-solid phase adsorption of oxalic acid and malonic acid onto charcoal, which is believed to be the earliest model pertaining to the adsorption rate based on the adsorption capacity.
Pseudo second order	$q_t = \frac{q_e^2 K_2' t}{1 + q_e K t}$	The adsorption rate of adsorbate depends on the concentration of adsorbate at the absorbent surface. Mechanism being the rate controlling step, involve valency forces through sharing or exchange of electrons between adsorbate and adsorbent. Kinetic performance is proportional to the adsorption rate. Based on the sorption equilibrium capacity [54].The adsorption process and the overall rate of the adsorption process appear to be controlled by the chemical reaction. Chemisorption significantly contributes to the adsorption process.
Intraparticle diffusion	$q_t = K_i t^{0.5}$	Intraparticle diffusion model [55] is used to identify the steps involved in

		adsorption. If it passes through origin it infers the applicability of intraparticle diffusion whereas presence of intercept shows the surface adsorption / boundary layer effects. The term *k* calculated from the slope is indicative of an enhancement in the rate of adsorption. [56]. Adsorption is said to be intra-particle diffusion controlled if the reaction sites are internally located in the porous adsorbents and the external resistance to diffusive transport process is much less than the internal resistance.
Bangham	$\text{LogLog}\left(\frac{C_0}{C_0 - q_t m}\right) = \text{Log}\left(\frac{K_m}{2.303V} + \propto \text{Log}t\right)$	Bangham equation [57] indicates that diffusion of adsorbate into the pores of adsorbent. It is a pore diffusion controlled process.
Liquid film diffusion	$\text{Ln}\left(1 - \frac{q_t}{q_e}\right) = -K_{FD}t$	When the transport of the solute molecules from the liquid phase up to the solid phase, boundary plays the most significant role in adsorption; the liquid film diffusion model may be applied [58] determines whether the main resistance to mass transfer is in the thin film (boundary layer) surrounding the adsorbent particle, or in the resistance to diffusion inside the pores. Applicable when flow of the reaction from the bulk liquid to the surface of the adsorbent determines the rate constant.

4.1.6 Sorption Dynamics

The kinetics of adsorption process describes the solute uptake, which, in turn governs the residence time of the adsorption reaction. The study was carried out at optimum conditions of pH, Dose, concentration and temperature with the variable in time.

In order to investigate the sorption process of the dyes Pseudo First order, Pseudo Second order, Intraparticle diffusion, Bangham, and Liquid film diffusion models were used as kinetic models (Table 1). The Values of correlation coefficients and standard deviation were used to compare the models.

4.1.7. Thermodynamics of Sorption Studies

The thermodynamic parameters of the sorption process could be determined from the experimental data obtained at various temperatures using the equations: The Gibbs free energy (ΔG◦) can be calculated from the equation:

$$\Delta G = -\mathbf{RTlnK}i \quad \text{.... eq. (5)}$$

Where K_l is Langmuir's equilibrium constant, T is the temperature (K) and R is the universal gas constant. The standard enthalpy change (ΔH◦) and standard entropy change (ΔS◦) of the adsorption process could be calculated using the equation:

$$\Delta G^0 = \Delta H^0 - T\Delta S^0 \quad \text{.... eq. (6)}$$

While the values of ΔH◦ and ΔS◦ could be calculated from the linear plot of ΔG versus T.

4.2. Results and Discussion

4.2.1. FT-IR spectroscopy

Figure 4.1, 4.2 and 4.3 shows the IR spectra of Chitosan (C), Nanoclay (NC), Chitosan nanoclay nanocomposite (CC) and the dye loaded adsorbents of C (C-RB,C-RR,C-RH), NC (NC-RB,NC-R,NC-RH) and CC (CC-RB,CC-RR and CC-RH).Table 4.2, 4.3 and 4.4 shows the Absorption frequencies and stretching frequencies for free and dye loaded adsorbents.

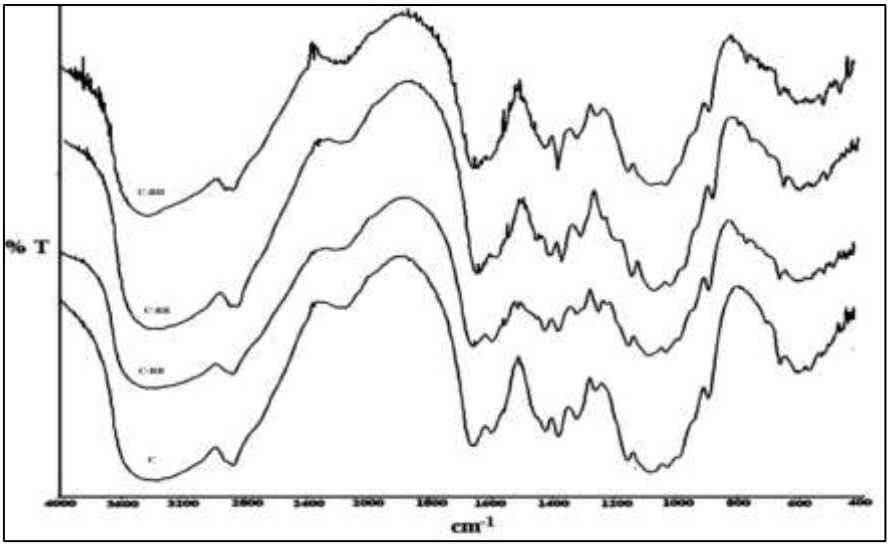

Figure 4.1 IR spectra of C, C-RB, C-RR and C-RH

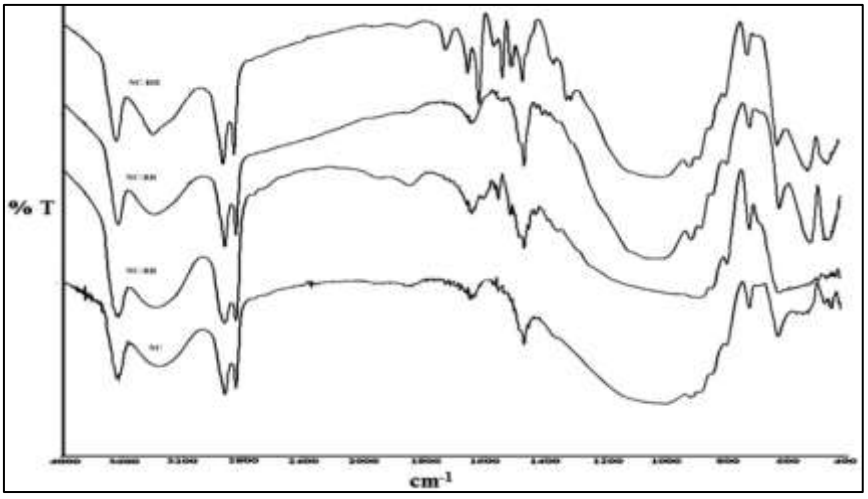

Figure 4.2 IR spectra of NC, NC-RB, NC-RR and NC-RH

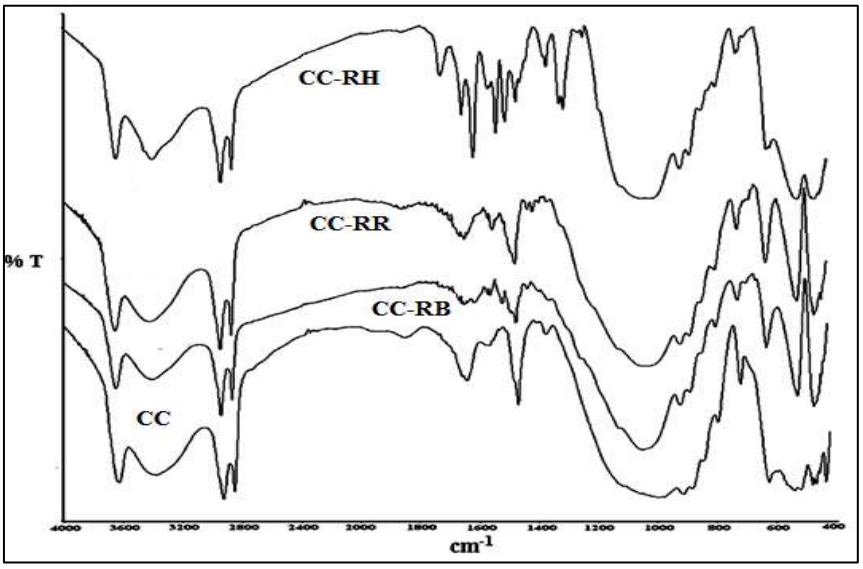

Figure 4.3 IR spectra of CC, CC-RB, CC-RR and CC-RH

The IR spectra of Chitosan (C) showed peaks at ~3362cm^{-1}(O-H and N-H stretching), 2879 cm^{-1}(aliphatic C–H stretching). The absorption bands at 1661, 1601, 1380, 1082 and 1026 cm-1 are attributed to C=O stretching of amide I, NH of amide III (combination of NH deformation and the =CN stretching vibration), C3-OH and C6-OH of chitosan respectively, while Nanoclay (NC) showed vibrational bands at 3626cm^{-1} (O-H stretching),1682 and 1660 cm^{-1} (H-O–H bending) and 911 cm^{-1}, 884 cm^{-1} (Al-OH and Si-OH vibrations respectively). The chitosan clay nanocomposite (CC) showed peaks at 3626 cm^{-1} (O–H stretching of Al-OH and Si-OH), 3382cm^{-1} (O-H and N-H stretching), 1643 cm^{-1} (C=O and N-H vibrations), 1850 cm^{-1} (C=O stretching vibration), 1570 cm^{-1} (a combination of N–H in plane bending and C–N stretching), as well as 996, 847 and 799 cm^{-1} (Al–OH and Si-OH vibrations) confirming the interaction of clay and chitosan in the composite [59]. Due to the interaction of the protons in chitosan with the oxygen species of Si–O and Al–O in nanoclay the tetrahedral symmetry of these moieties would have been distorted. The composite thus shows the presence of organic and inorganic groups which is due to intercalation of chitosan into layers of clay. FTIR analysis further shows that after adsorption of dye there is a significant shift in the O–H stretching and -CH_3, -CH_2 symmetric stretching frequency of chitosan, nanoclay and the composite. In all the dye loaded adsorbents. The intensity of symmetric Si–O–Si stretching vibrations at 799 cm^{-1} were reduced and the bands were shifted slightly in both dye loaded nanoclay and the composite. The peaks at 1682 and 1660 cm^{-1}in the case of nanoclay has been shifted to 1659 and 1643cm^{-1} in the case of NC-RB, 1644 cm^{-1} in the case of NC-RR and 1613 in the case of NC-RH indicating the interaction of the nanoclay with the dyes. The frequency of Al-OH stretching vibrations at 915 cm^{-1} and 995 cm^{-1} for the composite has also been shifted after loading of the dyes onto the adsorbents. The –N-H bending frequency at 1601 cm^{-1}of chitosan have been shifted 1649,1646 and 1643 cm^{-1}after loading of RB,RR and RH respectively which clearly shows the involvement of –N-H groups of chitosan in adsorption of dyes.

Table 4.2 Typical IR stretching frequencies of Infrared spectra for chitosan and dye loaded chitosan

Chitosan(C)	**C-RB**	**C-RR**	**C-RH**	**Inference**
3362	3435	3420	3438	-N-H, -O-H stretching
2879	2160,	2353	2350,2216	CH_3, $-CH_2$ symmetric stretch
		1759	1864,1738	
1601	1659	1662,1646,1603	1659,1643	-N-H bending, H-O-H bending
-	1599,1566,1515,	1553	1555	
-	1427	1427	1462,1426	$-CH_2$- stretching
1424	1384,1323,1252	1381,1322	1384,1323,1259	
	1155,1084,1032	1155,1086,1036	1157,1081,	
1380	1384,1323,1252	1381,1322	1384,1323,1259	-C-H stretch/ N-H bending
1158	1155,1084,1032	1155,1086,1036	1157,1081,	-C-O stretch
	712	710	770,728	-C-Cl /S-O

Table 4.3 Typical Absorption frequencies and stretching frequencies of Infrared spectra for nanoclay and dye loaded nanoclay

Nanoclay (C)	**NC-RB**	**NC-RR**	**NC-RH**	**Inference**
3627,3359	3626,3337	3633,3385	3626,3389	-N-H, -O-H stretching
2924,2851	2924,2852	2925,2851	2924,2851	$-CH_3$, $-CH_2$ symmetric stretch
	1851	-	1724	
1650	1659,1643	1644	1613	N-H bending
-	1565,1516	1563	1564,1535,1505	-N-H bending,
1470	1470,1433	1471,1409	1470,1367,1324	$-CH_2$- stretching
1001	-	1045	1003	-Si-O Stretch
915,882	887	916,884	915	Al-OH Stretch,Si-O Stretch
987,896	799,723	798,722	725	
	623	625,525	626,525	

Table 4.4 Typical Absorption frequencies and stretching frequencies of Infrared spectra for Chitosan clay nanocomposite and dye loaded nanocomposite

Chitosan clay nanocomposite (CC)	**CC-RB**	**CC-RR**	**CC-RH**	**Inference**
3626, 3382	3635,3386	3634,3408	3627, 3385	-N-H, -O-H stretching
2926,2851	2925,2852	2925,2852	2924,2851	$-CH_3$, $-CH_2$ symmetric stretch
1850		1737	1722	
1643	1643,	1657	1650,1611	-N-H bending,
				$-CH_2-$ stretching
1570	1563,1518	1563,1547	1563,1535,1503	CH_2- stretching
1471	1470,1433	1472,1428	1469,1455	
1378	-	-	1367,1323,1308	
995				Al-OH Stretch,Si-O Stretch
847,799				

4.2.2 SEM and TEM Micrographs

The SEM and TEM Micrographs in Figure 3.4 and Figure 3.5 of C, NC and CC indicate the uniform dispersion of clay into Chitosan matrix without any agglomeration**.** The fibrous nature of the composite CC seen from the figures suggests the suitability of the material for adsorption studies.

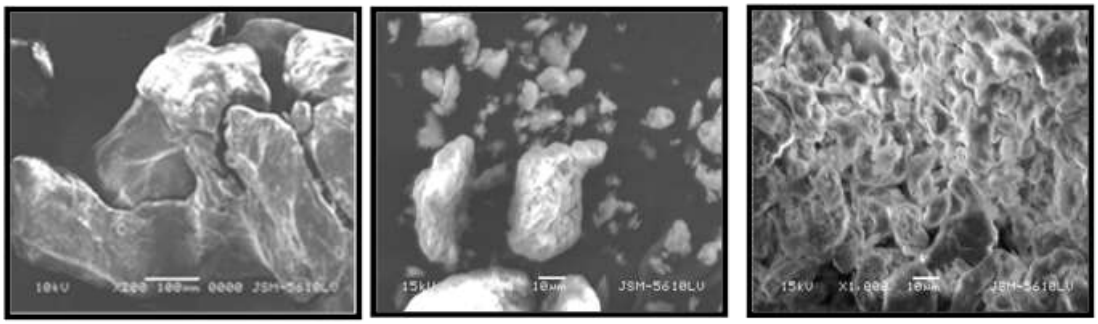

a) C **b) NC** **c) CC**

Figure 4.4 SEM Micrographs

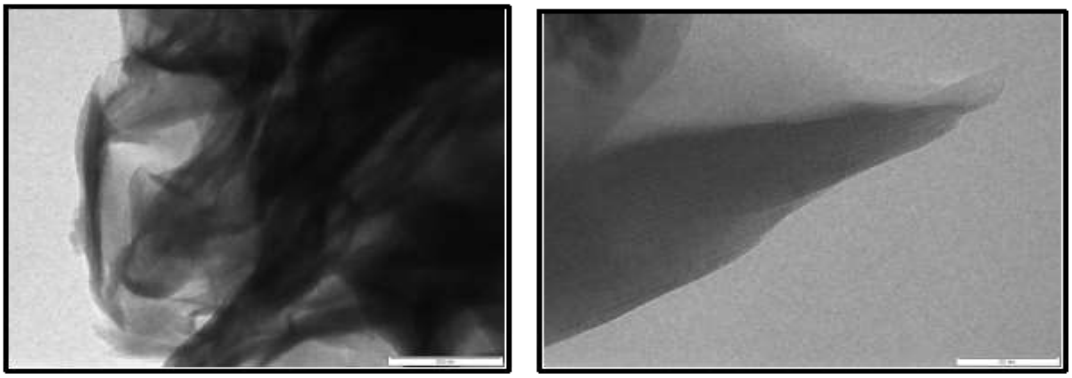

a) NC **b) CC**

Figure 4.5 TEM Micrographs

4.2.3. X-Ray diffraction studies

Figure 4.6, Figure 4.7 and Figure 4.8 show the XRD pattern of the adsorbents and dye loaded adsorbents.

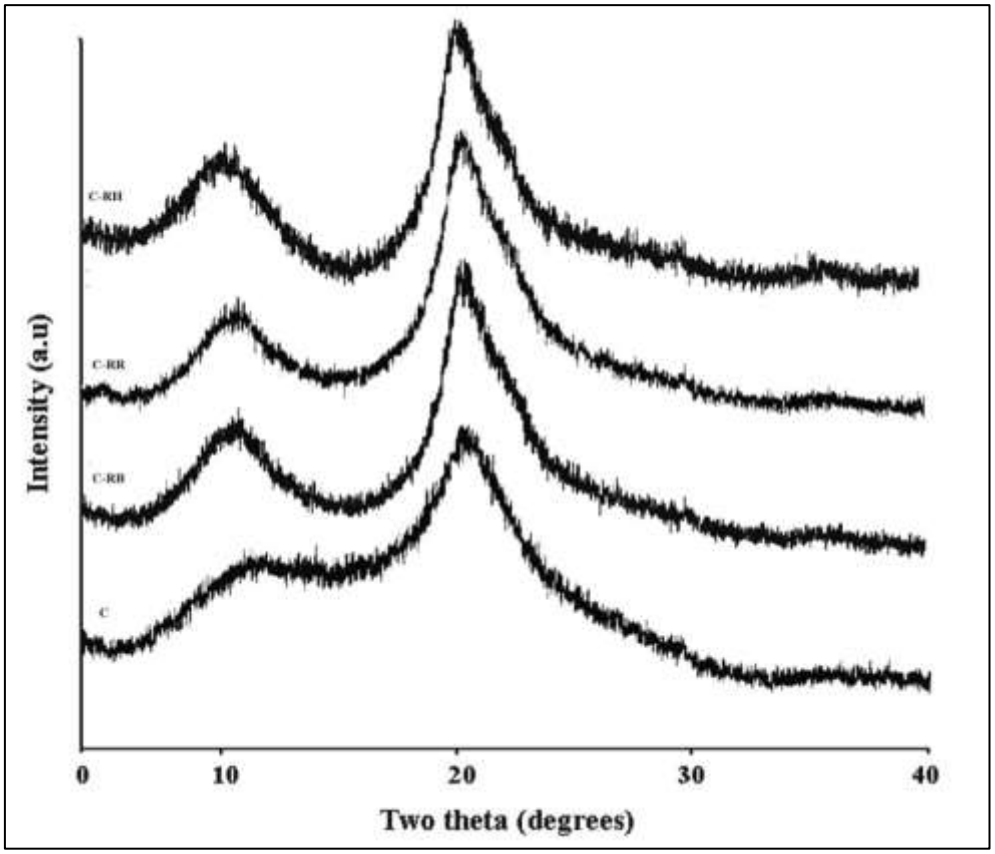

Figure 4.6 X-ray diffraction pattern of C, C-RB, C-RR and C-RH

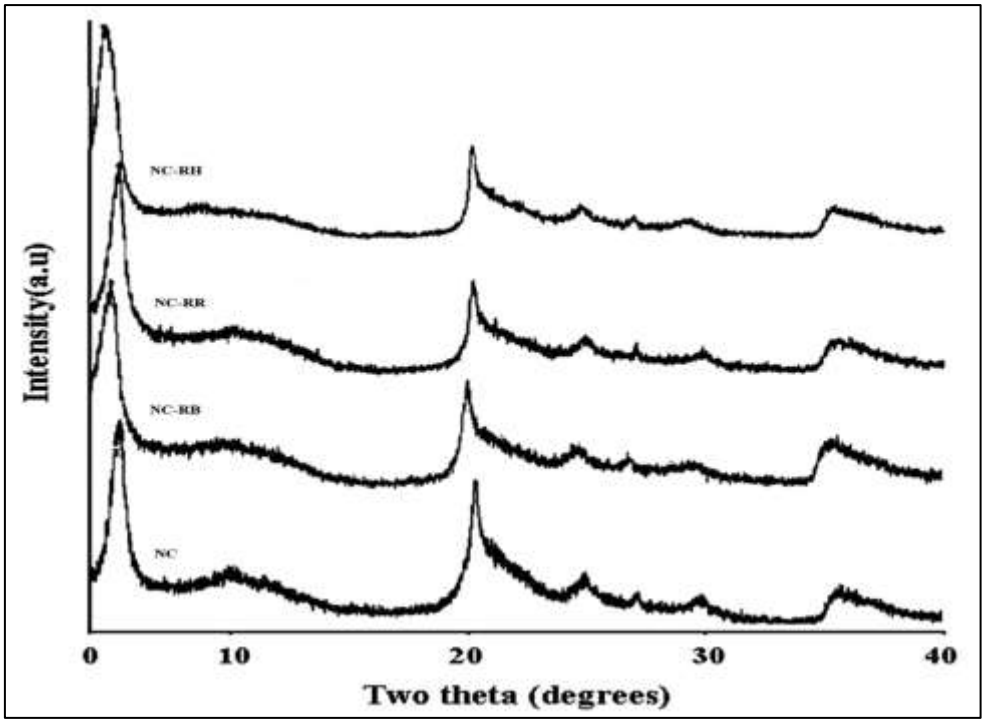

Figure 4.7 X-ray diffraction pattern of NC, NC-RB, NC-RR and NC-RH

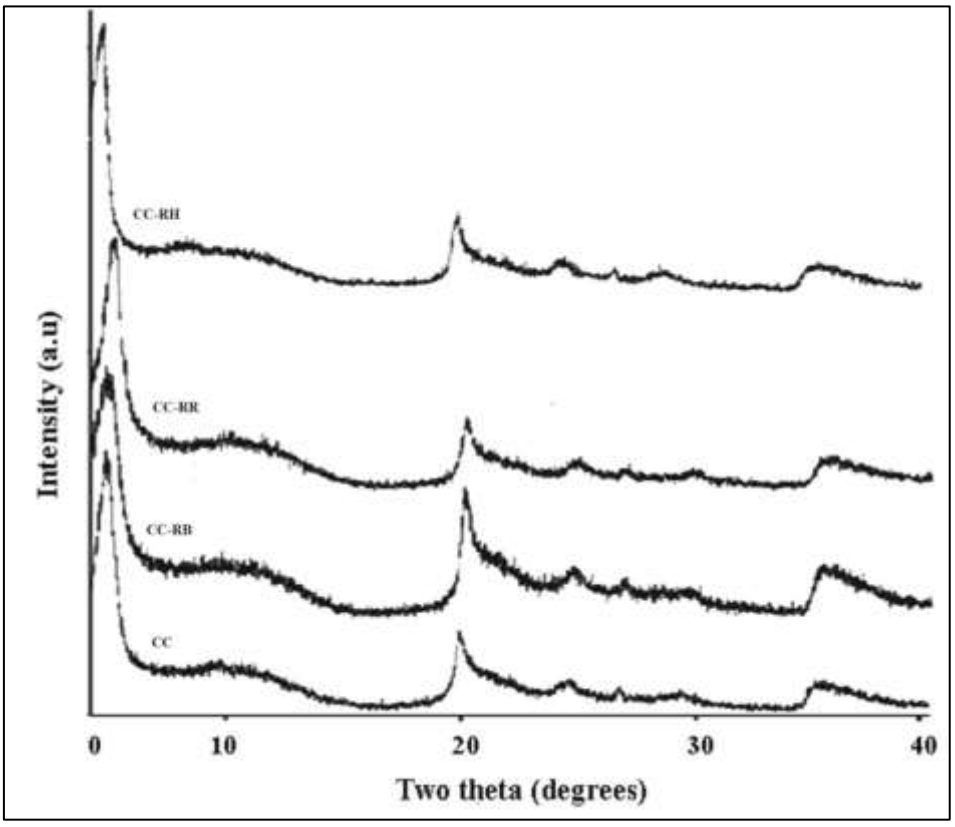

Figure 4.8 x-ray diffraction patterns of CC, CC-RB, CC-RR and CC-RH

The XRD pattern of Chitosan shows specific crystalline peaks at 10.746^0 and 19.994^0 attributed to crystal 1 and crystal 2 of chitosan [60, 61]. The characteristic peak of Nanoclay at 5.238^0 has been shifted to 4.985^0 with increase in d-spacing in CC. Furthermore in CC the peaks were seen to be broad with decreased intensity indicating intercalation. In the case of C-RH the reflections were seen to be shifted to higher angles while in the case of NC-RH and CC-RH the reflections were shifted to lower angles which could be attributed to compression and expansion of layers after adsorption of Rhodamine 6G. The superposition of the peaks of CC-RB, CC-RR and CC-RH with CC suggests that the dyes have been adsorbed onto CC instead of intercalation. The particle size calculated from XRD using Debye Scherrer equation was found to be 3.165 nm and 5.254 nm for CC and NC respectively.

4.2.4 Zeta potential analysis

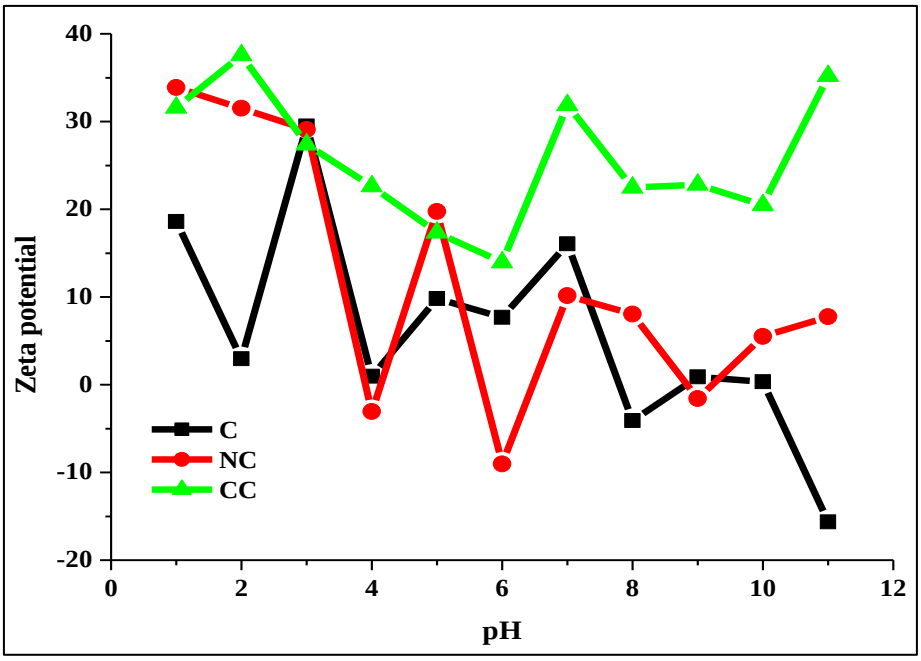

Figure 4. 9 Zeta potential of C, NC and CC

It is observed that the zeta potential is very sensitive to pH changes for the clays under study. The zeta potential for C was positive at acidic pH, had neglible or no surface charge from pH 6-10 and exhibited high negative zeta potential at pH 11. NC showed high positive zeta potentials upto pH 3 and at pH 5 while at other pH it showed low positive zeta potentials. On the other hand CC was relatively more stable to pH and showed large positive potentials of around 20- 35mV expect in the pH range 5-6.

4.2.5. Thermogravimetric analysis

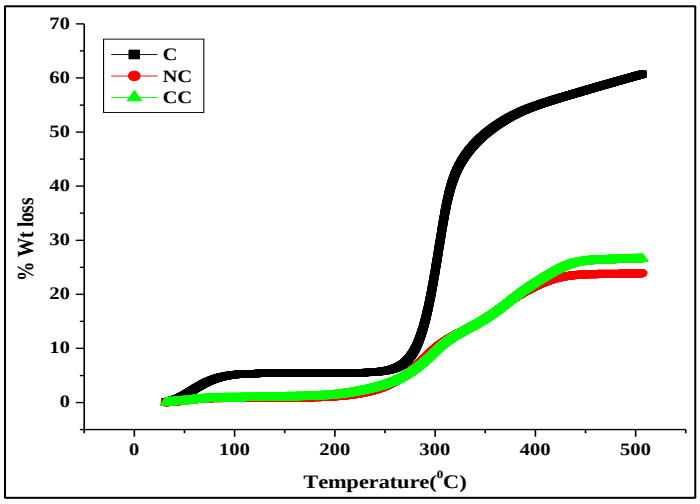

Figure 4.10 Thermogravimetric analysis of C,NC an CC

Figure 4.10 shows the Thermogravimetric analysis of C, NC and CC. The weight loss from 50^0 - $250^0$is attributed to loss of water in the case of C, NC and CC. The weight loss in C from 250^0 - 350^0 is attributed to degradation and deacetylation of Chitosan. The weight loss from 290^0 – 430^0 in NC can be attributed to the decomposition of organic material. The weight loss in CC from 290^0 – 340^0 can be attributed to deacetylation of Chitosan and the weight loss from 380^0 – 460^0 to the decomposition of organic material.

4.2.6 Photophysical properties of Rhodamine-6G loaded adsorbents

UV spectra of C-Rh,NC-Rh and CC-Rh

Figure 4.11 shows the UV spectra of dye loaded adsorbents. The typical peak observed at ~526 nm attributed to Rh6G monomers can be seen in NC and CC. It is seen as a low intensity broad peak only in Rhodamine loaded Chitosan (C-Rh) which could be due to the overlap of the band attributed to H- aggregates with monomers. However in the case of NC-Rh two peaks of increased intensity were observed at 500 and 526 nm while in the case of CC-Rh a sharp peak was observed at 526nm with two shoulders on either side at 500 and 560 nm. The peak at 500 nm in CC-Rh and NC-Rh can be attributed to vibronic component of electronic transitions and non-fluorescent H dimers. The small shoulder observed at~ 560nm in CC-Rh and C-Rh, could be attributed to aggregate formation which seemed to occur only in the presence of chitosan**.** Typical characteristic features of J-aggregates include light absorption at higher wavelengths and different fluorescence characteristics from that of the monomeric form. Thus after adsorption onto C, NC and CC the Rh6G molecule formed disordered molecular assemblies showing characteristics of J aggregates.

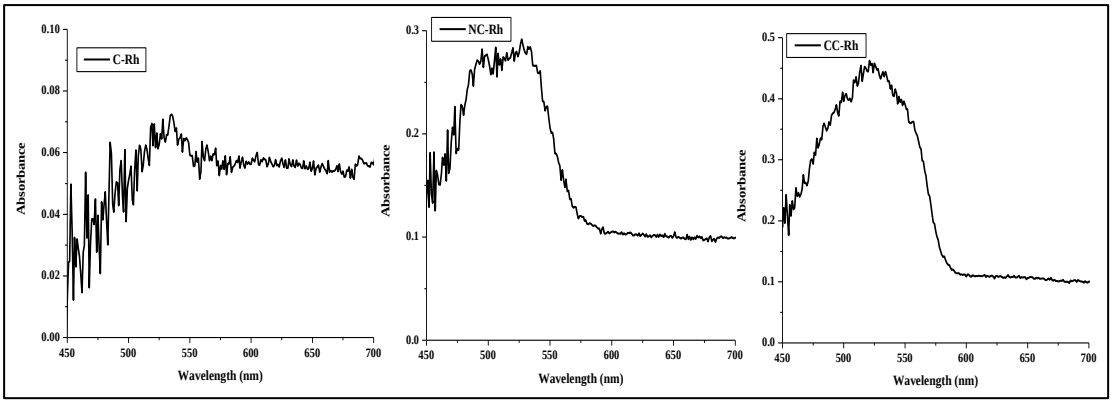

Figure 4.11 UV spectra of C-Rh, NC-Rh and CC-Rh

Emission spectra of C-Rh, NC-Rh and CC-Rh

Figure 4.12 (a & b) the emission spectra of Rh6G loaded C, NC and CC at different concentrations and excitation at 460 and 500 nm. The change in excitation wavelengths led to different profiles of Rh6G emission spectra. Excitation at 450nm led to a distinctive emission between 460 and 480 nm, attributed to the presence of fluorescent J-type dimers. The emission peak at ~ 477 nm in chitosan can be attributed to J dimer. In the case of NC and CC, two peaks were observed at 473 and 489 nm, with the peak at 473 nm being of increased intensity in NC while in CC the peak at 499 nm is of increased intensity which can be attributed to different J assemblies characterized with head to tail association. Furthermore, excitation with wavelength 450 nm led to selective excitation of monomers which radiatively relax at 560-570nm. On excitation at 500 nm, the emission spectrum was mainly dominated by the band at 550 nm, which was ascribed to the monomeric Rh 6G in all three adsorbents. In chitosan the main contribution to the fluorescence is given by the monomeric form of rhodamine 6G. However, the emission spectrum of NC and CC showed another band at 579 and 593nm respectively which can be attributed to J dimer. Furthermore an emission peak at 715 nm was also observed in NC and CC which can be attributed to J or J-H type aggregates which are reported to emit at longer wavelengths. The interaction of chitosan with Rh6G seems to change the dielectric environment around the dye thus reducing aggregation. Thus nanoclay and Chitosan-nanoclay composites are more conducive to the formation of aggregates. The compliance of chitosan as a matrix and its interaction with organoclay also favor the formation of different types of dimers. On the other hand chitosan alone does not favor the formation of high order aggregates. Chitosan probably allows the dimerization while limiting the formation of larger aggregates; this is also in

accordance with previous finding in polymeric films where aggregation is limited to the dimer form. It is observed that fluorescence intensity was highest in nanocomposite followed by nanoclay and chitosan.

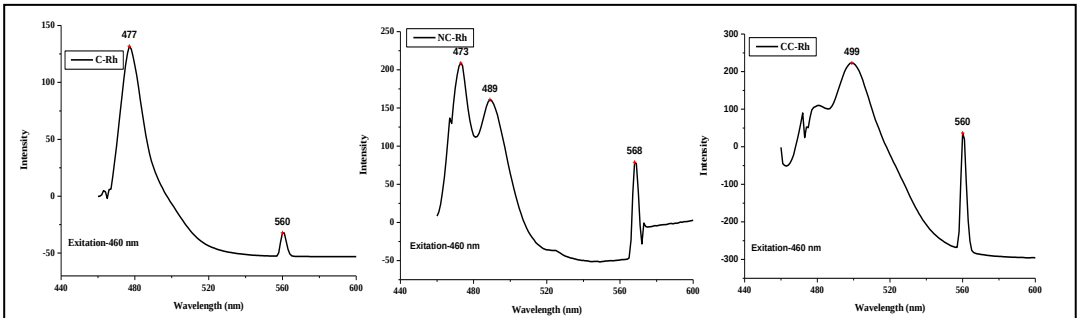

a) Emission spectra of C-Rh, NC-Rh and CC-Rh (Excitation at 460 nm)

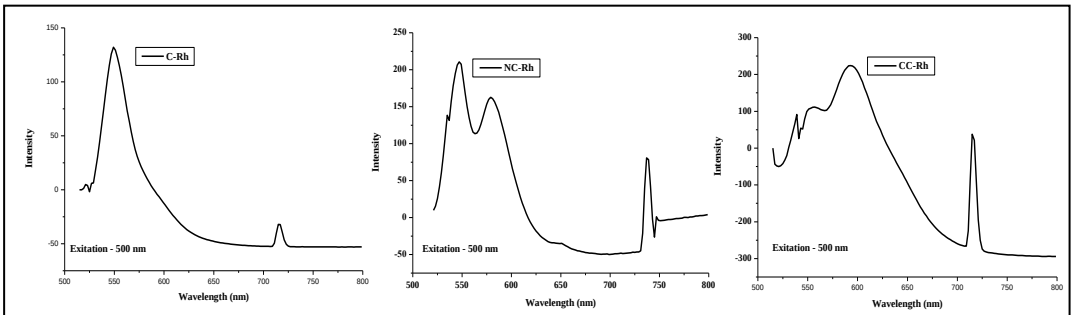

b) Emission spectra of C-Rh, NC-Rh and CC-Rh (Excitation at 500 nm)

Figure 3.12 Emission spectra of C-Rh, NC-Rh and CC-Rh –a) Excitation at 460 and b) 500 nm

4.2.7. Dye adsorption studies of single component dye systems

Effect of pH

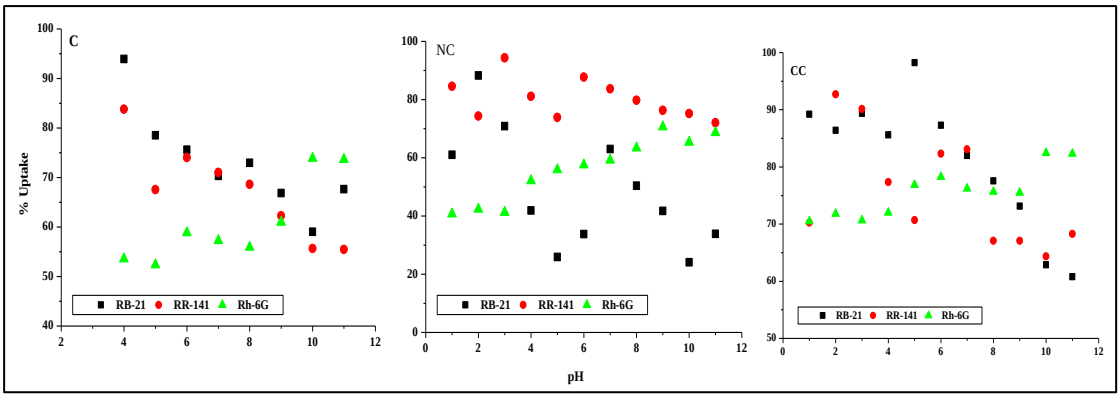

Operating parameters: agitation rate-180 rpm, 100 ppm of dye, 0.05g adsorbent, contact time-210 min, temperature 30^0C

Figure 4.13 Effect of pH on % uptake of RB-21, RR-141 and Rh-6G onto C, NC and CC

Figure.4.13 shows the **e**ffect of pH on % uptake of RB-21, RR-141 and Rh-6G onto C, NC and CC. Surface charge is the most important parameter for the adsorption of dye molecules and is primarily affected by the solution pH. In this study, the effect of solution pH on the adsorption of dyes was investigated in the range 1 to 11, while initial concentration and temperature were kept constant. The results in figure indicate maximum adsorption for RB-21and RR-141 is observed at acidic pH for C, NC and CC. All the three adsorbents have positive pH in acidic conditions resulting in conductive adsorption of anionic dyes RB-21and RR-141. C and NC have high negative potentials at basic pH thus being conducive for the adsorption of cationic Rh6G while CC had positive potential. However CC showed good adsorption potential for Rh6G probably due to the formation of aggregates whereby its positive charge gets masked and the amount adsorbed also would be higher

Effect of temperature

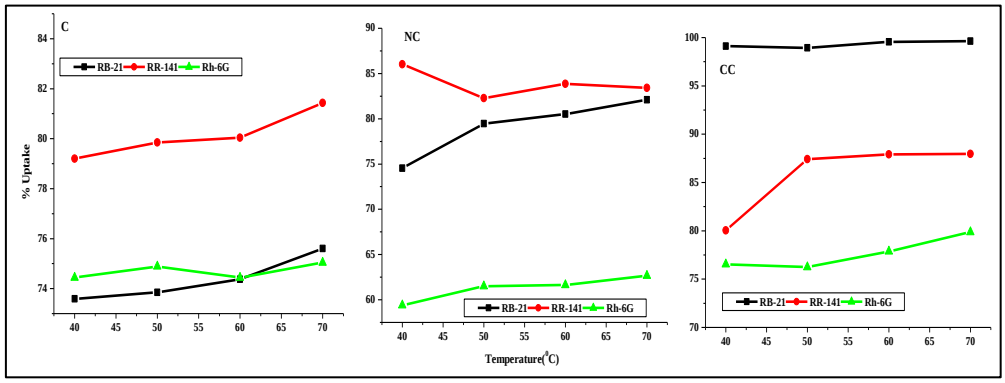

Operating parameters: 180 rpm, 100 ppm of dye, 0.05g adsorbent, time 300 min pH

Figure 4.14 Effect of temperature on % uptake of RB-21, RR-141 and Rh-6G onto C, NC and CC

Figure 4.14 shows the effect of temperature and it was observed that the adsorption process was not significantly affected by temperature for all the three dyes.

Effect of adsorbent dose

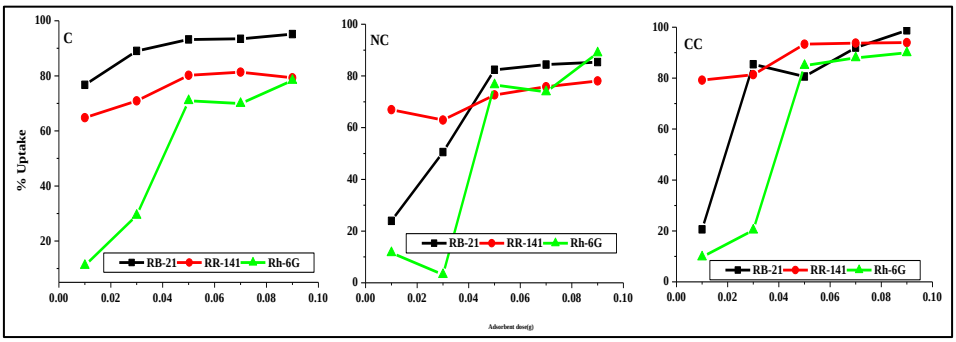

Operating parameters: 180 rpm, 100-1000 ppm of dye, 0.05g adsorbent, time300 min

Figure 4.15 Effect of adsorbent dose on % uptake of RB-21, RR-141 and Rh-6G onto C, NC and CC

Figure 4.15 shows the effect of adsorbent dose on the adsorption potential of C, NC and CC for the three dyes under study. The increase of adsorbent mass from 0.01 to 0.05 g for an initial concentration of 100 ppm dye solution resulted in increase in adsorption of the dyes which could be attributed to the availability of more sorption sites for the dyes due to higher amount of the adsorbents.

Effect of concentration

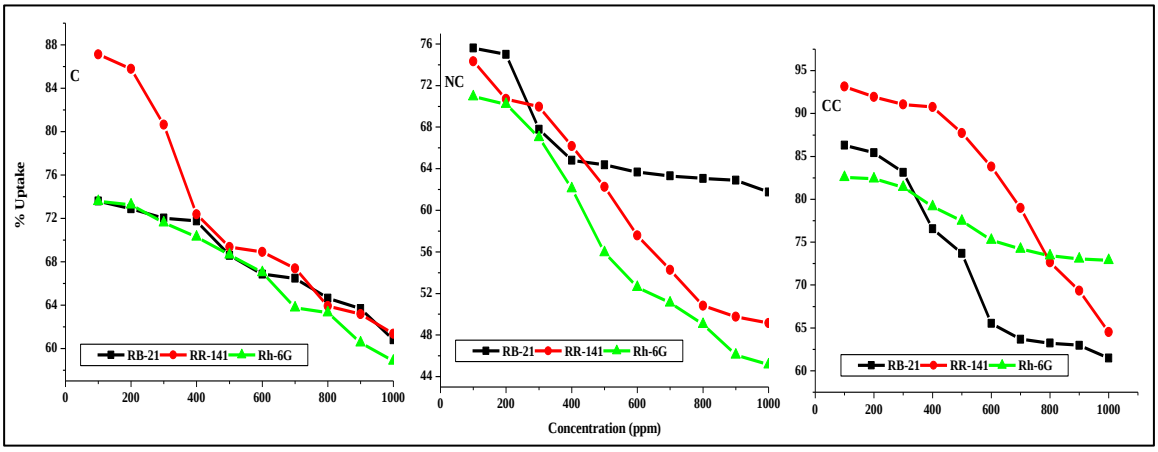

Operating parameters: 180 rpm, 100-1000 ppm of dye, 0.05g adsorbent, time300 min

Figure 4.16 Effect of concentration on % uptake of RB-21, RR-141 and RH-6G onto C, NC and CC

Figure 4.16 shows the effect of concentration. It was observed that as the initial dye concentration was increased from 100 ppm to 1000ppm the removal efficiency decreased. This could be attributed to hindrance in the diffusion of the dye into the boundary layer. Furthermore there might be a progressive decrease in the proportion of attraction forces and an increase in the electrostatic repulsive forces between dye molecules and adsorbent particles with increase in initial dye concentration.

Sorption isotherm

The isotherm models (Table 4.1) of Freundlich, Langmuir, Temkin, and Halsey models were studied and isotherm constants for the sorption of RB-2, RR-141 and RH-6G by C, NC and CC are presented in Table 4.5. Table 4.6 shows the comparision of adsorption capacity with respect to other adsorbents. The Freundlich constant, n > 1 implies that the adsorption intensity is favorable over the entire range of concentrations studied. The fitting of Langmuir showed that the correlation

coefficient values were best fitted and the calculated q_m values were in good correlation with q_{eexp} values. The fitting of Temkin model indicated favourable adsorption for all range temperature in the case of C, NC and CC which is clearly shown by the correlation coefficient values. The high regression values for Halsey model suggested multilayer adsorption [62]. Figure 4.17 (a, b & c) the shows the linear fit for isotherms of RB, RR and RH onto Chitosan (C). Figure 4.18 (a, b & c) the shows the linear fit for isotherms of RB, RR and RH onto Nanoclay (NC).). Figure 4.19 (a, b & c) the shows the linear fit for isotherms of RB, RR and RH onto Chitosan nanoclay composite (CC).

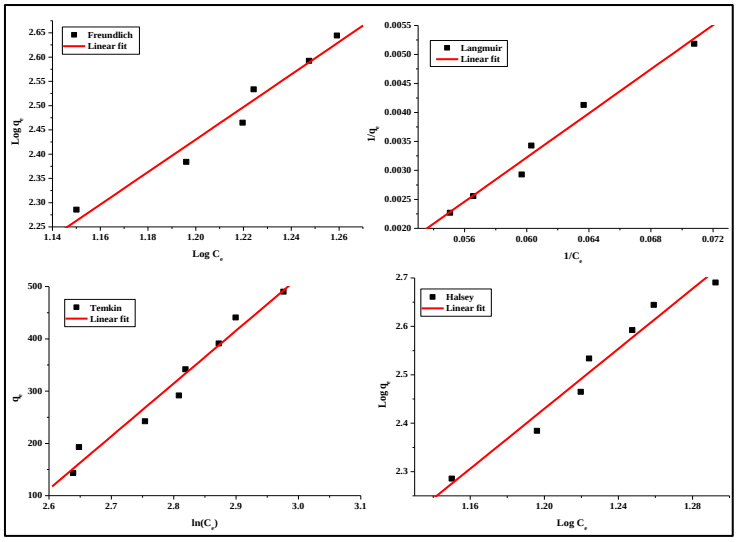

Operating parameters: 180 rpm, 100-1000 ppm of dye, 0.05g adsorbent, time 300 min, temperature 30^0C, optimum pH

Figure 4.17 a. Linear fit of isotherm for RB onto C

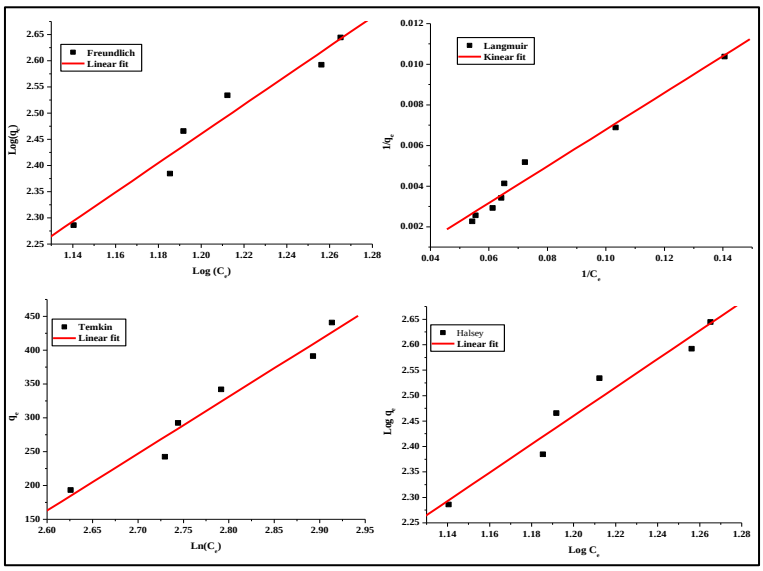

Operating parameters: 180 rpm, 100-1000 ppm of dye, 0.05 g adsorbent,

time 300 min, temperature 30^0C, optimum pH

Figure 4.17 b. Linear fit of isotherm for RR onto C

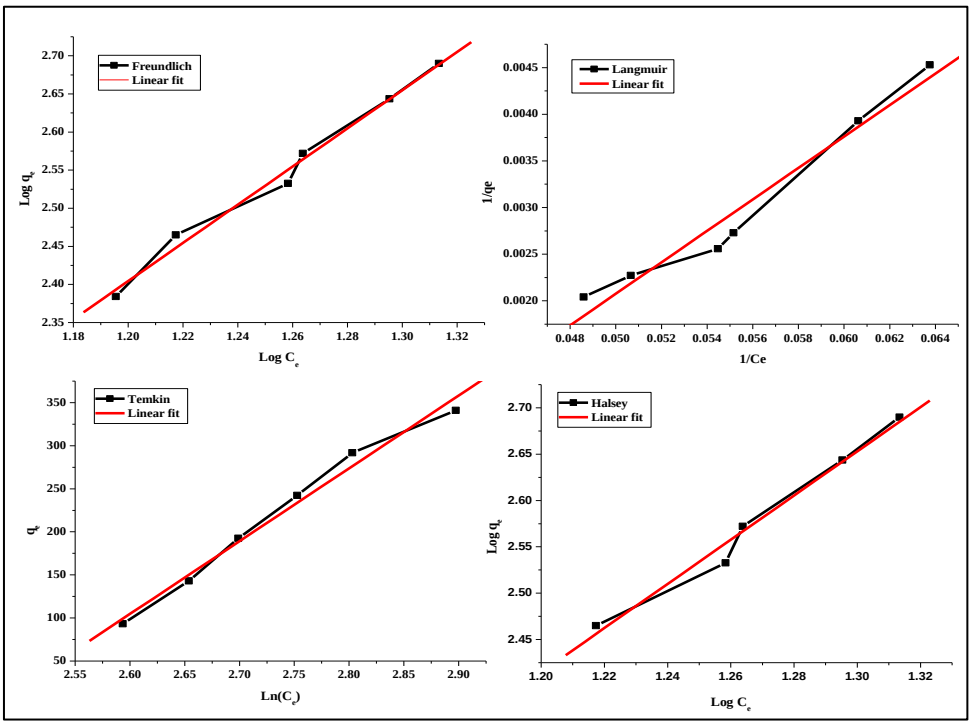

Operating parameters: 180 rpm,100-1000 ppm of dye, 0.05 g adsorbent, time 300 min, temperature 30^0C, optimum pH

Figure 4.17 c. Linear fit of isotherm for RH onto C

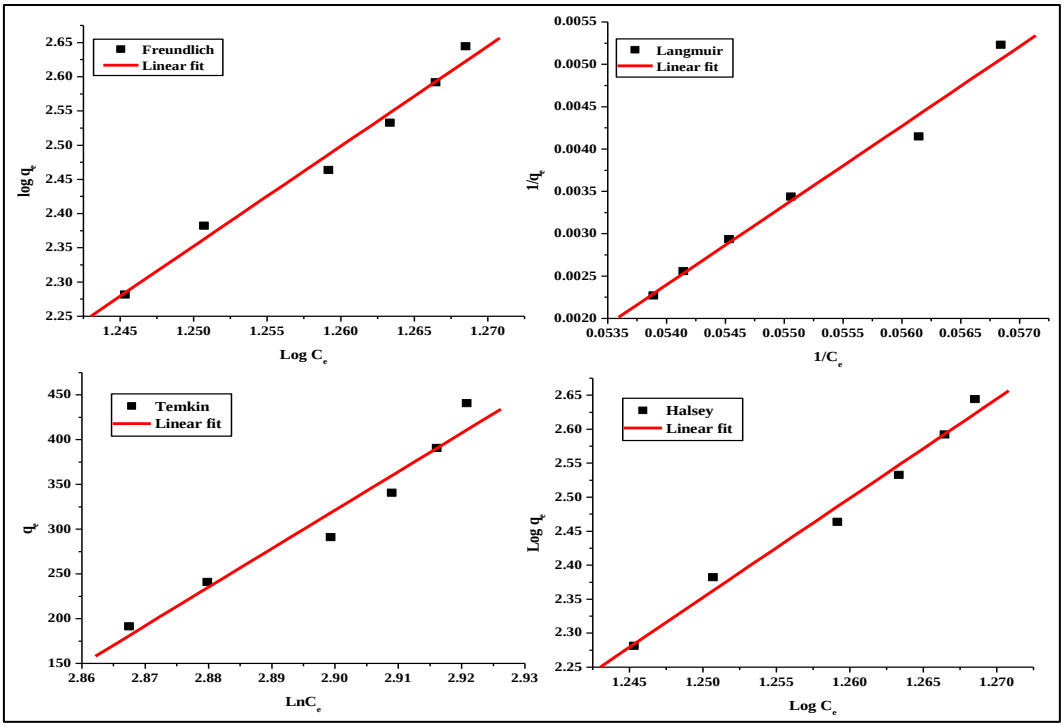

Operating parameters: 180 rpm, 100-1000 ppm of dye, 0.05g adsorbent, time 300min,

temperature 30^0C, optimum pH

Figure 4.18 a. Linear fit of isotherm for RB onto NC

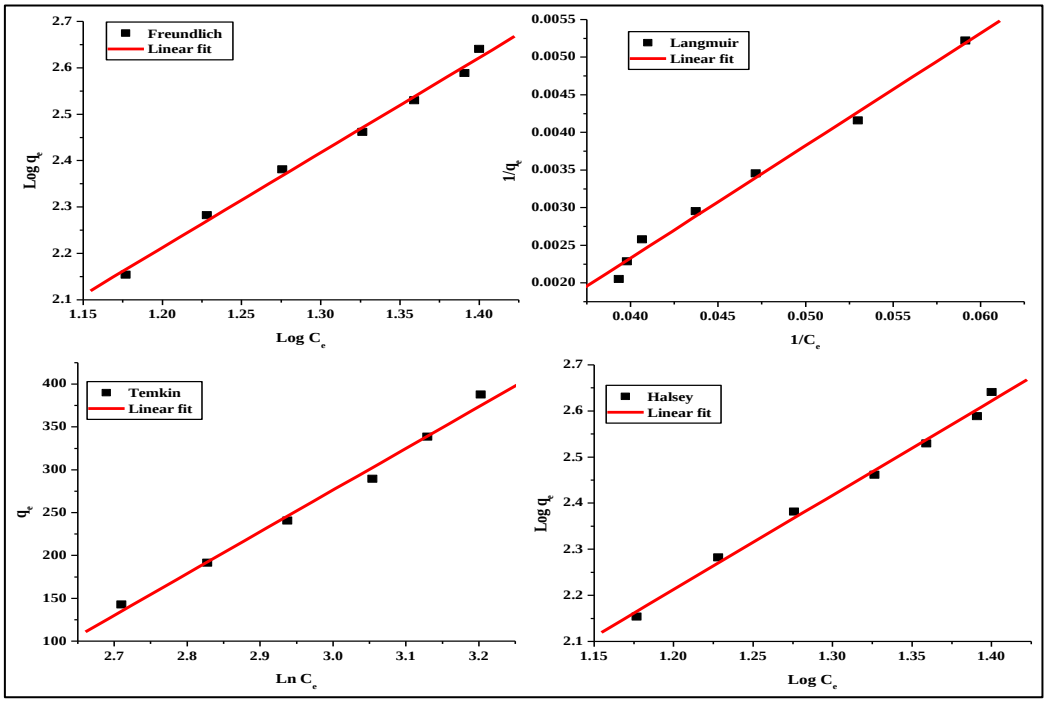

Operating parameters: 180 rpm, 100-1000 ppmof dye, 0.05g adsorbent, time 300min, temperature 30^0C, optimum pH

Figure 4.18 b. Linear fit of isotherm for RR onto NC

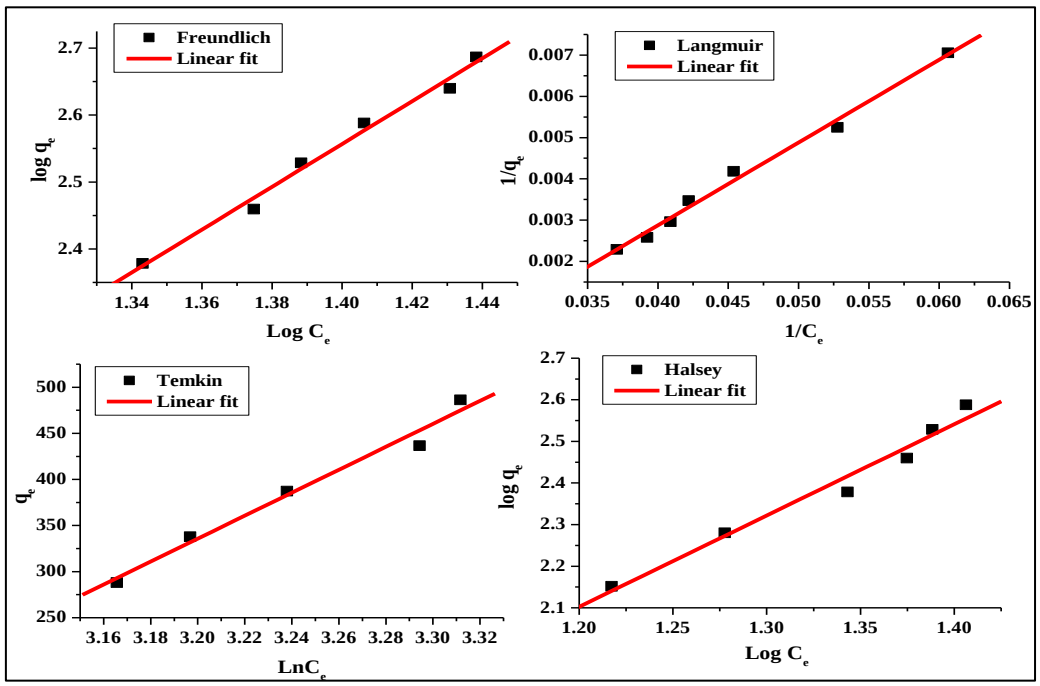

Operating parameters: 180 rpm, 100-1000 ppmof dye, 0.05g adsorbent, time 300min, temperature 30^0C, optimum pH

Figure 4.18 c. Linear fit of isotherm for RH onto NC

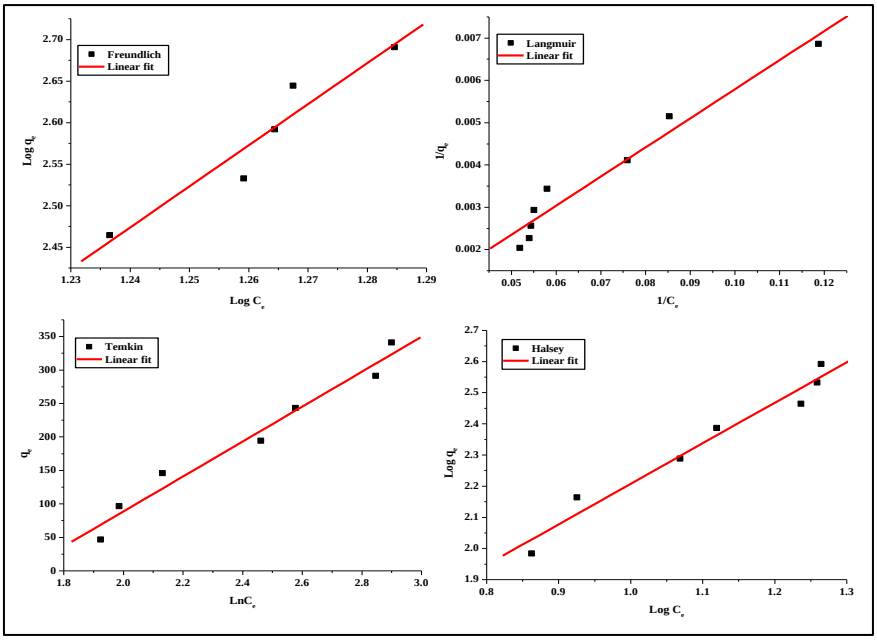

Operating parameters: 180 rpm, 100-1000 ppm of dye, 0.05g adsorbent, time 300min, temperature 30^0C, optimum pH

Figure 4.19 a. Linear fit of isotherm for RB onto CC

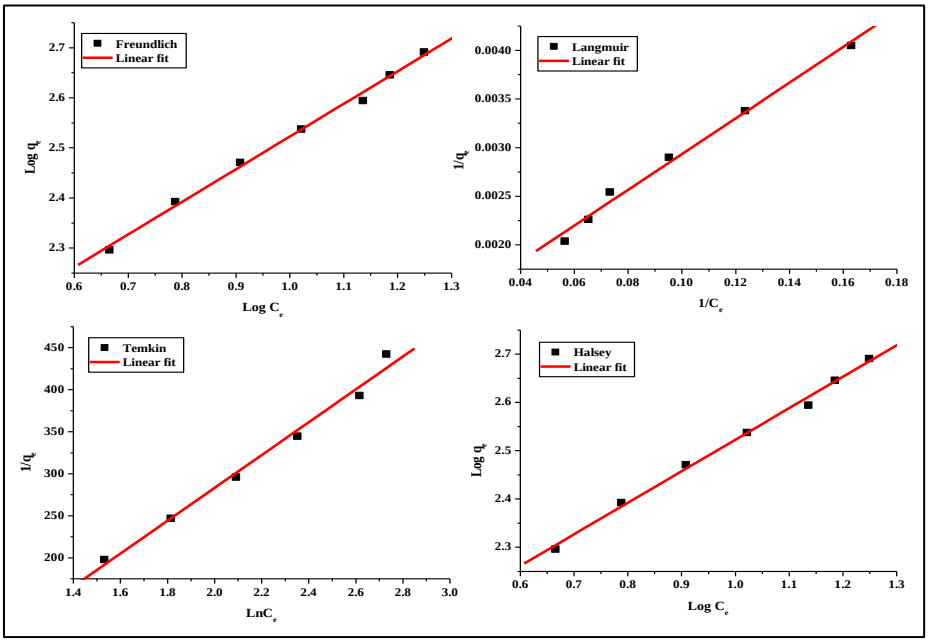

Operating parameters: 180 rpm, 100-1000 ppm of dye, 0.05 g adsorbent, time 300 min, temperature 30^0C, optimum pH

Figure 4.19 b. Linear fit of isotherm for RR onto CC

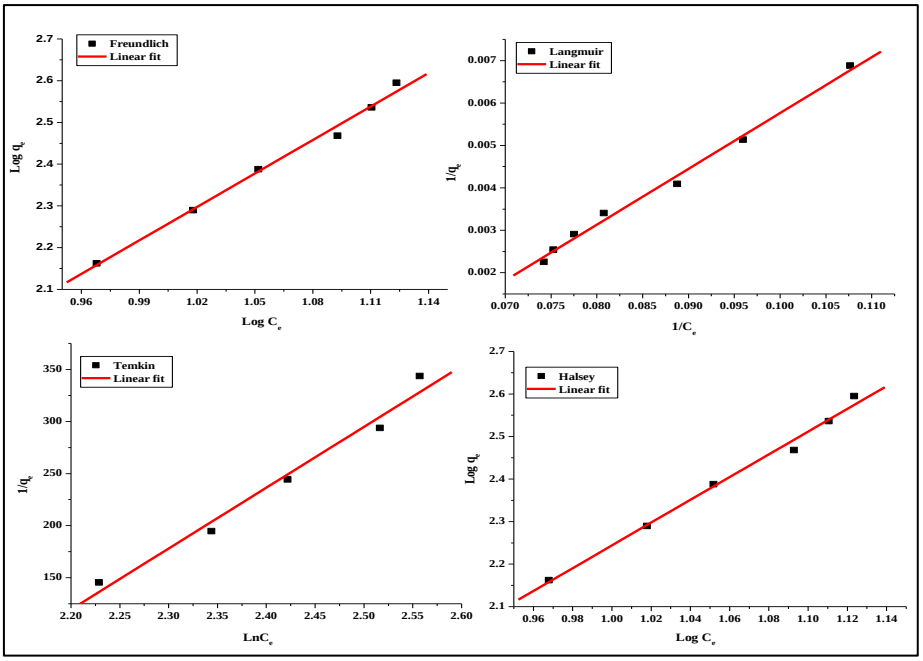

Operating parameters: 180 rpm, 100-1000 ppm of dye, 0.05 g adsorbent, time 300 min, temperature 30^0C, optimum pH

Figure 4.19 c Linear fit of isotherm for RH onto CC

Table 4.5 Isotherm parameters

	C			NC			CC		
	RB	**RR**	**RH**	**RB**	**RR**	**RH**	**RB**	**RR**	**RH**
Freundlich									
q_e(exp) ($mg.g^{-1}$)	402	410	411.3	401	423	428.9	490.37	442.6	440.90
Kf	0.025	0.129	7.277	0.012	0.571	6.902	4.5656	7.4259	0.0002
N	3.357	2.789	1.307	14.61	2.046	1.312	2.946	1.533	2.374
r^2	0.981	0.975	0.977	0.991	0.996	0.995	0.959	0.997	0.995
SD	0.028	0.032	0.04	0.019	0.015	1.69E-04	0.0292	0.010	0.016
Langmuir									
q_m ($mg.g^{-1}$)	434.78	419.28	410.84	425.53	403.22	434.54	476.19	439.30	446.42
K_L	0.0120	0.026	0.325	0.002	0.0166	0.010	0.0304	0.1239	0.0170
r^2	0.9891	0.9865	0.974	0.99178	0.995	0.995	0.9772	0.9953	0.996
SD	1.79E-04	4.86E-04	2.72E-04	1.58E-04	1.24E-04	1.69E-04	3.77E-04	8.06E-05	1.51E-04
Temkin									
β_T	1011.14	841.73	739.12	308.675	487.3498	244.43	261.02	195.36	584.34
K_T	0.083	0.090	0.081	0.059	0.087	0.055	0.1901	0.576	0.118
r^2	0.982	0.978	0.994	0.975	0.994	0.989	0.984	0.994	0.989
SD	24.152	21.54	0.04022	23.167	10.32	0.127	20.135	11.088	0.132
Halsey									
K_H	0.660	0.727	0.998	0.336	0.888	2.718	3.253	17.619	2.718
n_H	0.322	0.358	0.419	0.068	0.488	0.4558	1.300	1.533	0.374
r^2	0.9815	0.9758	0.994	0.991	0.996	0.986	0.982	0.997	0.995
SD	0.030	0.032	2.72E-04	0.019	0.015	0.029	0.044	0.010	0.016

Table 4.6 Comparison of adsorption capacity of CC with adsorbents reported in literature for RB-21, RR-141 and RH-6G

Adsorbent	Dye	Adsorption Capacity [mg/g]	Reference
Fly ash and Sepiolite	RB-21	106.71 and 66.67 respectively	[63]
Clay, Acivated Clay and Modified Clay	RB-21	44.32, 37.34 and 48.26 respectively	[64]
Clinoptilolite	RB-21	9.652	[65]
Cetyltrimethylammonium bromide-coated magnetite nanoparticles	RB-21	556.2	[66]
Polyurethane foam	RB-21	8.31	[67]
Activated carbon	RB-21	357 ± 24	[68]
Titanium dioxide (TiO_2),	RB-21	22.79	[69]
Ultra sound(US) + Titanium dioxide (TiO_2),	RB-21	37.28	[69]
Titanium dioxide (TiO_2)+ Praseodymium (Pr),	RB-21	148.08	[69]
Ultra sound (US) + Titanium dioxide (TiO_2) + Praseodymium (Pr)	RB-21	233.10	[69]
Titanium dioxide (TiO_2) + Lanthanum (La)	RB-21	149.95	[69]
Ultra sound (US) + Titanium dioxide (TiO_2), + Lanthanum (La)	RB-21	235.24	[69]
Titanium dioxide (TiO_2) +Gadolinium (Gd)	RB-21	156.50	[69]
Ultra sound(US) + Titanium dioxide (TiO_2) + Gadolinium(Gd)	RB-21	235.57	[69]
Titanium dioxide (TiO_2) + Cerium (Ce)	RB-21	165.50	[69]
Ultra sound(US + Titanium dioxide (TiO_2) + Cerium (Ce),	RB-21	236.02	[69]

Chitin and Modified Chitin	RR-141	133 and 124 respectively	[70]
Cattail, Water Lettuce and Activated Carbon	RR-141	1.63, 3.56 and 8.52 respectively	[71]
Treated flute-reed	RR-141	7.58	[72]
Zinc Stannate Oxide	RR-141	61.0	[73]
Banana Peel, Saw dust, Orange peel and TiO_2	RR-141	0.76,2.12,512 and 5.14 respectively	[74]
Exhausted coffee ground	Rh-6G	17.37	[75]
Trichodermaharzianummycelial waste	Rh-6G	3.40	[76]
Palm shell powder	Rh-6G	105	[77]
Graphene oxide	Rh-6G	23.30	[78]
Titanium phosphate	Rh-6G	217.39	[79]
Chitosan nanoclaynanocomposite	RB-21	490.37	This study
Chitosan nanoclaynanocomposite	RR-141	442.60	This study
Chitosan nanoclaynanocomposite	Rh-6G	440.90	This study

Sorption Kinetics

The kinetic models Pseudo First order, Pseudo Second order, Intraparticle diffusion, Bangham and Liquid film diffusion model were studied and the kinetic constants for the sorption of RB-21, RR-141 and RH-6G by C, NC and CC are presented in Table 4.7Fig. 4.20 (a, b & c), 4.21 (a, b & c) and 4.22 (a, b & c) shows the linear fit for Kinetics of RB,RR and RH onto C,NC and CC. The correlation coefficients for pseudo second order model were found to be greater than the other kinetic models for C, NC and CC and the calculated equilibrium adsorption capacity values were closer to those obtained experimentally. This supported the assumption behind the model that the surface complexation may be the rate-limiting step involving valence forces through sharing or exchanging of electron between adsorbent and adsorbate. The plot of qt versus $t_{1/2}$ did not pass through origin suggesting that intraparticle diffusion was not the only rate-controlling step but some degree of the boundary layer diffusion also controlled the adsorption process and that the overall rate of the dye adsorption process appeared to be controlled by more than one-step. It was thus concluded that the dye adsorption process was controlled by more than one step.

The plot for Liquid Film Diffusion Model did not pass though origin as required by the model for all the adsorbents under study but had very small intercepts (curves not shown) indicating that diffusion of the dyes from the liquid phase to the adsorbent surface might be having some role in deciding the rate processes. The double logarithmic plots of Bangham model showed good correlation coefficients indicating significant contribution of pore diffusion towards adsorption process.

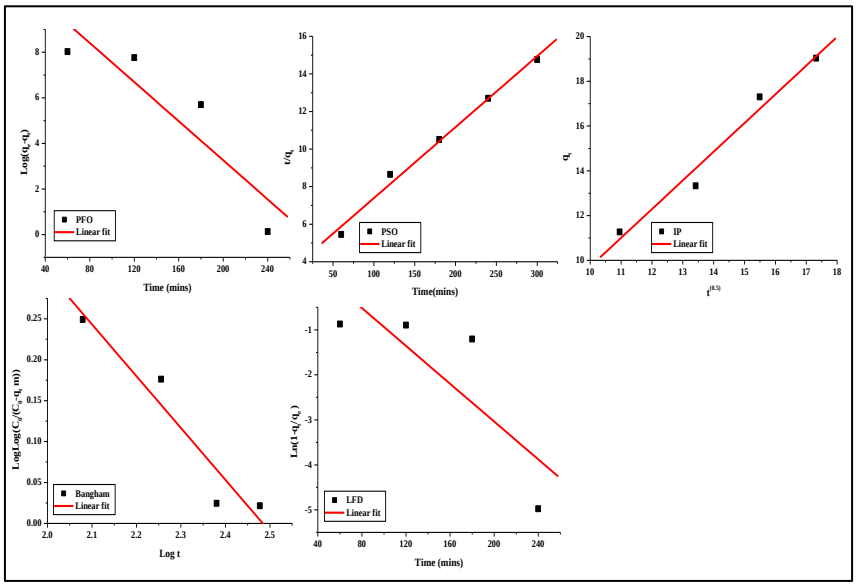

Operating parameters: 180 rpm, 100 ppm of dye, 0.05 g adsorbent, time 300 min, temperature 30^0C, optimum pH

Figure 4.20 a. Linear fit of kinetics for RB onto C

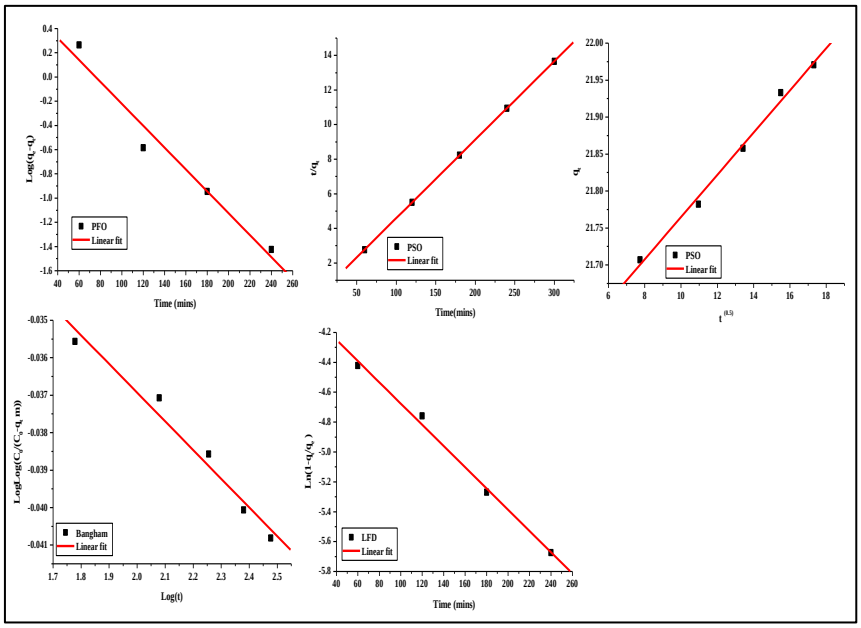

Operating parameters: 180 rpm, 100 ppm of dye, 0.05 g adsorbent, time 300 min, temperature 30^0C, optimum pH

Figure 4.20 b Linear fit of kinetics for RR onto C

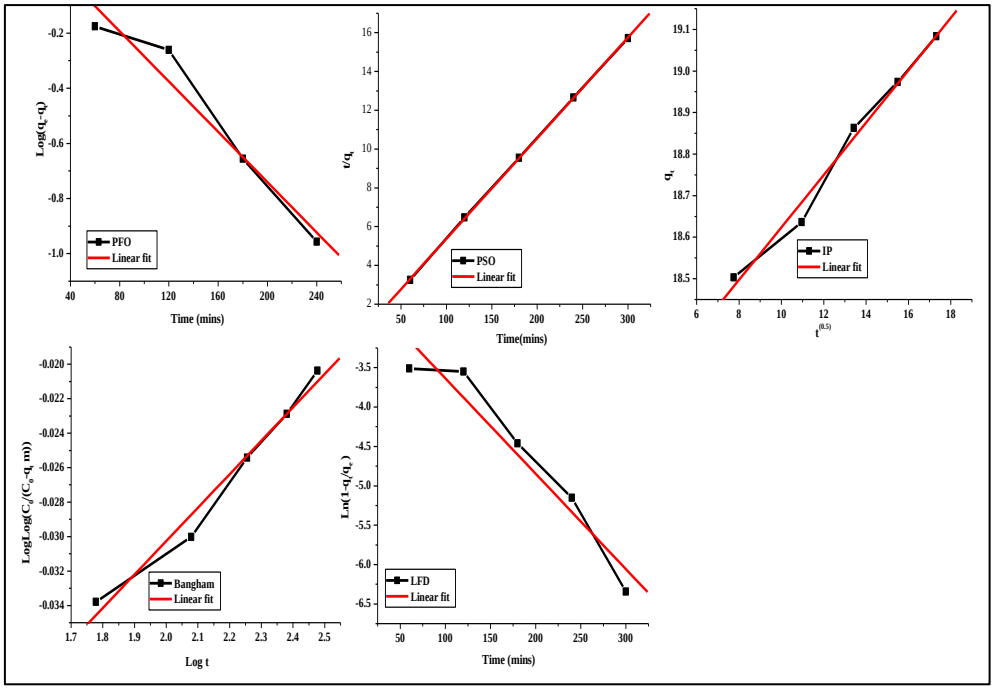

Operating parameters: 180 rpm, 100 ppm of dye, 0.05 g adsorbent, time 300 min, temperature 30^0C, optimum pH

Figure 4.20c Linear fit of kinetics for RH onto C

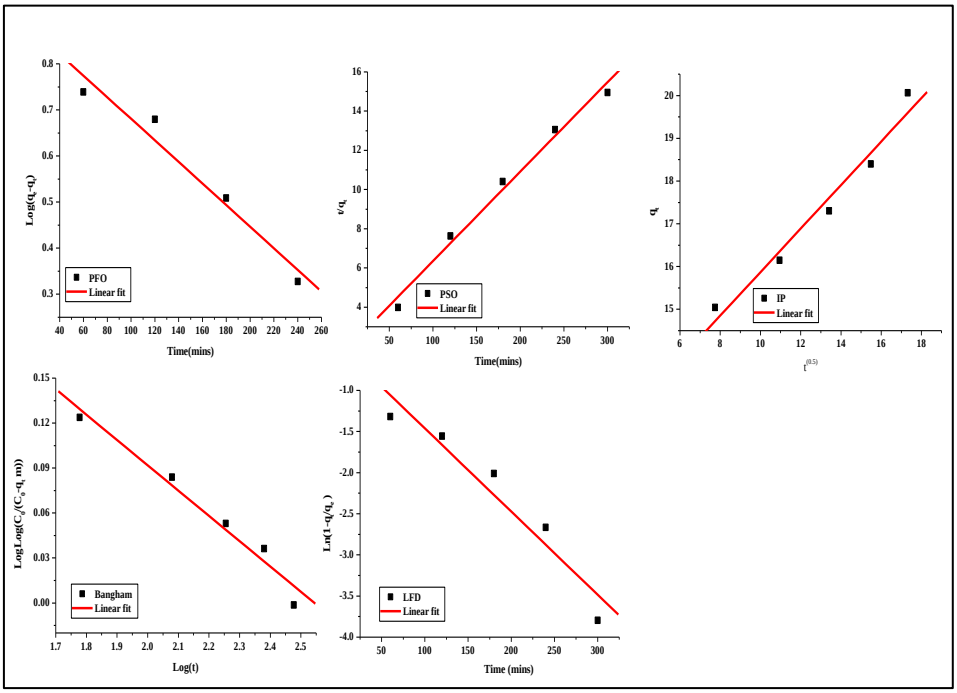

Operating parameters: 180 rpm, 100 ppm of dye, 0.05 g adsorbent, time 300 min, temperature 30^0C, optimum pH

Figure 4.21 a. Linear fit of kinetics for RB onto NC

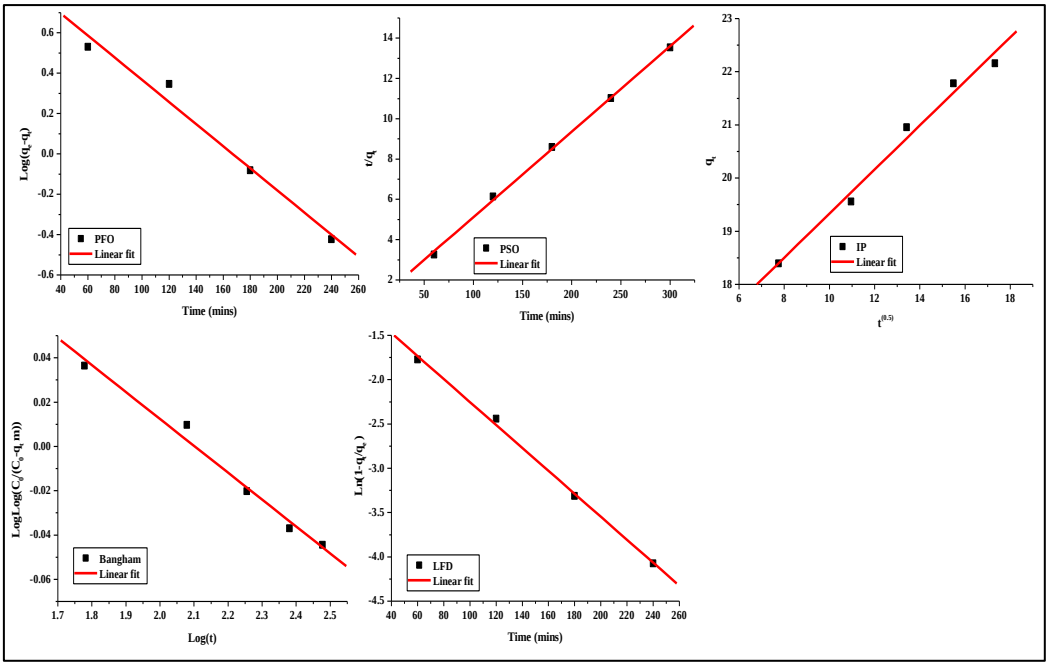

Operating parameters: 180 rpm, 100 ppm of dye, 0.05g adsorbent, time 300 min, temperature 30^0C, optimum pH

Figure 4.21 b. Linear fit of kinetics for RR onto NC

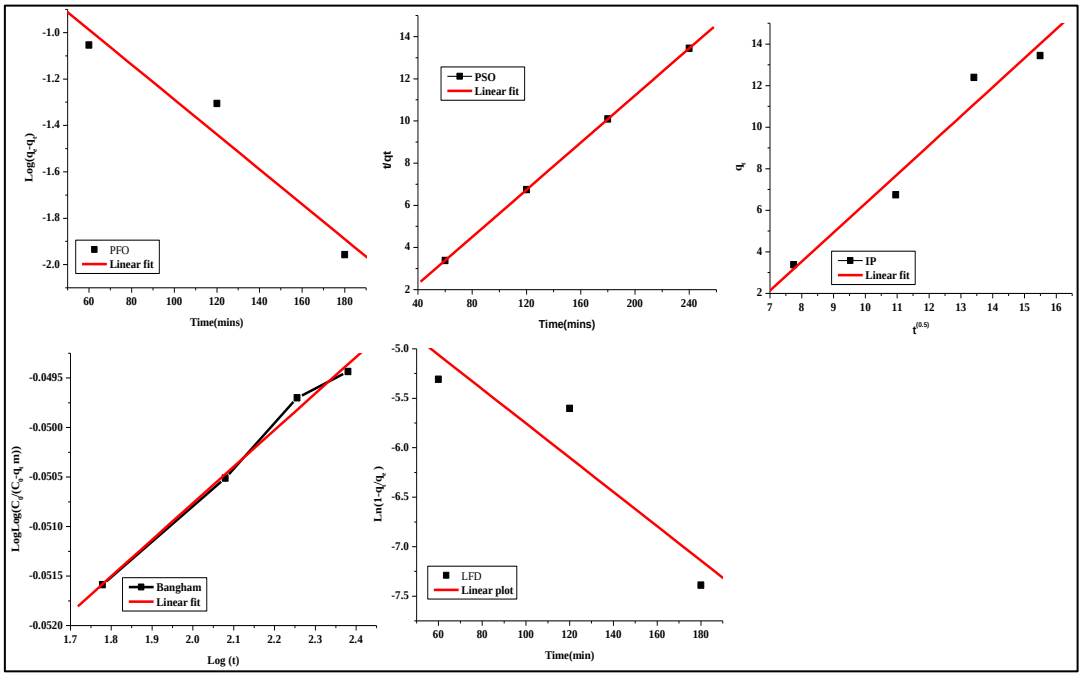

Operating parameters: 180 rpm, 100 ppm of dye, 0.05g adsorbent, time 300min, temperature 30^0C, optimum pH

Figure 4.21 c. Linear fit of kinetics for RH onto NC

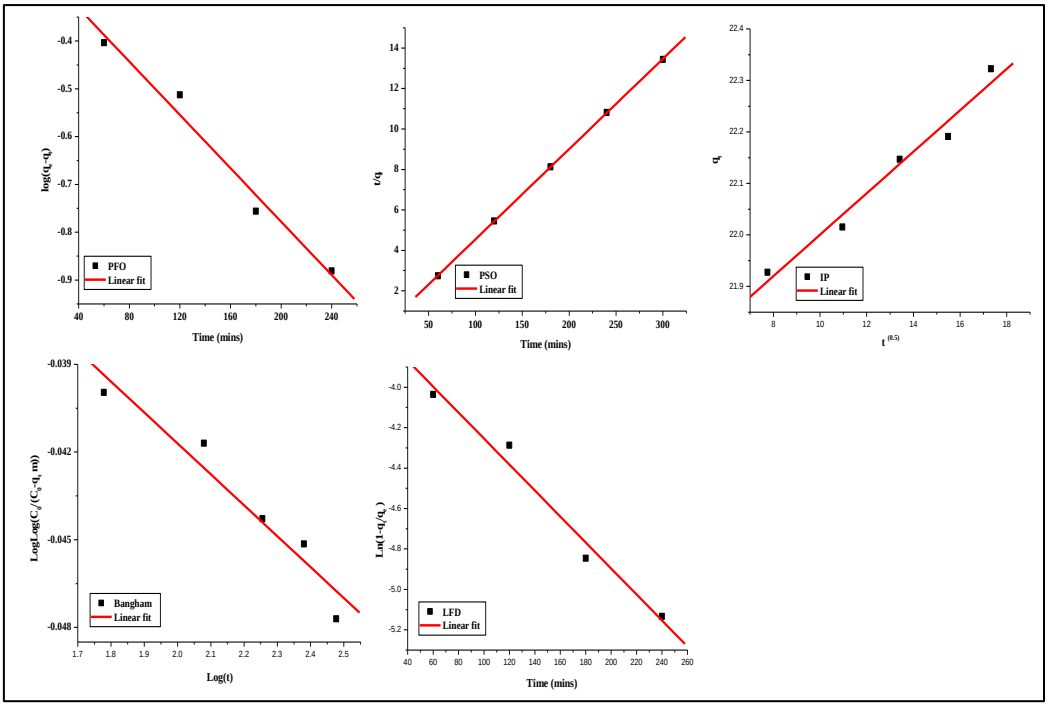

Operating parameters: 180 rpm, 100 ppm of dye, 0.05 g adsorbent, time 300 min, temperature 30^0C, optimum pH

Figure 4.22 a. Linear fit of kinetics for RB onto CC

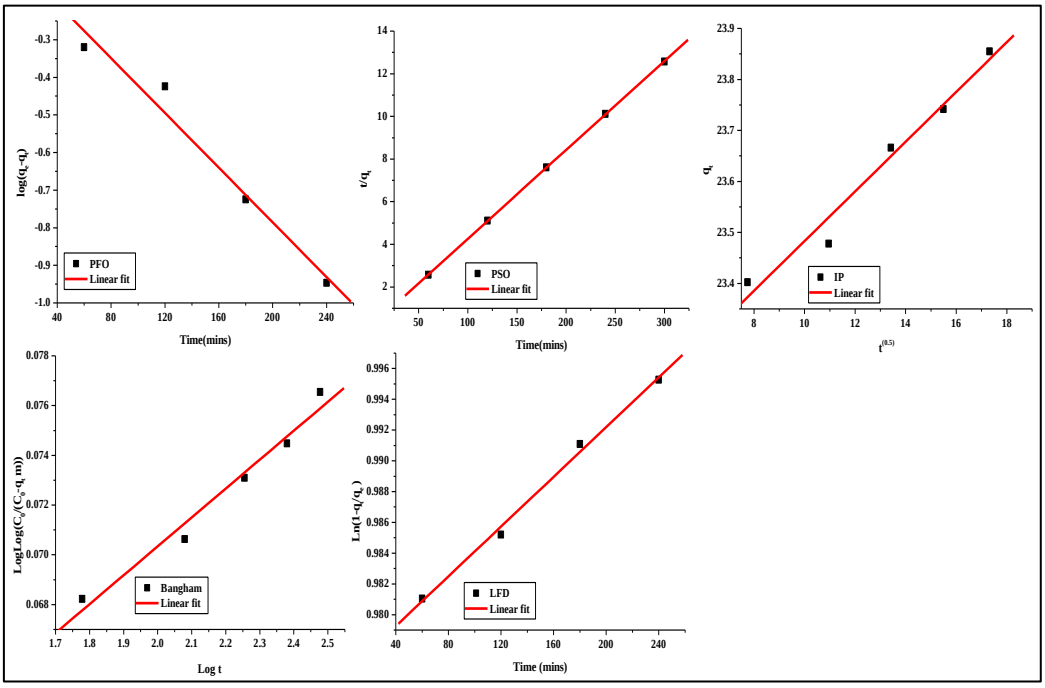

Operating parameters: 180 rpm, 100 ppm of dye, 0.05g adsorbent, time 300 min, temperature 30^0C, optimum pH

Figure 4.22 b. Linear fit of kinetics for RR onto CC

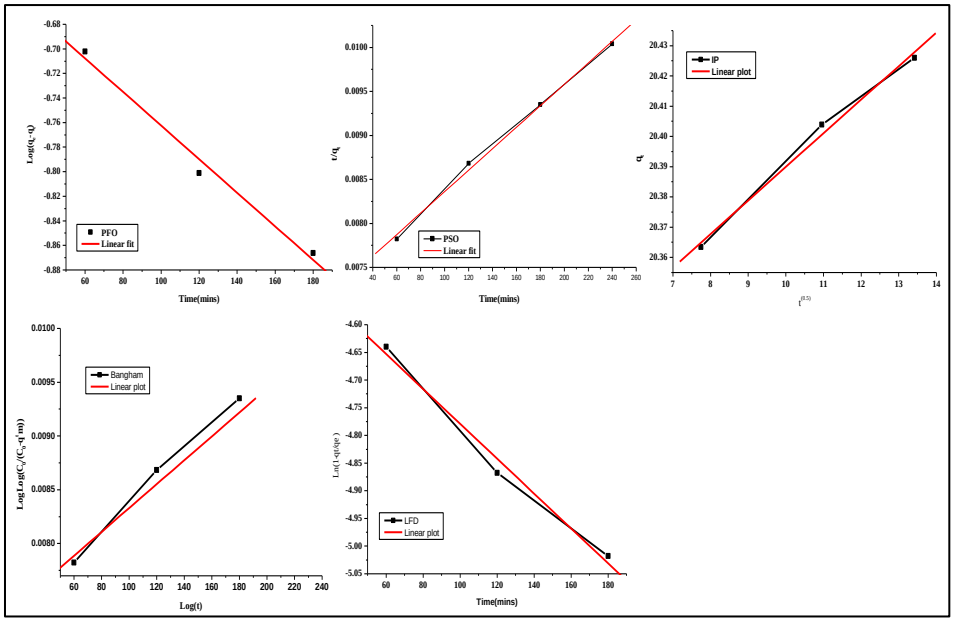

Operating parameters: 180 rpm, 100 ppm of dye, 0.05 g adsorbent, time 300 min, temperature 30^0C, optimum pH

Figure 4.22 c. Linear fit of kinetics for RH onto CC

Table 4.7 Kinetics

	C			NC			CC		
	RB	**RR**	**RH**	**RB**	**RR**	**RH**	**RB**	**RR**	**RH**
Pseudo first order									
q_e (exp)	19.03	21.97	18.75	20.52	22.15	15.56	22.19	23.74	20.56
q_e	12.462	10.197	1.294	8.219	8.237	0.205	18.26	9.480	0.575
K_1	0.098	0.0208	0.009	0.005	0.0126	0.011	0.023	0.064	0.0104
r^2	0.906	0.982	0.957	0.979	0.989	0.996	0.960	0.999	0.854
SD	0.1895	0.162	0.121	0.045	0.076	0.036	0.290	4.31E-4	0.261
Pseudo second order									
q_e	21.182	22.045	19.275	21.939	23.590	17.889	24.56	23.22	20.665
K_2	0.0006	0.0362	0.014	0.001	0.0020	0.109	0.053	2.9E-3	0.0358
r^2	0.995	1	0.992	0.993	0.999	1	0.998	0.995	0.999
SD	0.398	0.013	0.003	0.562	0.147	0.004	3.82E-4	0.405	0.026
Intraparticle diffusion									
K_{ip}	1.282	0.028	0.066	0.508	0.414	0.010	0.791	0.106	0.025
r^2	0.986	0.996	0.962	0.982	0.992	0.985	0.996	0.999	0.938
SD	0.705	0.009	0.081	0.421	0.218	0.007	0.259	0.013	0.041
Bangham									
K_m	3.308	1.244	-4.154	2.474	1.469	-3.339	20.270	3.908	-0.305
A	0.633	0.007	0.020	0.168	0.121	0.003	0.187	0.027	0.007
r^2	0.960	0.985	0.938	0.982	0.992	0.997	0.992	0.994	0.902
SD	0.038	4.20E-04	0.002	0.010	0.004	8.94E-05	0.008	9.6E-4	0.001
Liquid film diffusion									
K_{fd}	0.021	0.007	0.009	0.010	0.012	0.011	3.611	0.002	0.010
r^2	0.815	0.997	1	0.962	0.998	0.996	0.989	0.999	0.854
Sd	1.416	0.050	3.31E-16	0.310	0.057	0.084	0.092	9.9E-4	0.602

The Thermodynamic studies

The negative values of ΔG (Table 4.8) for both RB-21 and RR-141 indicate the spontaneous and favourable nature of the adsorption process. The very low positive values of ΔH in the case of Rh-6G adsorption onto C, NC and CC indicate the adsorption process to be physical in nature and further affirm the fact that the adsorption process is independent of temperature. The negative values of ΔH in the case of RB–21 and RR-141 adsorption onto C, NC and CC suggested the adsorption process to be thermodynamically feasible. The positive values of ΔS suggested that and also the increase in randomness at the solid-solution interface during the though fixation of the dye molecule onto the active site of the adsorbent should have caused an entropy decrease, the entropy of dye molecules in aqueous phase could be much greater, leading to high entropy of the whole system. This further facilitated the adsorption of RB-21 and RR-141 onto C, NC and CC. The negative value of ΔS^0 in Rh-6G adsorption indicates orderliness at the solid/liquid interface and also the irreversible nature of adsorption.

Table 4.8 Thermodynamic parameters

ΔG[KJ/mol]									
	C			**NC**			**CC**		
	RB	**RR**	**RH**	**RB**	**RR**	**RH**	**RB**	**RR**	**RH**
303	-16.639	-19.792	8.374	-12.126	-18.569	9.984	-18.947	-23.726	14.634
313	-17.188	-20.445	8.650	-12.526	-19.182	10.313	-19.573	-24.509	15.117
323	-17.738	-21.098	8.926	-12.926	-19.795	10.643	-20.198	-25.292	15.599
333	-18.287	-21.752	9.203	-13.326	-20.407	10.972	-20.824	-26.075	16.082
343	-18.836	-22.405	9.479	-13.726	-21.020	11.302	-21.449	-26.858	16.565
	C			**NC**			**CC**		
	RB	**RR**	**RH**	**RB**	**RR**	**RH**	**RB**	**RR**	**RH**
ΔH[KJ/mol]	-3.11E-05	-4.42E-05	3.15E-09	-2.60E-05	-2.39E-05	1.16E-09	-0.0000229	-3.36E-05	1.00E-08
ΔS[J/molK]	54.916	65.32163	-0.027	40.019	61.28512	-0.032	62.534	78.303	-0.048

3.2.8 Dye adsorption studies of binary dye systems

In dye containing effluents, generally a variety of dyes would be present and these dyes will show different adsorption behaviour. There would be a competitive adsorption with respect to the nature of the dye and the adsorbent. In this work, we report an investigation of cationic and anionic dye adsorption onto Chitosan clay nanocomposite. Extensions of several common isotherms were used to model the experimental data, namely, the extended Langmuir equation, the Jain and Snoeyink modified extended Langmuir model and the P-factor.

Extended Langmuir Equation was developed by Butler and Ockrent (1930) for competitive adsorption. This model assumed (i) a homogeneous surface with respect to the energy of adsorption, (ii) no interaction between adsorbed species, and (iii) that all desorption sites are equally available to all adsorbed species.

$$q_{e,i} = \frac{K^0_{L,i} C_{e,i}}{1+\sum a^0_{L,i} C_{e,i}} \qquad \text{…. eq. (7)}$$

Where, K_l and a_l are the Langmuir isotherm constants. For example, using components 1 and 2

$$q_{e,1} = \frac{K^0_{L,1} C_{e,1}}{1+a^0_{L,1} C_{e,1}+a^0_{L,2} C_{e,2}} \qquad \text{…. eq. (8)}$$

$$q_{e,2} = \frac{K^0_{L,2} C_{e,2}}{1+a^0_{L,1} C_{e,1}+a^0_{L,2} C_{e,2}} \qquad \text{…. eq. (9)}$$

Jain and Snoeyink Modified Extended Langmuir Model. Jain and Snoeyink (1973) investigated competitive sorption on activated carbon from aqueous bicomponent solutions of organic sorbates and developed model that predicts sorption equilibria in such non ideal systems. According to Jain and Snoeyink, the Langmuir theory for binary sorbate systems is based on sorption without competition. Therefore, to account for competition in the Langmuir theory, the Jain-Snoeyink (JS) model proposed to add an additional term to the extended Langmuir equation.

$$q_{e,1} = \frac{(Q^0_{m,1}-Q^0_{m,2}) a^0_{L,1} C_{e,1}}{1+a^0_{L,1} C_{e,1}} + \frac{Q^0_{m,2} a^0_{L,1} C_{e,1}}{1+a^0_{L,1} C_{e,1}+a^0_{L,2} C_{e,2}} \qquad \text{…. eq. (10)}$$

$$q_{e,2} = \frac{Q^0_{m,2} a^0_{L,2} C_{e,2}}{1+a^0_{L,1} C_{e,1}+a^0_{L,2} C_{e,2}} \qquad \text{…. eq. (11)}$$

Where, Q°m is the monolayer saturation capacity for the Langmuir isotherm. The first term on the right-hand side of eq 10 refers to the amount of species 1 adsorbed without competition with species 2, while the second term gives the amount of species 1 adsorbed in competition with 2, as described by applying the competition to the Langmuir model. Further a correlative technique was developed (McKay and Al Duri, 1987) and applied to dye/carbon systems. It is an easy-to-use method based on introducing a “lumped” capacity factor *P*

$$P_i = \frac{(K_{L,i}/a_{L,i})_{singlesolute}}{(K_{L,i}/a_{L,i})_{multisolute}} \quad \text{.... eq. (12)}$$

Figure.4.23 (a, b & c), 4.24 (a, b & c) and 4.25 (a. b & c) shows the linear fit for isotherms of RB+RR, RB+RH and RB+RR onto C, NC and CC.

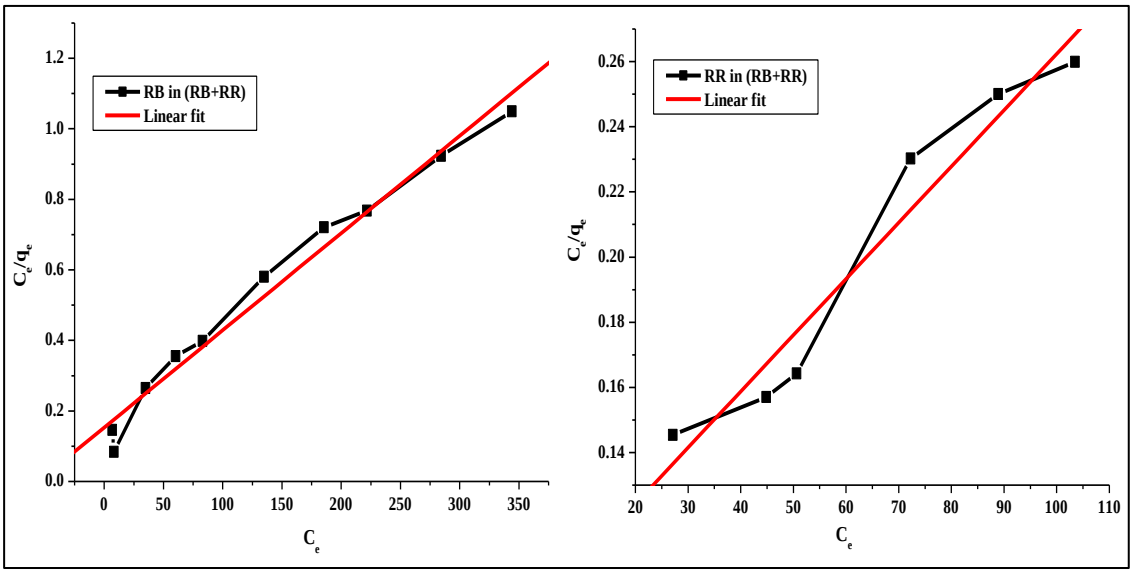

Operating parameters: 180 rpm, 100 ppm of dye, 0.05 g adsorbent, time 210 min, temperature 30^0C, optimum pH

Figure 4.23 a Linear fit of isotherm for RB and RR in (RB+RR) onto C

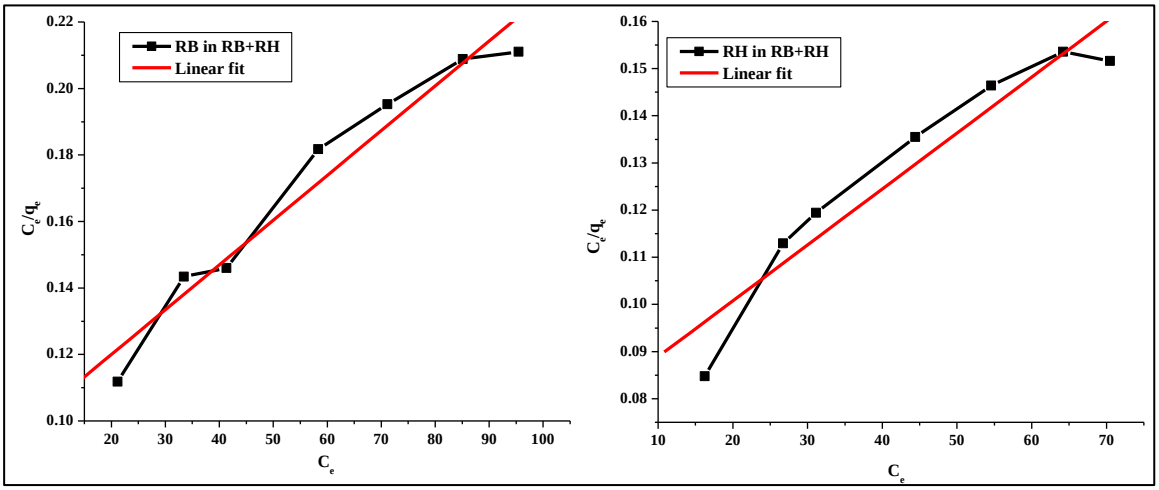

Operating parameters: 180 rpm, 100 ppmof dye, 0.05g adsorbent, time210 min, temperature 30^0C, optimum pH

Figure 4.23 b Linear fit of isotherm for RB and RH in (RB+RH) onto C

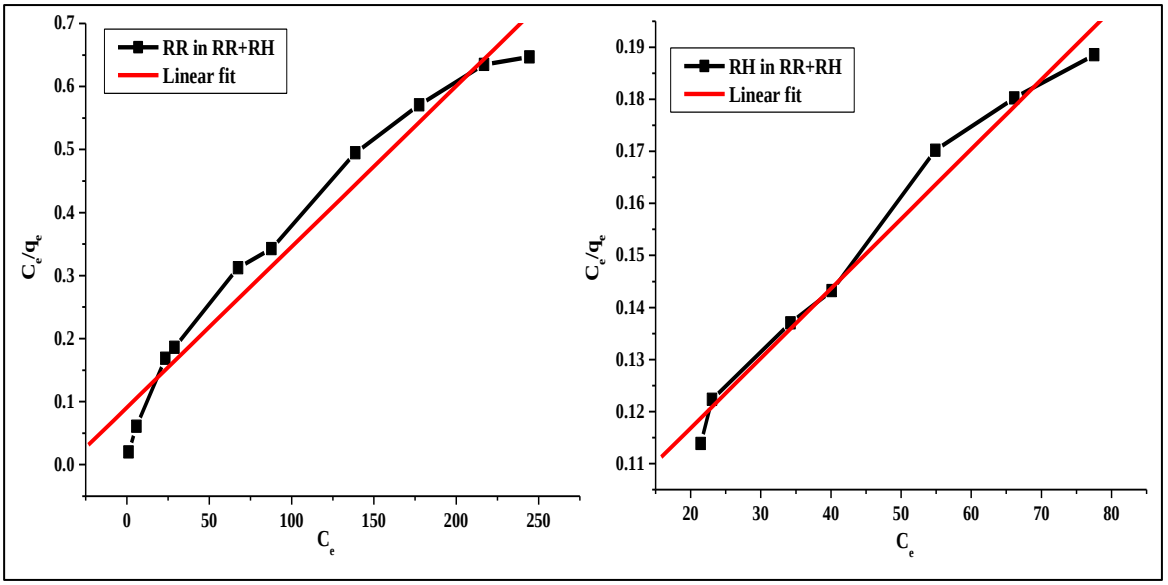

Operating parameters: 180 rpm, 100 ppm of dye, 0.05g adsorbent, time 210 min, temperature 30^0C, optimum pH

Figure 4.23 c Linear fit of isotherm for RR and RH in (RR+RH) onto C

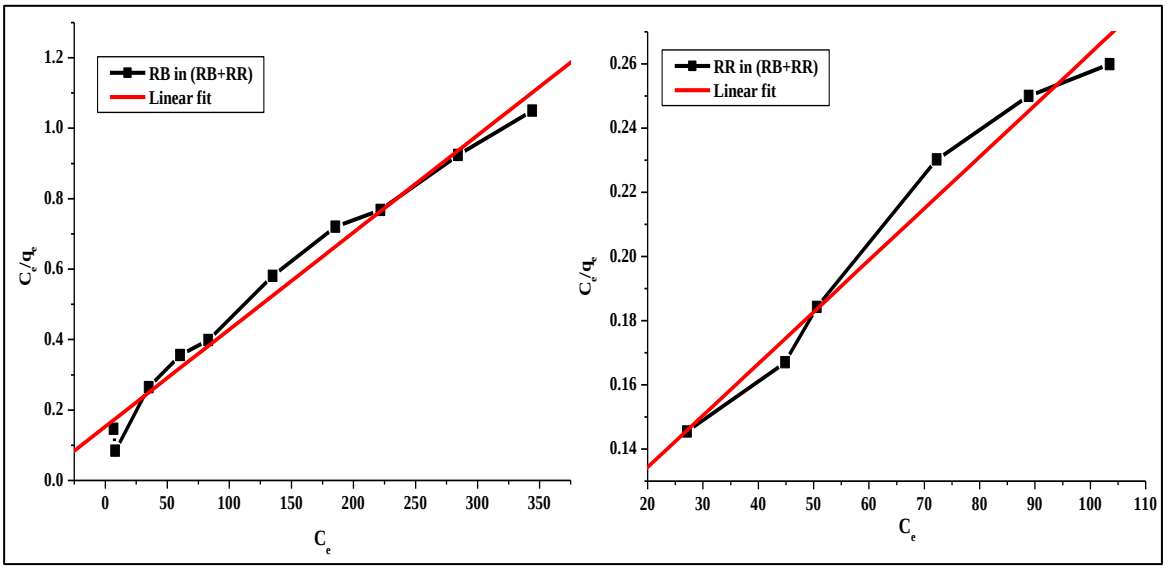

Operating parameters: 180 rpm, 100 ppm of dye, 0.05g adsorbent, time 210 min, temperature 30^0C, optimum pH

Figure 4.24 a Linear fit of isotherm for RB and RR in (RB+RR) onto NC

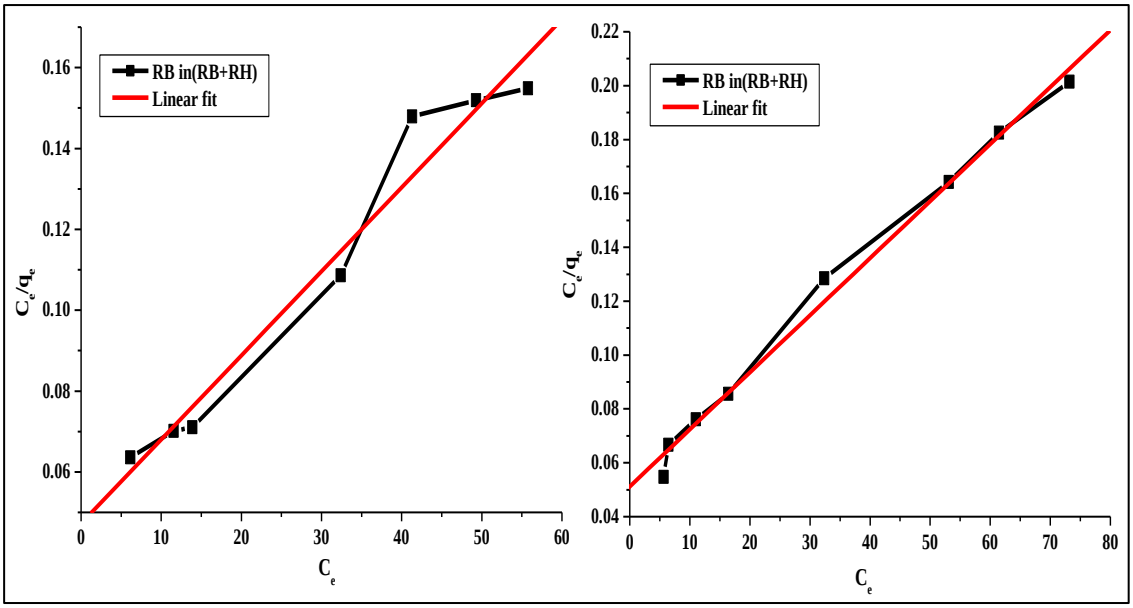

Operating parameters: 180 rpm, 100 ppm of dye, 0.05 g adsorbent, time 210 min, temperature 30^0C, optimum pH

Figure 4.24 b Linear fit of isotherm for RB and RH in (RB+RH) onto NC

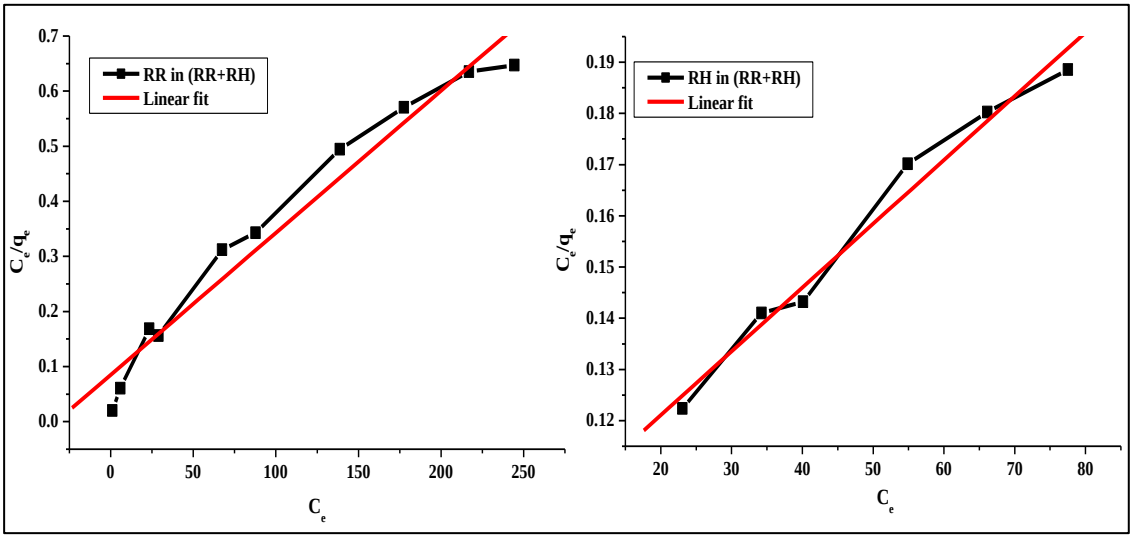

Operating parameters: 180 rpm, 100 ppm of dye, 0.05g adsorbent, time 210 min, temperature 30^0C, optimum pH

Figure 4.24 c. Linear fit of isotherm for RR and RH in (RR+RH) onto NC

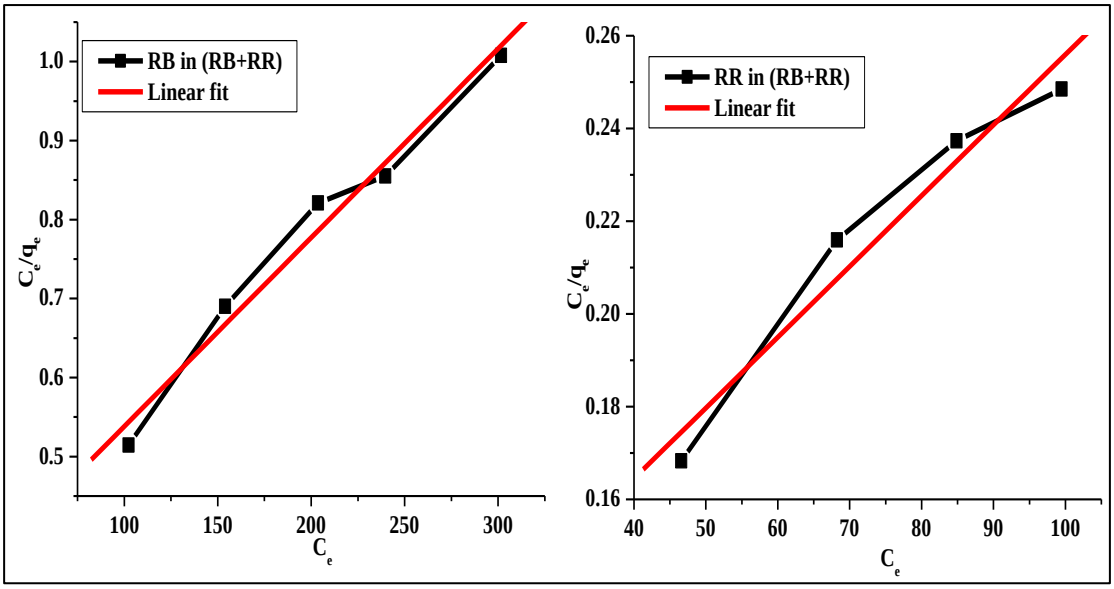

Operating parameters: 180 rpm, 100 ppm of dye, 0.05g adsorbent, time 210 min, temperature 30^0C, optimum pH

Figure 4.25 a. Linear fit of isotherm for RB and RR in (RB+RR) onto CC

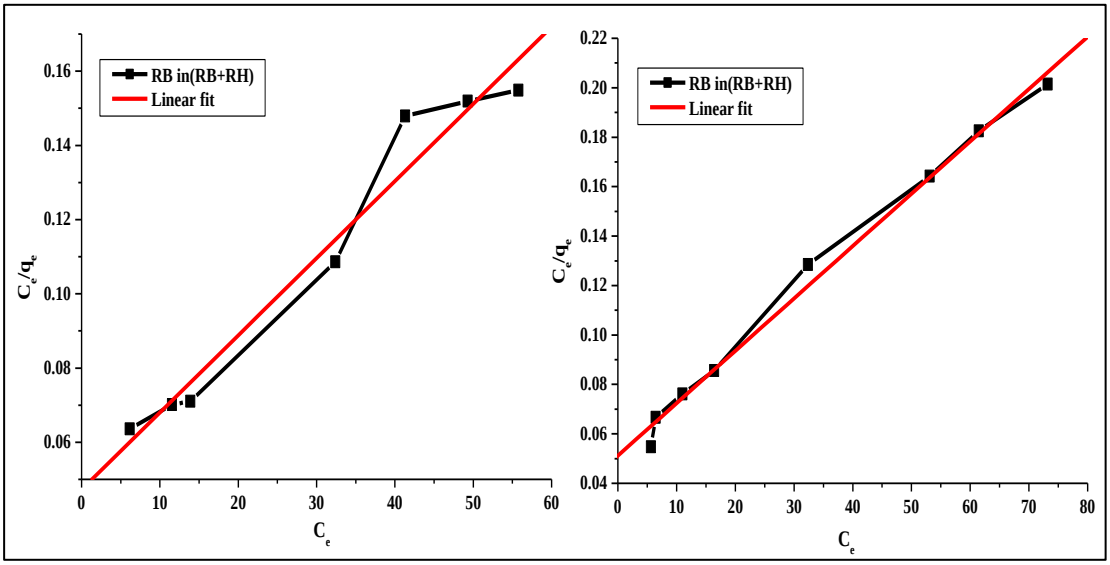

Operating parameters: 180 rpm, 100 ppm of dye, 0.05g adsorbent, time210 min, temperature 30^0C, optimum pH

Figure 4.25 b. Linear fit of isotherm for RB and RH in (RB+RH) onto CC

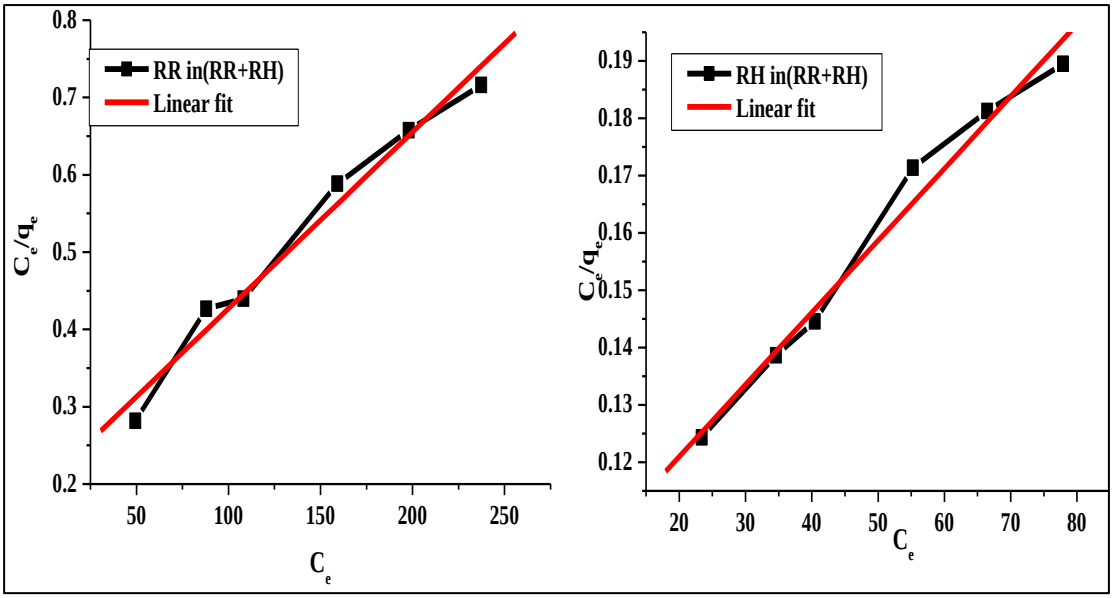

Operating parameters: 180 rpm, 100 ppm of dye, 0.05gadsorbent, time 210 min, temperature 30^0C, optimum pH

Figure 4.25 c. Linear fit of isotherm for RR and RH in (RB+RH) onto CC

Table 4.9 isotherm constants for binary systems

Langmuir isotherm constants for binary systems												
	Binary component system ((RR+RB)											
	C				NC				CC			
	RB+RR											
	K_l	a_l	q_m	r^2	K_l	a_l	q_m	r^2	K_l	a_l	q_m	r^2
RB	6.539	0.018	362.31	0.989	6.539	0.018	324.71	0989	4.784	0.013	346.020	0.988
RR	11.14	0.032	341.29	0.972	11.148	0.032	341.29	0.986	9.660	0.022	434.78	0.976
	RB+RH											
	K_l	a_l	q_m	r^2	K_l	a_l	q_m	r^2	K_l	a_l	q_m	r^2
RB	10.665	0.028	378.78	0.987	19.527	0.041	394.10	0.996	10.902	0.025	388.71	0.986
RH	12.980	0.032	401.60	0.976	21.177	0.044	384.43	0.992	15.966	0.046	342.46	0.980
	RR+RH											
	K_l	a_l	q_m	r^2	K_l	a_l	q_m	r^2	K_l	a_l	q_m	r^2
RR	11.008	0.028	392.15	0.980	11.008	0.028	362.1	0.980	5.031	0.015	322.580	0.988
RH	11.106	0.027	409.83	0.989	11.106	0.027	396.43	0.999`	10.432	0023	365.21	0.990

Table 4.10 Jain Soeinyk isotherm constants for binary systems

			Qm	% of dye adsorbed without competitive adsorption
C				
	RB+ RR	RB	318	50.54
		RR	230	5.21
	RR + RH	RR	363	43.24.
		RH	172	
	RB+RH	RB	296	58.34
		RH	185	
NC				
	RB+ RR	RB	365	32.54
		RR	276	65.73
	RR + RH	RR	386	42.12
		RH	293	59.32
		RB	326	26.54
		RH	164	28
CC				
	RB+RH	RB	296	47
		RH	142	33
	RR+RH	RH	294	96
		RR	287	04
	RB+RH	RB	287	61
		RH	176	39

Table 4.9 shows the K_l and a_L for binary systems The linear isotherm fitting constants showed that the binary mixture fitted well with Langmuir model and the JS model (Table 4.9) clearly explains the competitive adsorption of one over the other.

Sorption kinetics of binary system

The sorption kinetics of binary system was fitted to pseudo first order, pseudo second order and intra particle diffusion models. The adsorption kinetics was well explained by pseudo second order model for all the systems onto C, NC and CC. Figure4.26 (a, b& c), 4.27 (a, b & c) and 4.28 (a, b & c) shows the linear fit for kinetics of RB+RR, RB+RH and RB+RR onto C, NC and CC.

The kinetic constants show the behaviour of the adsorption process,

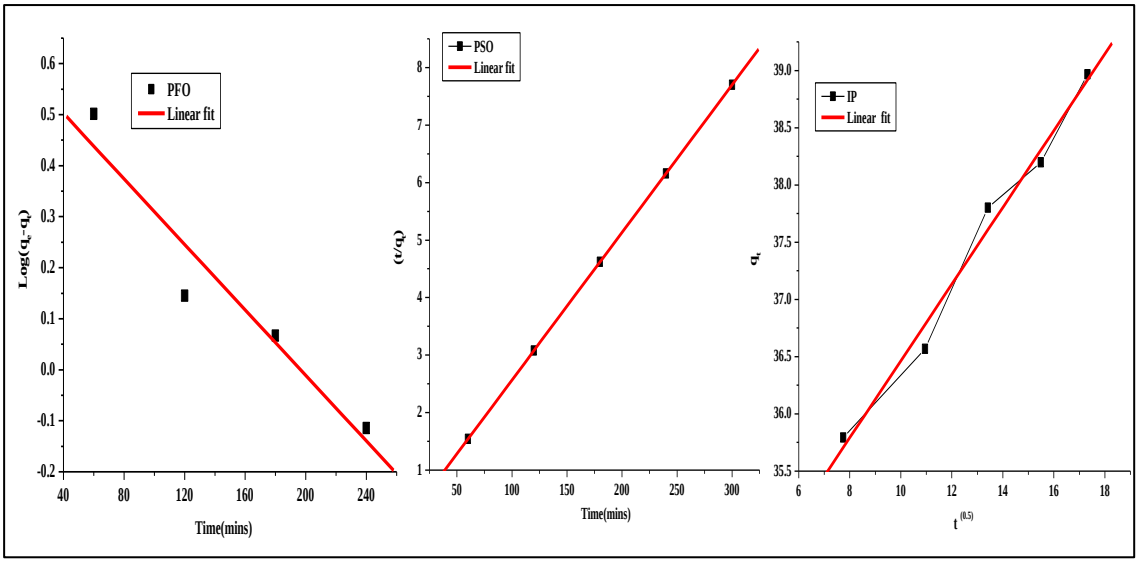

Operating parameters: 180 rpm, 100 ppmof dye, 0.05gadsorbent, time 300 min, temp 30^0C, optimum pH

Figure 4.26 a. Linear fit of Kinetics for RB and RR in (RB+RR) onto C

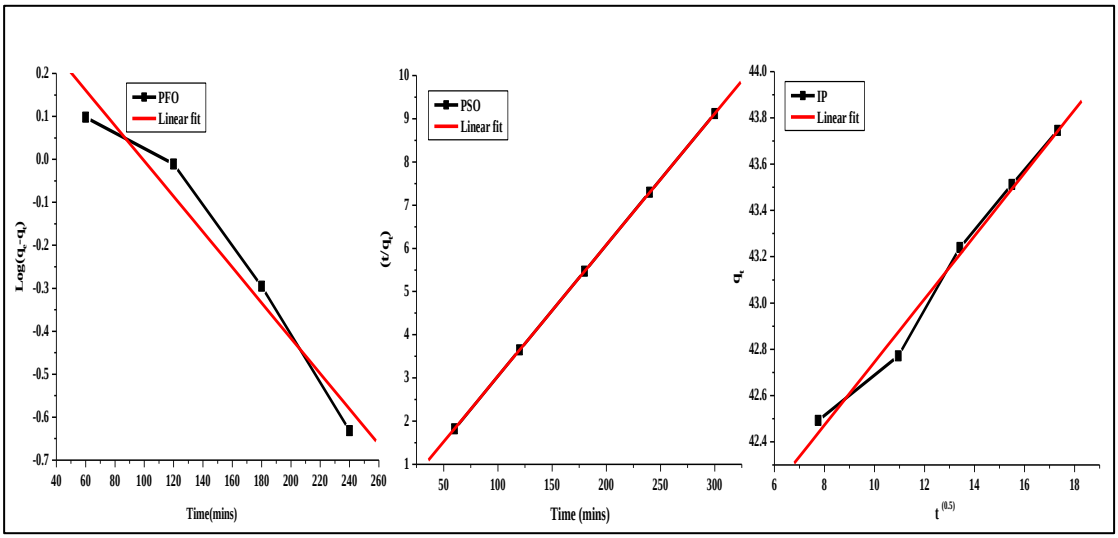

Operating parameters: 180 rpm,100 ppm of dye, 0.05 g adsorbent,time 300min, temp 30^0C, optimum pH

Figure 4.26b. Linear fit of Kinetics for RB and RH in (RB+RH) onto C

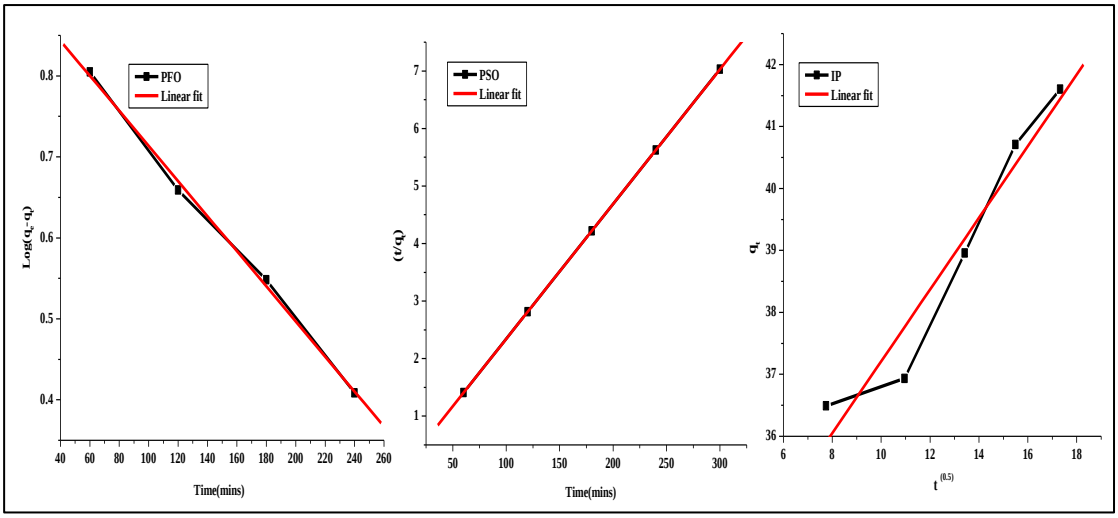

Operating parameters: 180 rpm, 100 ppm of dye, 0.05g adsorbent, time 300 min, temp 30^0C, optimum pH

Figure 4.26 c. Linear fit of Kinetics for RR and RH in (RR+RH) onto C

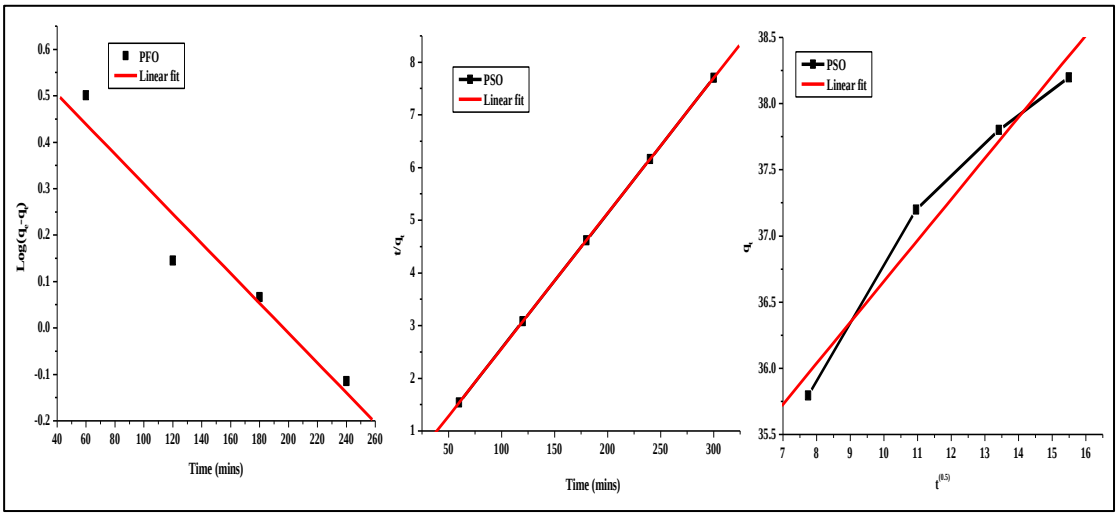

Operating parameters: 180 rpm, 100 ppm of dye, 0.05g adsorbent, time 300 min, temp 30^0C, optimum pH

Figure 4.27 a. linear fit of Kinetics for RB and RR in (RB+RR) onto NC

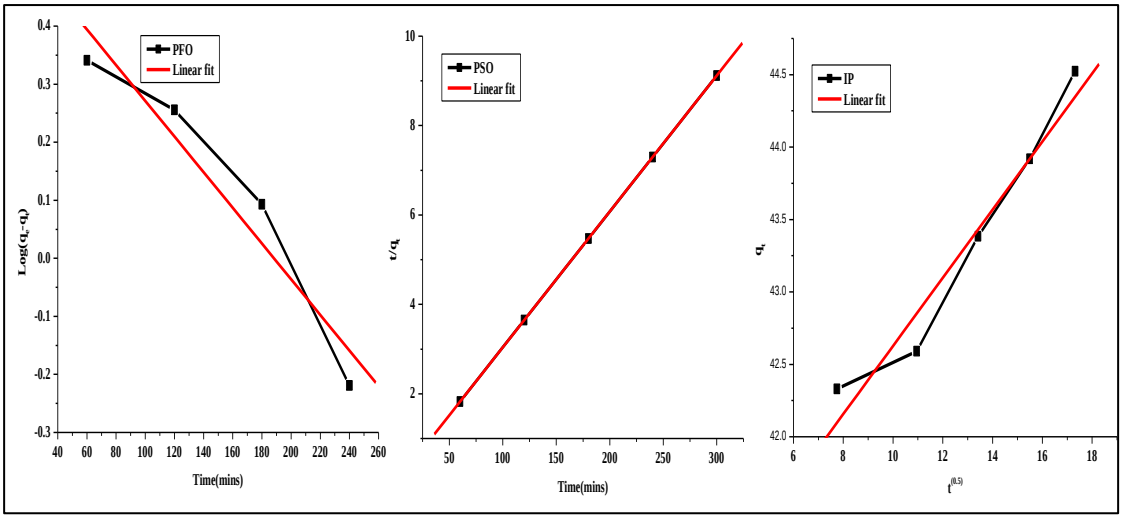

Operating parameters: 180 rpm, 100 ppm of dye, 0.05g adsorbent, time 300 min, temp 30^0C, optimum pH

Figure 4.27 b. Linear fit of Kinetics for RB and RH in (RB+RH) onto NC

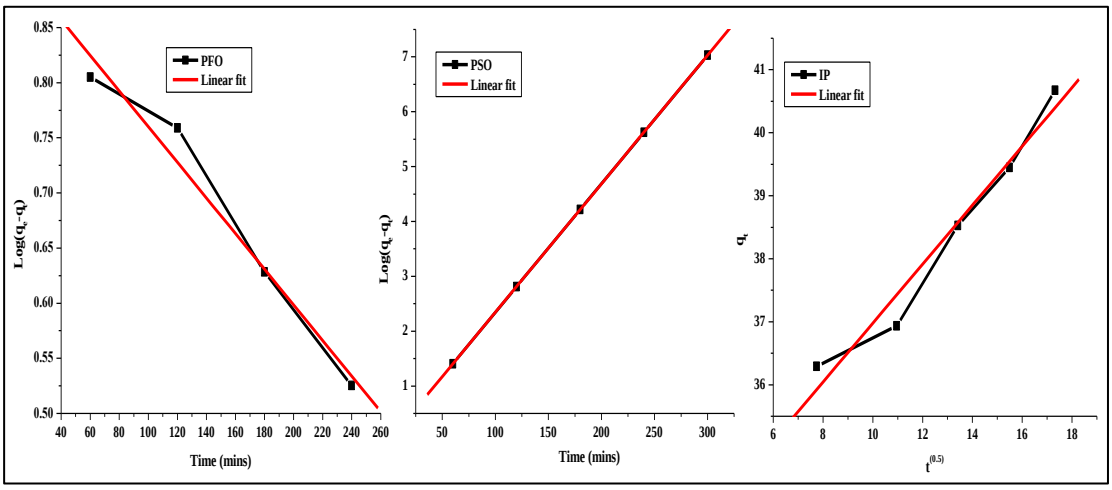

Operating parameters: 180 rpm, 100 ppm of dye, 0.05g adsorbent, time 300 min, temp 30^0C, optimum pH

Figure 4.27 c. Linear fit of Kinetics for RR and RH in (RR+RH) onto NC

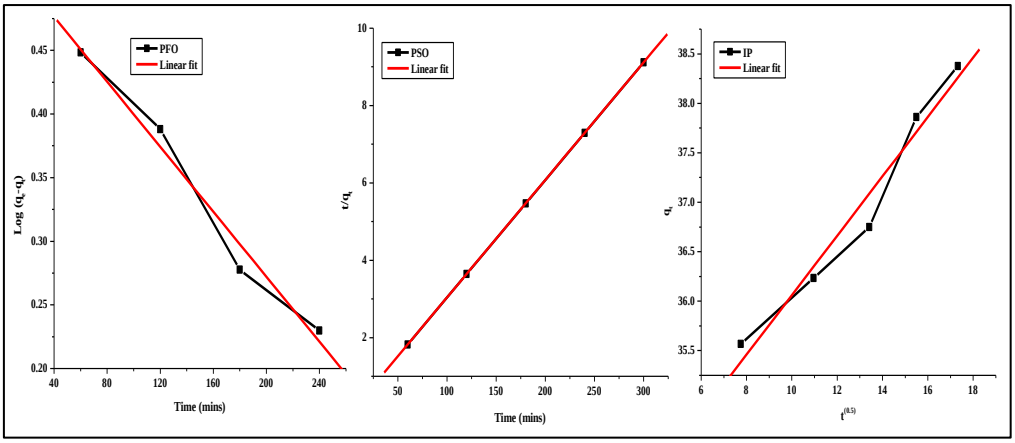

Operating parameters: 180 rpm, 100 ppm of dye, 0.05g adsorbent, time 300min, temp 30^0C, optimum pH

Figure 4.28 a. Linear fit of Kinetics for RB and RR in (RB+RR) onto CC

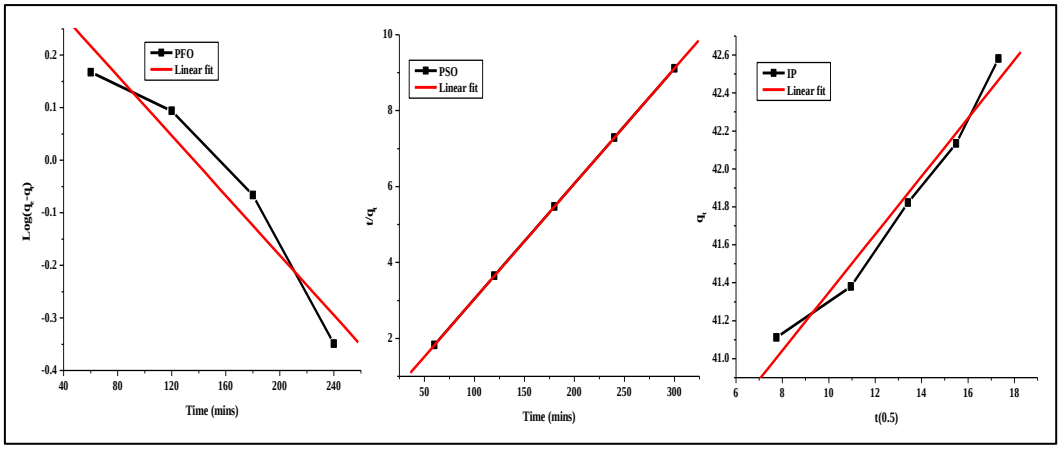

Operating parameters: 180 rpm, 100 ppm of dye, 0.05g adsorbent, time 300 min, temp 30^0C, optimum pH

Figure 4.28 b. Linear fit of Kinetics for RB and RH in (RB+RH) onto CC

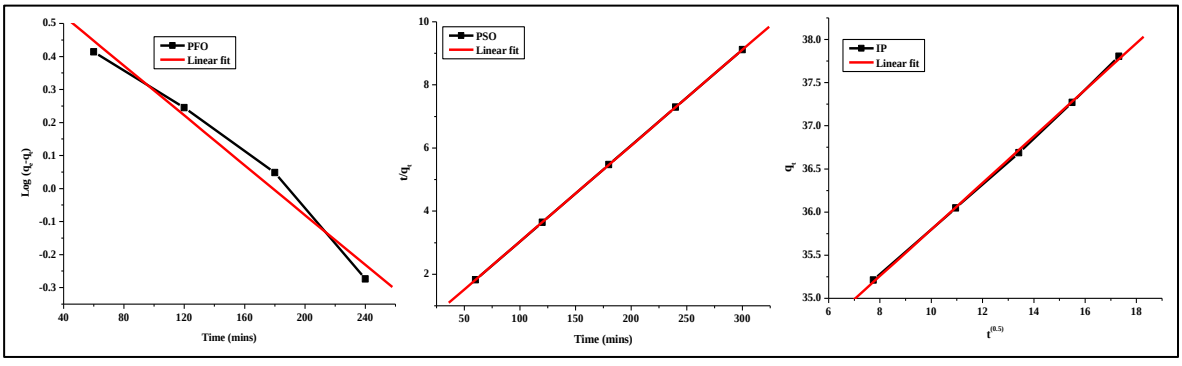

Operating parameters: 180 rpm, 100 ppm of dye, 0.05g adsorbent, time 300 min, temp 30^0C, optimum pH

Figure 4.28 c Linear fit of Kinetics for RR and RH in (RR+RH) onto CC

Table 4.10 Kinetics for binary mixture of dyes

Kinetics	**C**			**NC**			**CC**		
	RB+RR	RB+RH	RR+RH	RB+RR	RB+RH	RR+RH	RB+RR	RB+RH	RR+RH
	Pseudo first order								
q_e (exp)	38.96	43.74	42.67	47.51	44.52	42.86	42.73	42.58	37.80
q_e	4.623	2.559	8.512	4.278	3.787	8.512	3.2973	3.0387	1.669
K_1	0.028	9E-03	5E-03	0.073	7.07E-03	5E-03	8E-04	5E-03	2E-03
r^2	0.994	0.988	0.998	0.962	0.963	0.998	0.957	0.988	0.947
SD	0.076	0.037	0.104	0.086	0.081	0.104	0.009	0.037	0.034
	Pseudo second order								
q_e	35.8s71	36.21	42.72	38.971	32.93	42.70	32.90	33.87	32.90
K_2	0.023	0.012	0.036	1.01E+08	1.10E+11	7.81E+07	6E-03	1E+11	1E+08
r^2	1	1	1	1	1	1	1	1	1
SD	0.098	0.024	0.045	3.16E-10	3.16E-10	3.16E-10	3.16E-10	3.16E-10	3.16E-10
Intraparticle diffusion									
K_{ip}	0.321	0.990	0.578	0.335	0.235	0.57873	0.488	0.990	0.037
r^2	0.996	0.983	0.988	0.992	0.973	0.98806	0.983	0.983	0.988
SD	0.176	0.110	0.018	0.186	0.240	0.0189	0.396	0.110	0.018

4.2.9. Conclusion

Chitosan-Organically modified Nanoclay (Cloisite 30B) nano biocomposite was found to have good adsorption potential for removal of cationic xanthene dye and Reactive dyes RB-21 and RR-141from water. The X-ray diffraction pattern shows that the nanocomposite has intercalation and exfoliation in the structure. The adsorbents were found to be unique due to their optical properties, such as large fluorescence due to of molecular aggregation. The nanoclay chitosan composites with enhanced hydrophobicity due to organically modified clay and further modified by Rh6G, could have potential use as coloring additives.

The Freundlich constant, n was less than unity implied that the adsorption intensity was favourable over the entire range of concentrations studied for all the adsorbents. The positive values of ΔG for Rh-6G indicated the non-spontaneous nature of adsorption. The negative values of ΔG for RB-21 and RR-141 and low ΔH values indicate the spontaneous nature and temperature independent behaviour of adsorption. The adsorption kinetics data fitted well with the pseudo-second-order kinetic model. Chitosan clay nanocomposite showed higher adsorption capacity than most of the earlier reported adsorbents, reflecting a promising future for the utilization of the nanocomposite as an adsorbent for removal of dyes from aqueous solution.

The qm values for binary system was very less on comparison with single component system which clearly indicated that one of the dye from the mixture is adsorbed to a greater extent which is because of the availability of large number active sites utilized by the first dye of the mixture . Also the kinetic study indicates the fitness to Pseudo second order model for binary systems.

Synthesis, Characterization and Adsorption of individual and binary mixture of dyes on to Hydrotalcite and Chitosan-hydrotalcite composite

4.3 Introduction

Anionic clays have been identified as potential adsorbents due to their large surface areas, anion exchange capacities, low cost and non-toxicity [80]. The term ‘‘anionic clays’’ is used to designate Layered double hydroxides (LDHs)]. LDHs comprise a class of layered materials with positively charged layers and charge balancing anions in the interlayer regions [81]. LDH is generally expressed by the formula $M(II)_{1-x}\ M(III)_x\ (OH)_2\ (A^{n-})_{x/n}\ x\ yH_2O$, where M(II) and M(III) are divalent and trivalent cation, A= interlayer anion, n is the inter layer charge and x and y are fraction constants. Hydrotalcite [HT] is the most widely used layered double hydroxide with the formula $Mg_6Al_2(OH)_{16}(CO_3).4H_2O$]. The interlayer anions in LDHs and HT can be easily exchanged by other simple anions as well as complex bio molecules and dyes [82, 83]. The presence of these highly exchangeable interlayer anions and the bronsted basicity of the layer surfaces has resulted in the use of LDHs in wide range of applications such as catalysis, ion exchange, molecular stabilization, separation, membrane technology and controlled release of anions.

Nowadays, LDHs have become the focus of research in removing dyes from aqueous solutions. Mg–Fe-LDH [84] was used as an adsorbent of congo red and $NiFeCO_3$ hydrotalcites [85] were used for removal of Evans blue while calcined Mg–Al LDHs [86] were used for removal of acid orange from aqueous solutions. And there are few studies on the comparison of removing different red dyes from aqueous solutions by Mg–Al- LDH. In a separate study, the feasibility of using Mg–Al-LDH [87] as adsorbent for red dyes (RR, CR and AR1) was examined. The adsorbent property of the HT surface can be modified through the exchange of inorganic interlayered anions for organic anions to form an organocomposite [88, 89]. The hydrophilic hydrotalcites can be made hydrophobic by intercalating anionic surfactants like dodecylsulfate (DS) and dodecylbenzenesulfonate (DSB), which also increases the interlamellar space. This hydrophobic nature and accessibility of the interlayer region of organocomposites make these materials potential adsorbents for non-ionic organic pollutants [90-93]. However, reports on the removal of cationic pollutants, by LDH, from aqueous solutions are little reported in the literature [88].

Due to their anionic exchange capacity, HT are suitable for sorption of anionic species, but are not applicable for positively charged ones. The synthesis of surfactant-intercalated layered double hydroxides reported in the literature led to the sorption of many types of organic molecules including basic dye safranine [94-99, 88].

Natryasamy Viswanathan and Meenakshi had investigated the adsorption of fluoride onto Chitosan hydrotalcite [100]. Although the adsorption of anionic dyes onto LDHs is well known [101-103], very few studies have focused on the uptake of reactive dyes onto hydrotalcite [104,105]. Our aim in this study was to establish the potential of HT (Hydrotalcite) and CHT (Chitosan-hydrotalcite) composite to remove individual and binary mixture of Reactive and Xanthene dyes.

4.3.1 Materials and methods

Hydrotalcite (HT) was a gift sample from Heubach Colour Private Limited, Ankleshwar, Gujarat, India. The characteristics of Hydrotalcite are shown in Table. 1.

4.3.2 Synthesis of Chitosan-hydrotalcite composite

0.25 g hydrotalcite was added to 1% Chitosan solution in 1% acetic acid. The dispersion was maintained on stirring condition at for 12 h. The obtained composite was then filtered and washed with deionized water which is then dried at 60°C for 12 h.

4.4. Results and Discussion

4.4.1 FT-IR spectroscopy

Figure 4.2.9 shows the IR spectra of Hydrotalcite (HT) and the dye loaded adsorbents (HT-RB, HT-RR and HT-RH). Figure 4.30 shows the IR spectra of Hydrotalcite (CHT) and the dye loaded adsorbents (CHT-RB, CHT-RR and CHT-RH). Table 4.11and 4.12 shows the absorption frequencies and stretching frequencies for free and dye loaded adsorbents.

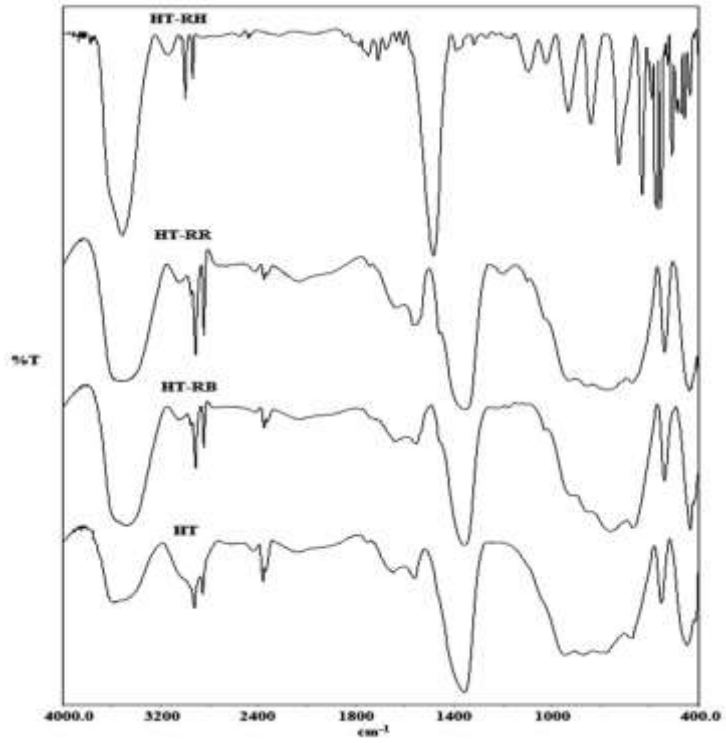

Figure 4.29 IR spectra of HT, HT-RB, HT-RR and HT-RH

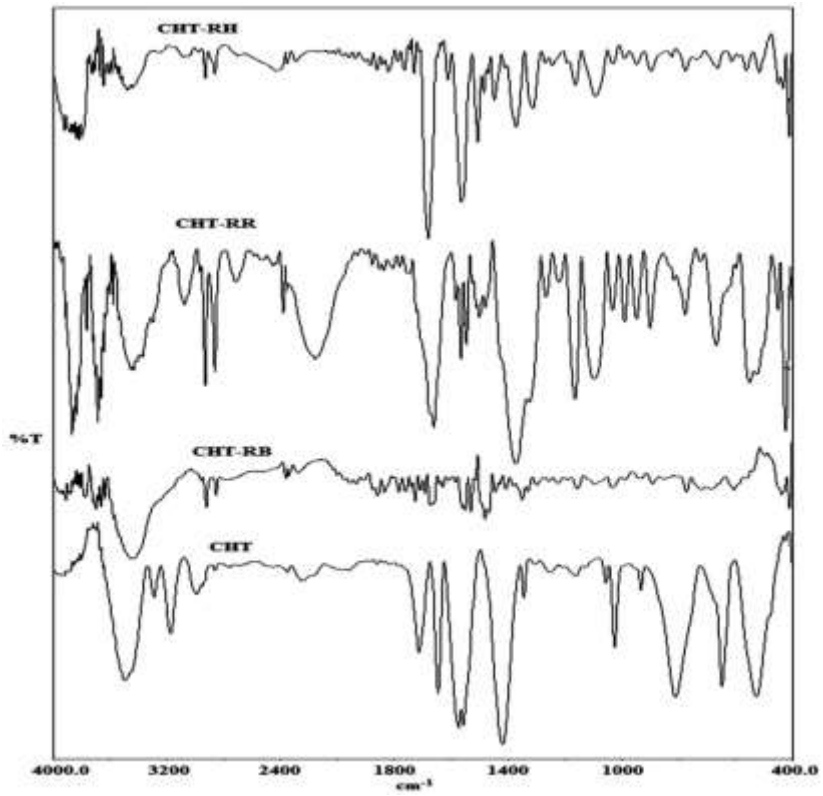

Figure 4.30 IR spectra of CHT, CHT-RB, CHT-RR and CHT-RH

The FTIR spectra of HT, HT-RB, HT-RR and HT-RH (Figure 4.39) show peaks at 3586, 3478 3513 and 3473 cm^{-1} respectively, which could be attributed to the presence of O-H stretching of hydroxyl group.

Similarly the peaks at for CHT, CHT-RB, CHT-RR and CHT-RH (Figure 4.40) at 3479, 3660, 3823 and 3787 cm^{-1} are attributed to the stretching modes of hydroxyl groups. Further, the hydroxyl stretching groups of HT and CHT were shifted after loading of dyes which clearly indicates the interaction of hydroxyl groups with the dye molecules. The peaks at 2900 - 3000 cm^{-1} are attributed to the hydrogen bonding with carbonate ions present in the inter layer space of adsorbents and the dye loaded adsorbents [106].

The peaks at 1654, 1656, 1652,1604 cm^{-1} can be attributed to the vibration of bending mode of interlamellar water molecules in HT, HT-RB, HT-RR and HT-RH respectively. These peaks are shifted to 1640, 1674, 1655 and 1676 cm^{-1} in the case of CHT, CHT-RB, CHT-RR and CHT-RH.

The bending mode of interlamellar carbonate ions has resulted in peaks at 1356, 1364 and 1358 cm^{-1} for HT, HT-RB and HT-RR. In the case of the composite the peaks of the bending mode of interlamellar carbonate ions have been shifted to a higher wave number 1413, 1480, 1368 and 1367 cm-1 for CHT, CHT-RB, CHT-RR and CHT-RH respectively. The peaks below 1000 cm^{-1} corresponded to Al-OH stretching absorption. The metal-oxygen

peak at 872 cm-1 in HT was found to be shifted to 772, 771, 773 cm^{-1} due to the interaction of hydrotalcite with dye molecules while in the case of CHT the metal –oxygen peak at 803 cm-1 was shifted to 893,896 and 892 after loading of dye molecules. The band at ~ 449 cm^{-1} in HT, HT-RB and 452 cm^{-1} in HT-RR and 448 cm^{-1} in HT-RH was assigned to the superposition of the characteristic stretching bands of magnesium and aluminum oxide [96].

Table. 4.11. IR stretching frequencies of Infrared spectra for Hydrotalcite and dye loaded hydrotalcite

HT	**HT-RB**	**HT-RR**	**HT-RH**	**Inference**
3586	3478	3513	3472,3072	stretching modes of hydroxyl groups
2920,2855,2360	2917,2850	2917,2850	2918,2850	H2O carbonate bridging mode / C-H stretching frequencies in dye loaded samples
1654	1656	1652	1604	Bending mode of water molecules
1558	1559	1558	1574,1500	Asymmetric stretching absorption Of the C=O group.
1356	1364	1358	1126,1187	Symmetric bending absorption of the C=O group.
872	772	771	,773,672	Metal – Oxygen stretching mode
553	552	552	551	stretching bands of Aluminum oxide
449	449	452	448,367,318,295228	stretching bands of magnesium and aluminum oxide

Table. 12. IR stretching frequencies of Infrared spectra for Chitosan-Hydrotalcite nanocomposite and dye loaded CHT

CHT	CHT-RB	CHT-RR	CHT-RH	Inference
3479,3280,3162	3660,3435	3823,3676,3424,3064	3787,3070	stretching modes of hydroxyl groups
2979,2847	2919	2918,2850,2714,2444,23712148	2918,2408	H_2O carbonate bridging mode /C-H stretching frequencies in dye loaded samples
1413,1338	1480, 1349	1368	1444,1367	bending mode of interlamellar carbonate
928,807	893	896	892	stretching bands of Aluminum oxide
643,543	773,606	773,663,546,447	772,658	stretching bands of magnesium and aluminum oxide

4.4.2 SEM Micrographs

The scanning electron micrographs of HT and the dye adsorbed HT are shown in Figure 4.31. The SEM image of HT shows the clear plate like morphology of typical layered double hydroxides. The particles are of irregular size ranging from a few to tens of microns. The SEM image of CHT shows a fibrous morphology which might be due to the intercalation of chitosan into the layered structure of hydrotalcite.

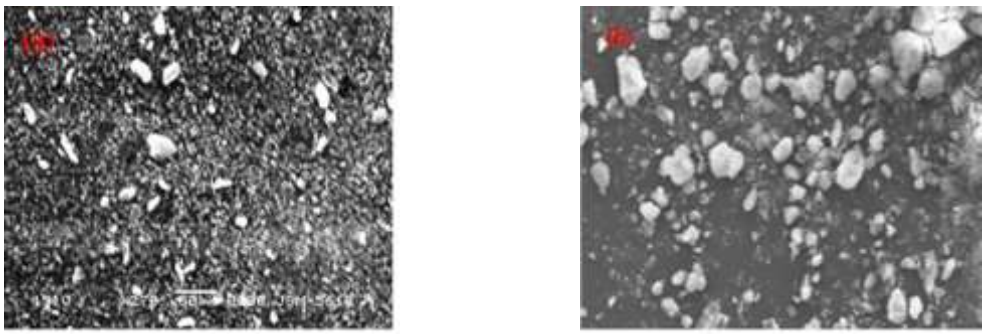

Figure 4.31SEM images of a) HT and b) CHT

4.4.3 X-Ray diffraction studies

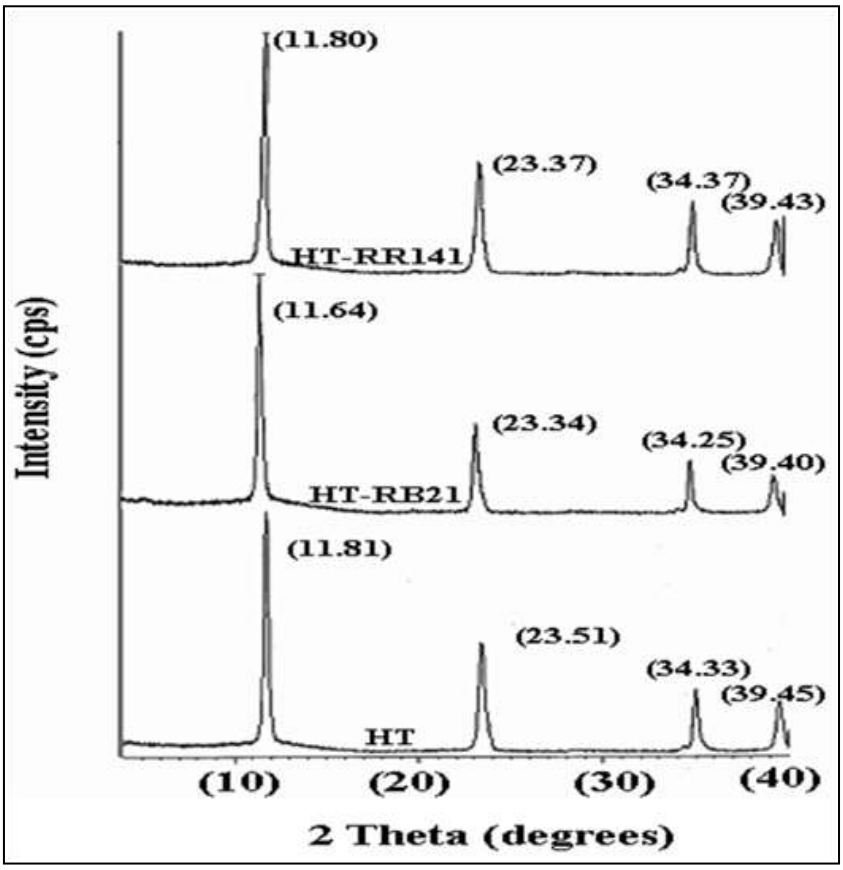

Figure 4.32 XRD spectra of HT, HT-RB21 and HT-RR141

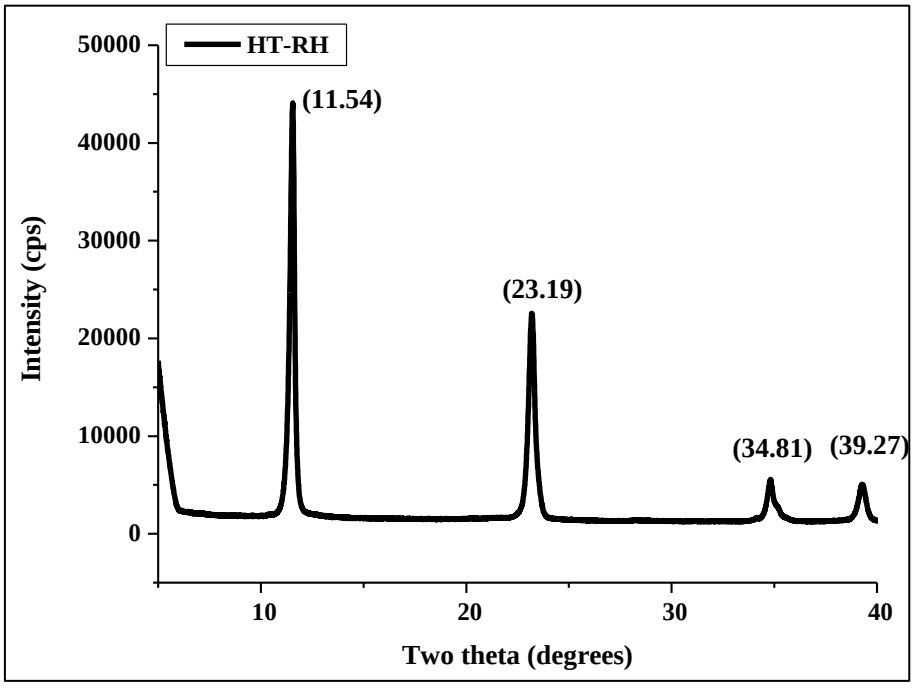

Figure 4.33 XRD spectra of HT-RH

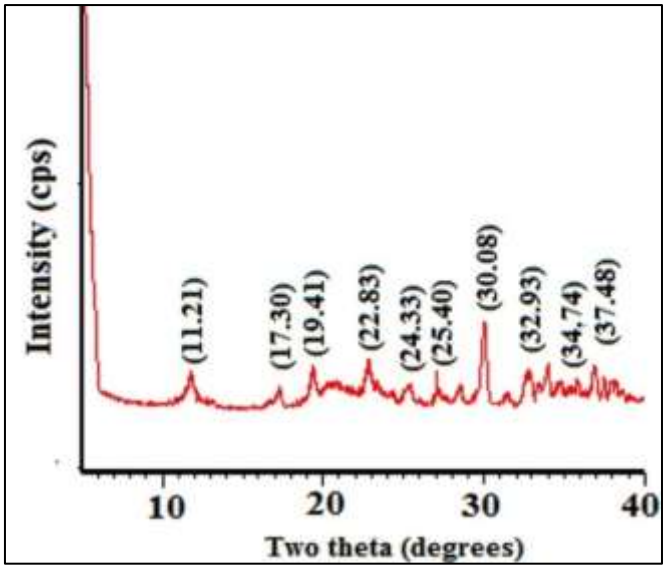

Figure 4.34 XRD spectra of CHT

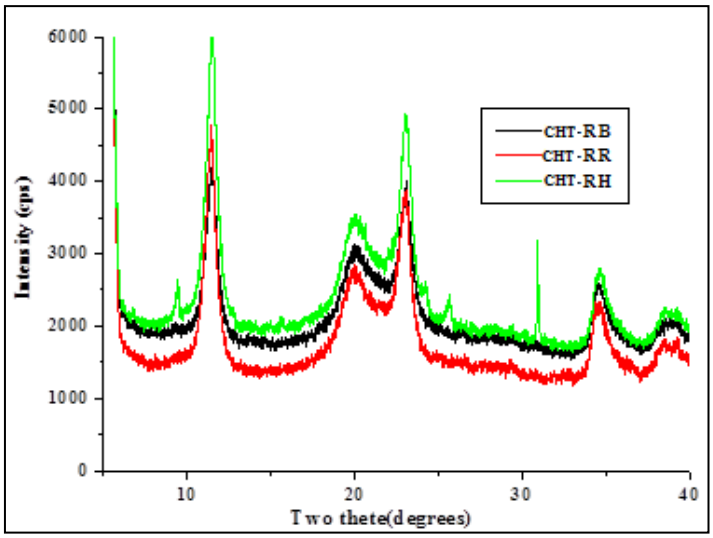

Figure 4.35 XRD spectra of CHT-RB, CHT-RR and CHT-RH

The powder XRD of hydrotalcite (HT), Chitosan hydrotalcite composite (CHT) and dye loaded adsorbents (HT-RB, HT-RR) are shown in Figure. 4.32 (HT-RH) figure 3.33, CHT (figure 3.34,) CHT-RB, CHT-RR and CHT-RH (figure 4.35). It was observed that the diffraction pattern of hydrotalcite has characteristic sharp and symmetric peaks at 2θ values of 11.8° (003), 23.5° (006) and 34.3° (009). In the case of HT-RB21 it was observed that the reflections were shifted to lower angles indicating the expansion of layers due to reconstruction of the layered structure after RB-21 adsorption. However, HT-RR 141 gave a basal spacing of 7.49 Å similar to that of HT, which could be due to the affinity of dye ion towards HT being lesser than that of carbonate, rendering the ion-exchange of RB-141 for

carbonate in the HT interlayer difficult. We thus presume that the uptake of RB-141 by HT mainly occurs by physisorption. In the case of CHT there are new peaks at 2θ - 17.30, 19.14, 24.33 and 25.04^0 which might be due to the interaction of chitosan with hydrotalcite. Further in CHT-RB and CHT-RR there was negligible change in 2θ values suggesting that the dyes were adsorbed onto CHT without affecting the structure of CHT. In the case of CHT-RH a new peak at 9.43^0 was observed which might be due to intercalation of rhodamine moiety within CHT leading to reformation of the structure of CHT

4.4.4 Zeta potential analysis

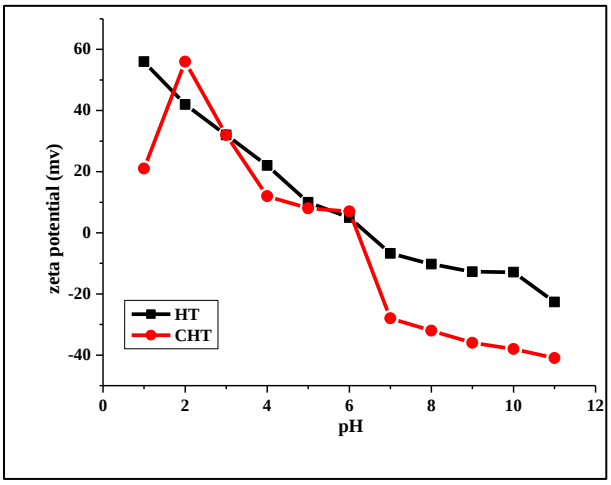

Figure 4.36 Zeta potential of HT and CHT

Figure 4.36 shows the surface charge distribution of HT and CHT where it is highly positive (~58 mV) at acidic pH and highly negative (~42 mV) at basic pH. The isoelectric point for HT and CHT was pH 6.

4.3.5 Thermogravimetric analysis

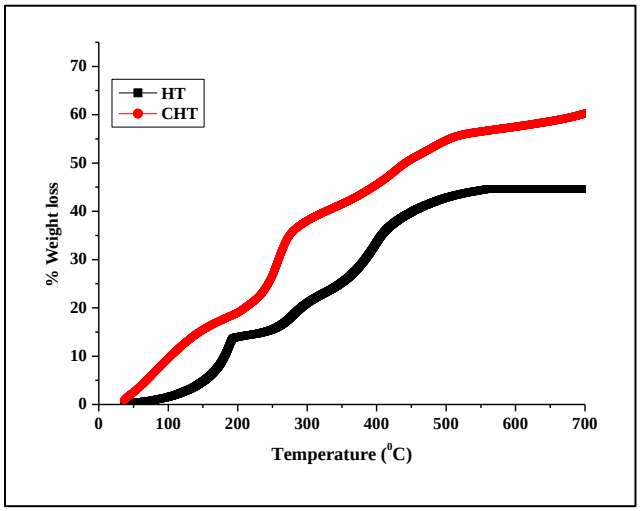

Figure.4.35 Thermogravimetric analysis of HT and CHT

Figure 4.35 shows the thermogravimetric analysis of HT and CHT. The weight loss from 500C–200^{0}C is due to the loss of physically bonded water. The weight loss in C from 250^0-350^0 is attributed to degradation and deacetylation of Chitosan. The weight loss from 300^0 – 450^0 in HT and CHT can be attributed to the decomposition of organic material.

4.3.6 Dye adsorption studies of single component dye systems

Effect of pH

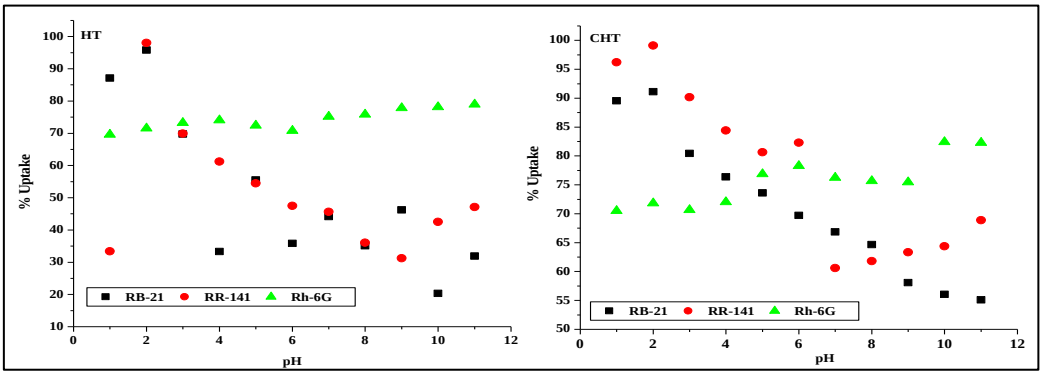

Operating parameters: 180 rpm, 100 ppm of dye, 0.05 g adsorbent, time 300 min

Figure 4.36 Effect of pH on % uptake of RB-21, RR-141 and RH-6G onto HT and CHT

The effect of initial pH on the adsorption of RB-21, RR-141, Rh-6G onto HT and CHT was investigated by varying the pH of solution from 1 to 11 using 0.1N NaOH/HCl. The maximum removal was found to be at pH 2 for RB- 21, RR-141and pH 10 for Rh6G. The high amount of dye adsorbed by HT at as low a pH as 2 could be explained by two mechanisms:

One mechanism could be the acidic condition favoring displacement of interlayer carbonate, which facilitates the penetration of anionic dyes into the interlayer spaces according to reaction.

$$[Mg_3Al\ (OH)_8]_2CO_3.x\ H_2O + 2\ Dye^- \rightarrow [Mg_3Al(OH)_8]_2\ 2Dye^-.xH_2O + CO_3^{2-}$$

Another mechanism may be attraction by electrostatic forces between the protonated surface of hydrotalcite and the negatively charge anionic dyes [96].

$$HT_{sur}\text{-}OH_2^+ + Dye^- \rightarrow HT_{Sur}\text{-}OH_2^+ \text{---} Dye^-$$

As the pH of the solution increased above 2.0, the efficiency of HT for removal of dyes decreased. As the pH increases, the positive charge on the surface of HT decreases and displacement of carbonate also becomes difficult which could have resulted in decrease in the dye removal efficiency. At pH values above the zpc value the adsorbent surface becomes

negatively charged due to deprotonation resulting in lesser uptake of anionic dyes but increase in uptake of cationic dye. Furthermore, the anionic dyes compete with the OH^- ions in the solution for exchange with the CO_3^{2-} ions that are associated with the surface or interlayers of HT.

Effect of temperature

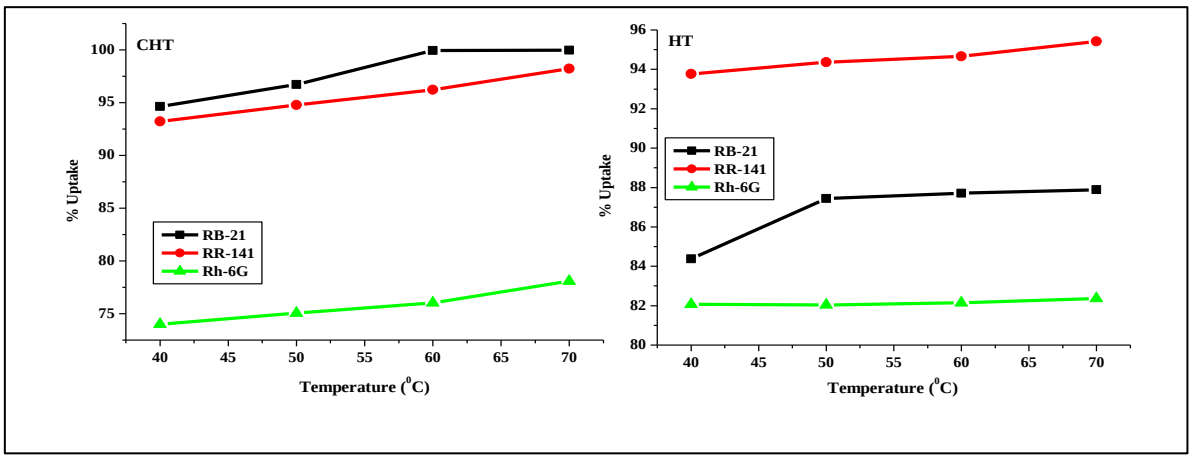

Operating parameters: 180 rpm,100 ppm of dye, 0.05 g adsorbent, time 300 min

Figure 4.37 Effect of temperature on % uptake of RB-21, RR-141 and RH-6G onto HT and CHT

Figure 4.37 show the effect of adsorption of RR-141 and RB-21 as a function of temperature. The removal of RB21 and RR141 onto CHT was found to a weak endothermic process. In all the other cases there was not much of change in uptake of dyes with respect to temperature.

Effect of adsorbent dose

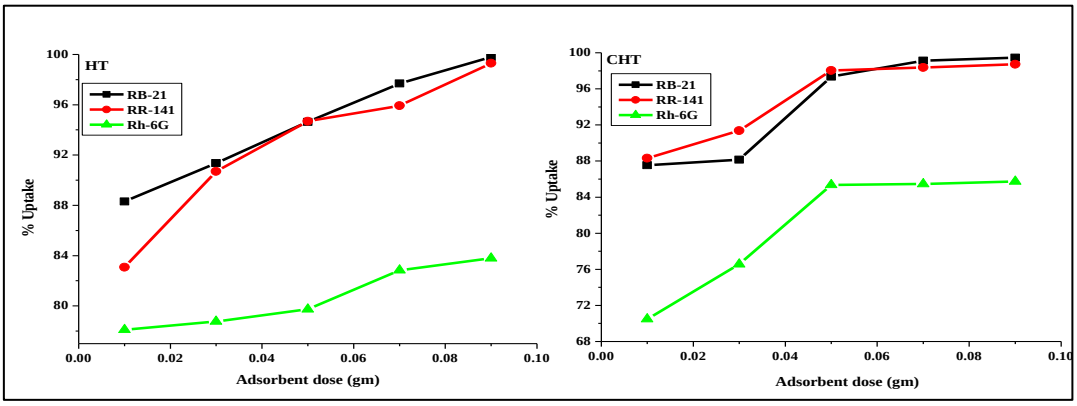

Operating parameters: 180 rpm,100-1000 ppm of dye, 0.05 g adsorbent, time 300 min

Figure 4.38 Effect of adsorbent dose on % uptake of RB-21, RR-141 and RH-6G onto HT and CHT

Figure 4.38 shows the effect of amount of HT on the removal of RR-141 and RB-21. The study was done by varying the amount of HT from 0.01 to 0.15 g in 25mL of solutions containing 100 ppm of dye while maintaining other parameters constant. It was observed that the percentage removal increased when the adsorbent dose was increased from 0.01 to 0.1 g for both HT and CHT. This indicates larger availability of active sites for the same number of adsorbate molecules.

Effect of concentration

The effect of variation in concentration of dyes on the adsorption potential of HT and CHT was investigated and is shown in Figure. 4.39. It was found that the percentage uptake decreases with increase in concentration of the dyes which could be due to the limited availability of adsorption sites and thus saturation of sorption sites by the dyes at high concentrations.

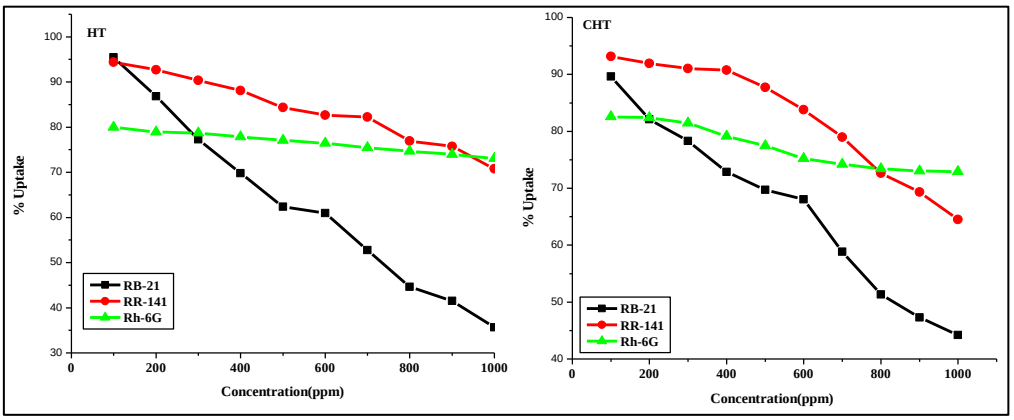

Operating parameters: 180 rpm, 100-1000 ppm of dye, 0.05 g adsorbent, time 300 min

Figure 4.39 Effect of concentration on % uptake of RB-21, RR-141 and RH-6G onto HT and CHT

Sorption isotherm

The isotherm models Freundlich, Langmuir, Temkin, and Halsey models were studied a isotherm constants for the sorption of RB-2, RR-141 and RH-6G by HT and CHT are presented in Table 13. The low SD values obtained for the Langmuir model implies that the adsorption of dyes onto HT and CHT follows the Langmuir model. The experimental data also showed a good fit to Freundlich model. The magnitude of n indicates a measure of favourability of adsorption. A value of $n < 1$ indicates favourable adsorption intensity over the entire range of concentration studied while $n > 1$ indicates favorable adsorption intensity at high concentrations but much less at lower concentration [97]. In the present study, the value of n for RR-141onto HT, RB-21onto CHT and Rh-6G onto CHT was less than 1 implying a favourable adsorption process over the entire range of concentration while for

RB-21, Rh6G onto HT and RR-141 onto CHT the value of n was greater than 1 indicating that favorable adsorption at high concentrations. The high adsorption capacity of HT and CHT reflects a promising future for the utilization of HT and CHT in the removal of dyes from aqueous solution. The Temkin isotherm assumes that the adsorption energy of all the molecules in the layer decreases linearly rather than logarithmically with coverage, due to adsorbent–adsorbate interactions and that the adsorption is characterized by a uniform distribution of the binding energies, up to some maximum energy. On comparison of Temkin model with the Langmuir and Freundlich isotherm models, it was observed that the Temkin isotherm model did not fit well with the experimental data. However, as seen from Table. 13 the high K_T value for CHT suggests strong interaction between the dye and the adsorbent surface. The high linear regression values of Halsey model suggests the adsorption to be favourable. Figures 4.40 (a, b& c) and 4.41 (a, b& c) shows the linear fit for isotherm of RB, RR and RH onto HT and CHT.

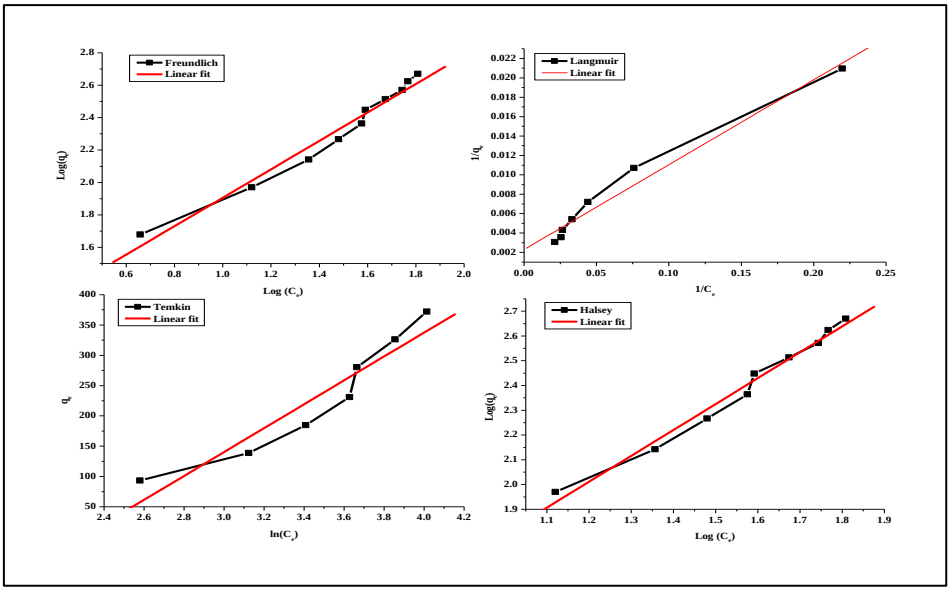

Operating parameters: 180 rpm,100-1000 ppm of dye, 0.05g adsorbent, time 300min, temperature 30^0C, optimum pH

Figure 4.40 a. Linear fit of isotherm for RB onto HT

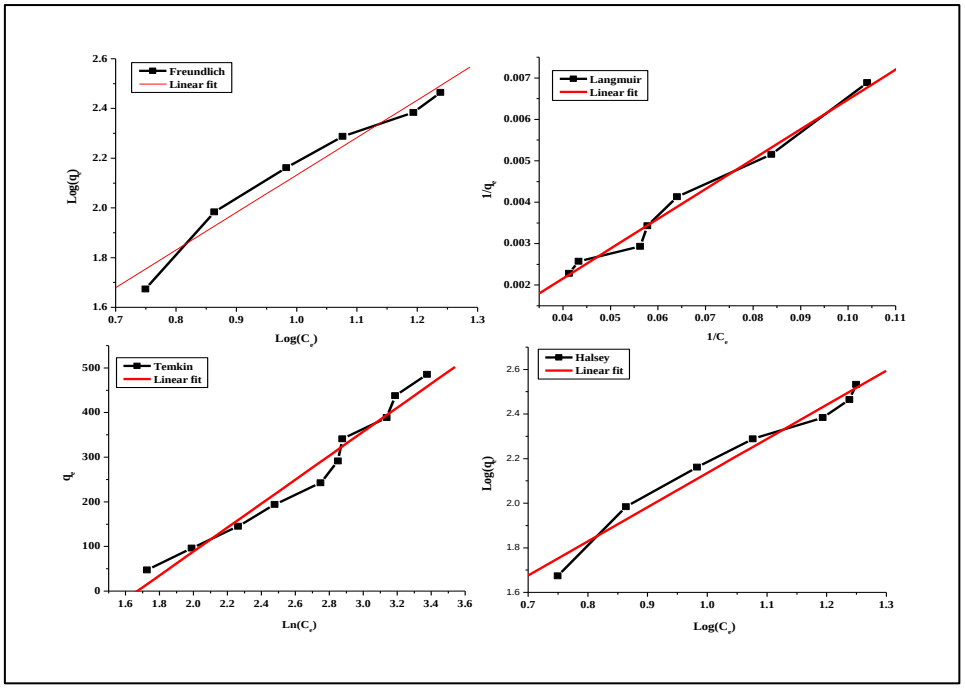

Operating parameters: 180 rpm, 100-1000 ppm of dye, 0.05g adsorbent, time 300 min, temperature 30^0C, optimum pH

Figure 4.40 b. Linear fit of isotherm for RR onto HT

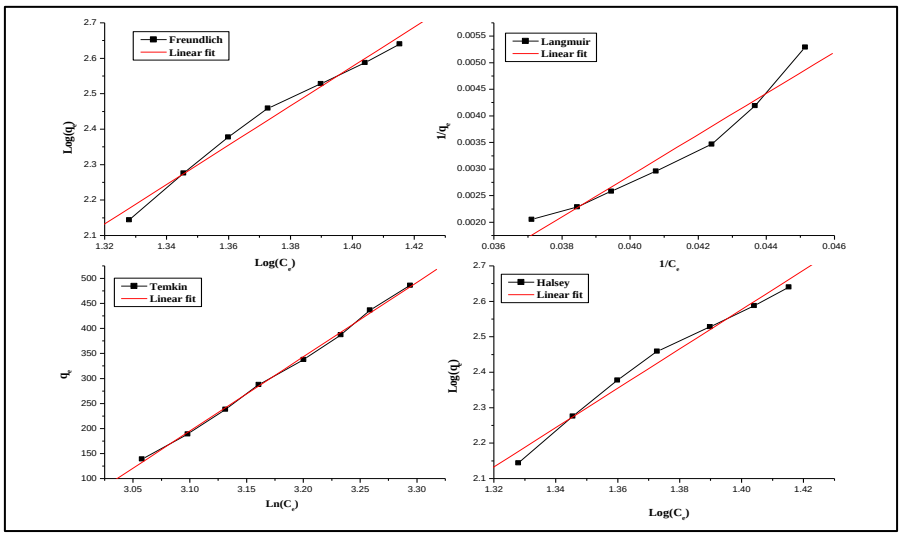

Operating parameters: 180 rpm, 100-1000 ppm of dye, 0.05 g adsorbent, time 300 min, temperature 30^0C, optimum pH

Figure 4.40 c. Linear fit of isotherm for RH onto HT

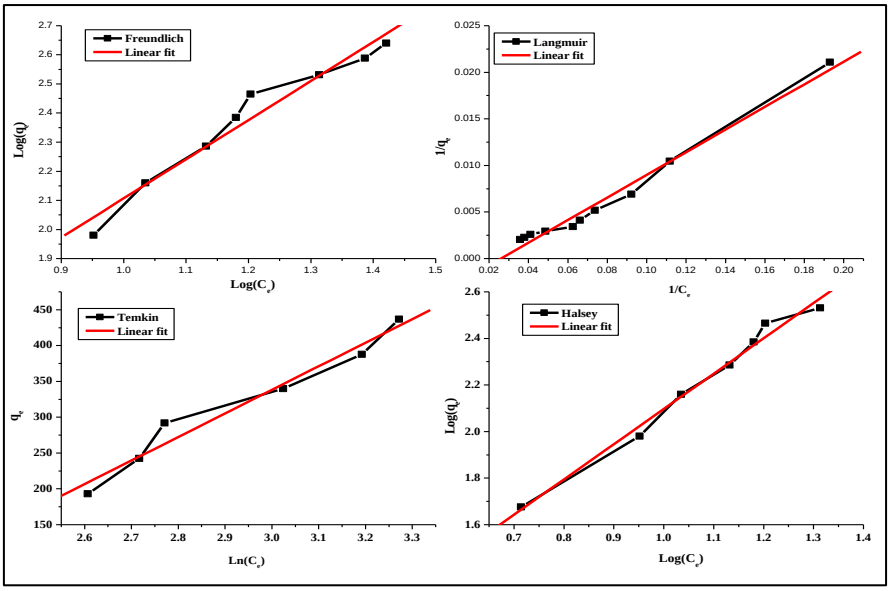

Operating parameters: 180 rpm, 100-1000 ppm of dye, 0.05 g adsorbent, time 300 min, temperature 30^0C, optimum pH

Figure 4.41 a. Linear fit of isotherm for RB onto CHT

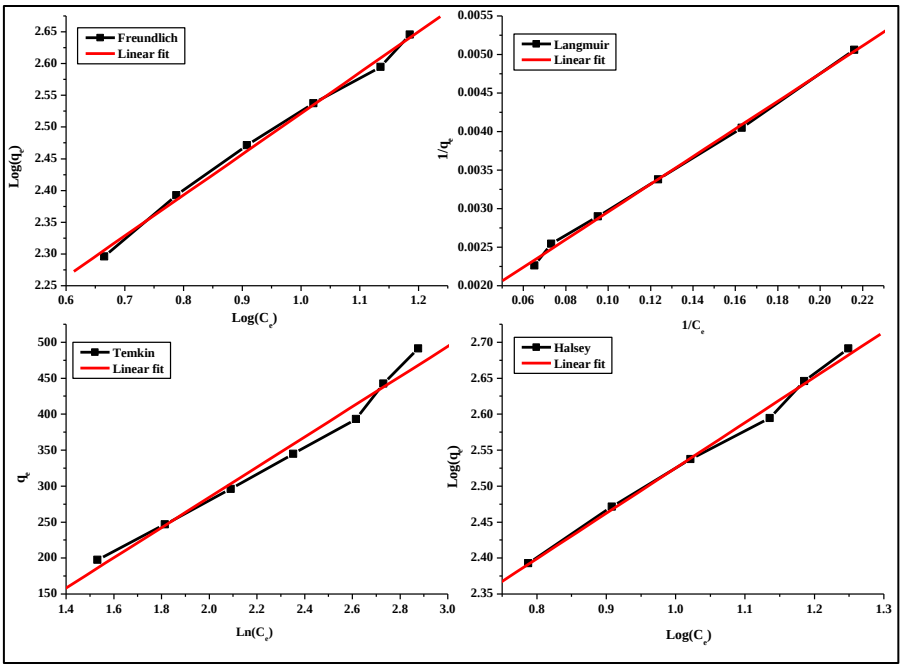

Operating parameters: 180 rpm, 100-1000 ppm of dye, 0.05 g adsorbent, time 300 min, temperature 30^0C, optimum pH

Figure 4.41 b. Linear fit of isotherm for RR onto CHT

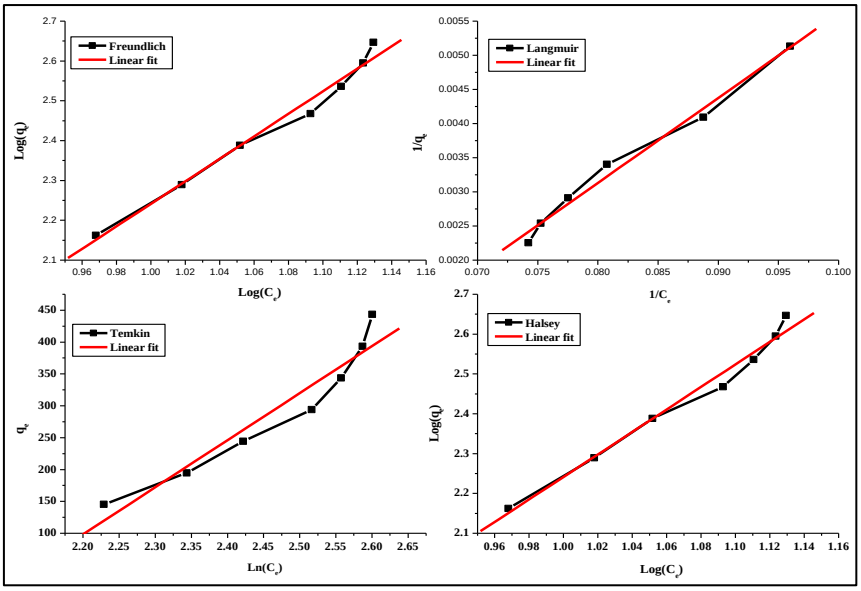

Operating parameters: 180 rpm, 100-1000 ppm of dye, 0.05 g adsorbent, time 300 min, temperature 30^0C, optimum pH

Figure 4.41 c Linear fit of isotherm for RH onto CHT

Table 4.13 Isotherm parameters

	HT			CHT		
	RB	**RR**	**RH**	**RB**	**RR**	**RH**
Freundlich						
q_e(exp) (mg.g^{-1})	**467.82**	**485.32**	**486.52**	**486.05**	**491.13**	**493.22**
$_{Kf}$(mg.g^{-1})	4.204	14.97	10.67	3.829	7.540	10.261
N	0.6625	1.361	1.139	0.660	1.557	0.354
R^2	0.980	0.994	0.986	0.992	0.997	0.990
SD	0.064	0.03	0.055	0.039	0.010	0.025
Langmuir						
q_m(mg.g^{-1})	412.35	436.66	429.30	415.457	462.06	446.84
K_L(L.mmol^{-1})	0.031	0.045	0.0325	0.0260	0.064	0.054
R^2	0.981	0.975	0.971	0.990	0.998	0.992
SD	0.0019	0.0108	2.98E-04	8.64E-04	5.61E-05	1.42E-04
Temkin						
β_T	197.167	268.45	484.53	328.726	209.93	738.13
K_T (L.mmol^{-1})	0.226	0.093	0.0513	0.139	0.5242	0.1266
R2	0.999	0.997	0.999	0.982	0.989	0.960
SD	3.169	4.8832	5.661	18.83	16.35	32.77
Halsey						
K_{FH}	0.110	0.025	1.068	2.596	0.333	4.846
n_{FH}	0.8936	1.3617	0.180	0.660	1.585	0.354
R2	0.9924	0.9895	0.990	0.992	0.996	0.990
SD	0.045	0.075	2.62E-02	0.039	0.0097	0.025

Sorption Kinetics

The kinetic models Pseudo First order, Pseudo Second order, Intraparticle diffusion, Bangham and Liquid film diffusion model were studied and the kinetic constants for the sorption of RB-21, RR-141 and RH-6G by HT and CHT are presented in Table 4.42.Fig. 4.43 (a, b& c) and 4.44 (a, b& c) shows the linear fit for kinetics of RB, RR and RH onto HT and CHT. Low SD values and high correlation coefficients were obtained for pseudo second order model suggesting that chemisorptions played an important role during the adsorption of both the dyes onto HT and CHT. The theoretical q_e values were closer to the experimental q_e values reinforcing the fact that pseudo second order model produces a better fit with the experimental data. The adsorption process of the dyes onto HT and CHT may involve the following steps: [98] (1) solute transfers to the sorbent particle surface (film or external diffusion); (2) transfer from the sorbent surface to the intraparticle active sites (intraparticle diffusion); and (3) retention on the active sites. The third step is very rapid and can be considered negligible, while either first or second steps may be the slowest step to be considered as the rate-limiting step for the sorption process [99]. The first and second steps can be modeled by the liquid film diffusion model and intraparticle diffusion model, respectively. The adsorption kinetic data were thus analyzed using the intraparticle diffusion model and liquid diffusion model to elucidate the adsorption mechanism. The plots of intraparticle diffusion and liquid film diffusion models have intercepts instead of starting from origin (not shown), suggesting that neither the film diffusion nor intra particle diffusion processes are the sole rate-limiting steps in the adsorption process. However, the low correlation coefficient for the liquid film diffusion model as compared to that of the intraparticle diffusion model suggested that intraparticle diffusion mainly controlled the adsorption process of dyes onto HT and CHT along with a significant contribution of film diffusion process. Also the linear coefficient values of the Bangham model suggests that the diffusion of dye molecules onto the pores of the adsorbent.

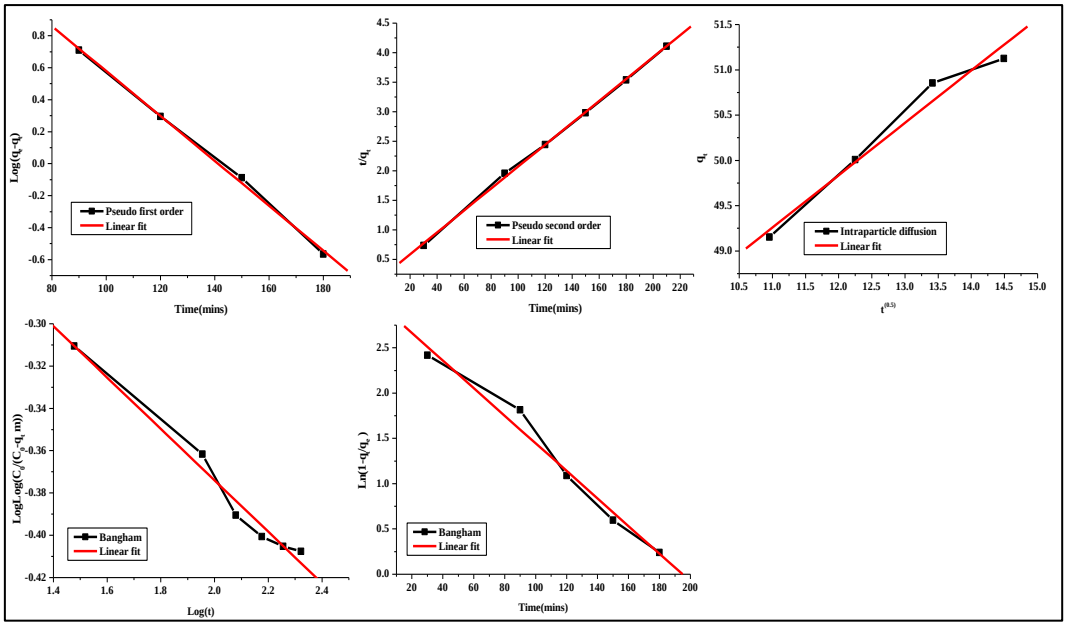

Operating parameters: 180 rpm,100 ppm of dye, 0.05 g adsorbent, time 300 min, temperature 30^0C, optimum pH

Figure 4.42 a Linear fit of Kinetics for RB onto HT

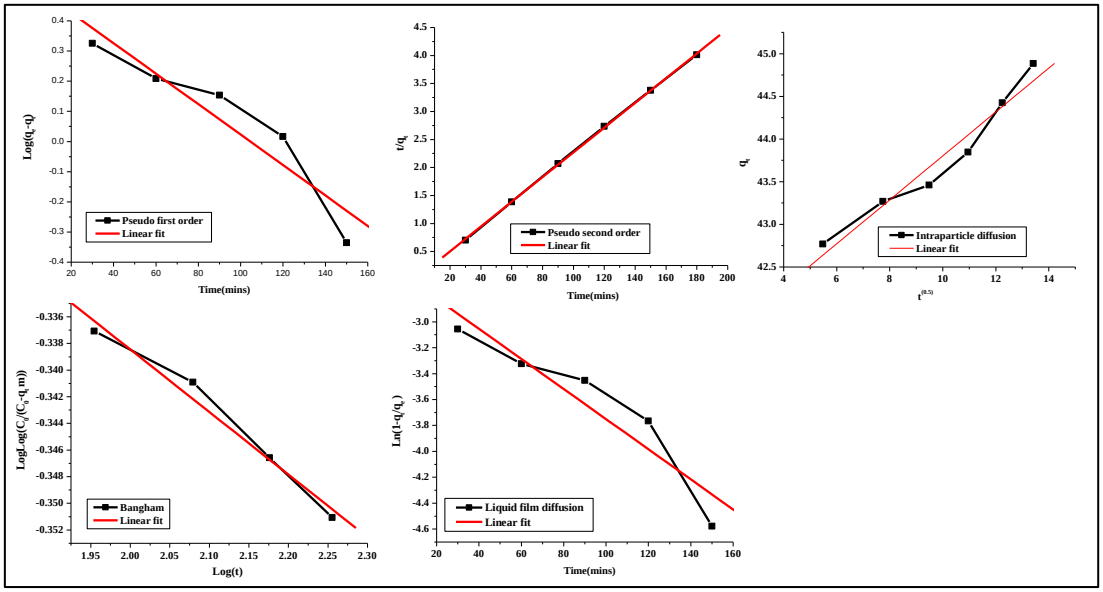

Operating parameters: 180 rpm, 100 ppm of dye, 0.05 g adsorbent, time 300 min, temperature 30^0C, optimum pH

Figure 4.42 b. Linear fit of Kinetics for RR onto HT

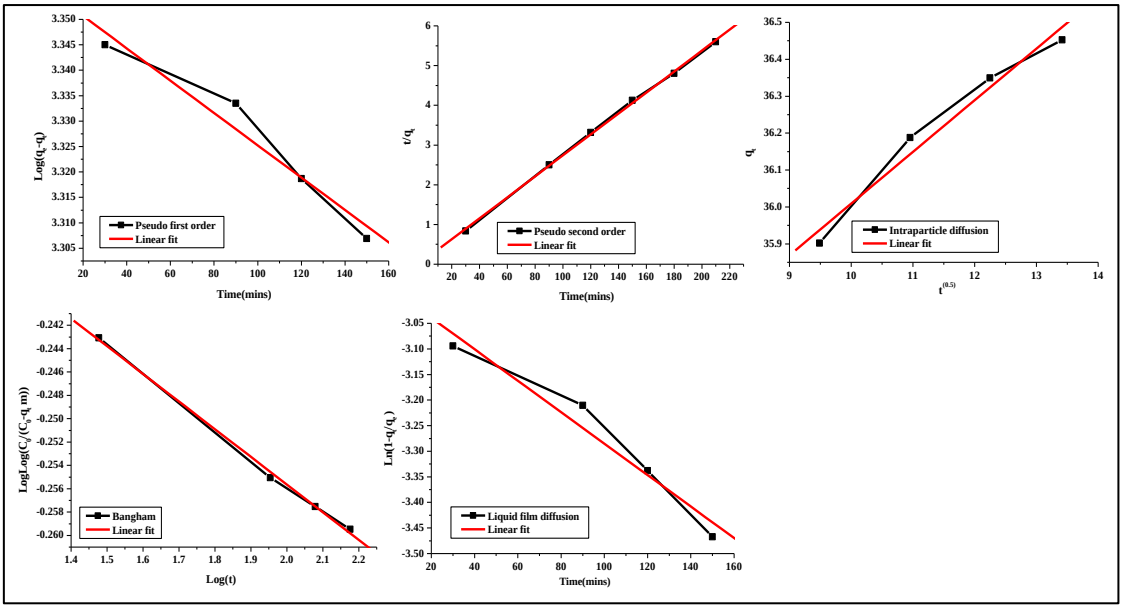

Operating parameters: 180 rpm, 100 ppm of dye, 0.05 g adsorbent, time 300 min, temperature 30^0C, optimum pH

Figure 4.42c Linear fit of Kinetics for RH onto HT

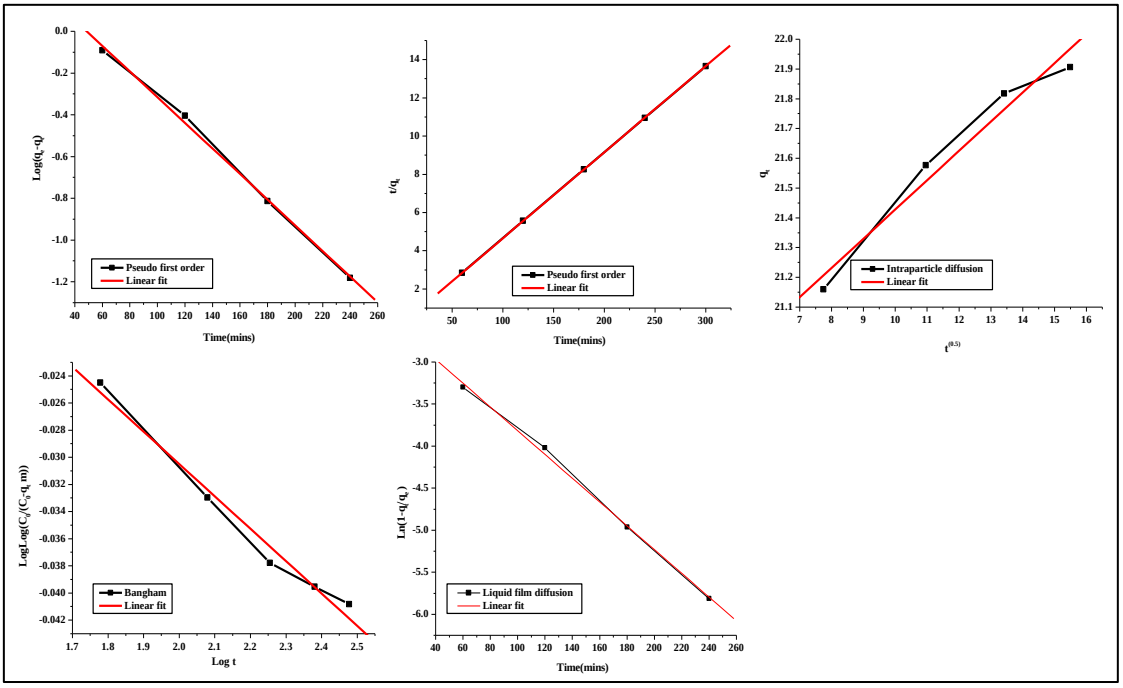

Operating parameters: 180 rpm, 100 ppm of dye, 0.05 g adsorbent, time 300 min, temperature 30^0C, optimum pH

Figure 4.43 a Linear fit of Kinetics for RB onto CHT

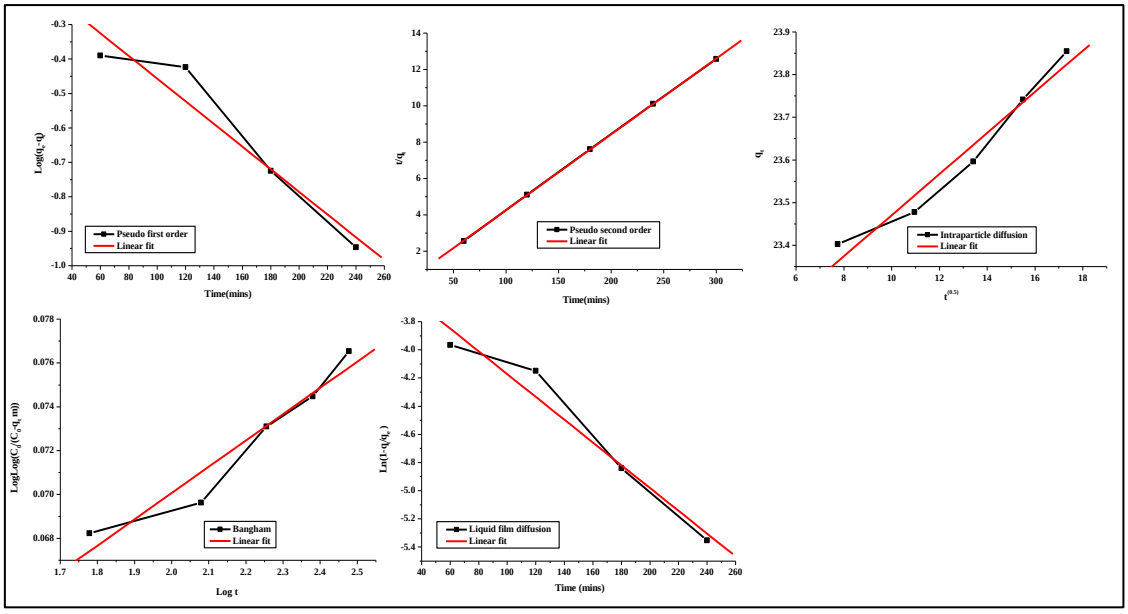

Operating parameters: 180 rpm, 100 ppm of dye, 0.05 g adsorbent, time 300 min, temperature 30^0C, optimum pH

Figure 4.43 b Linear fit of Kinetics for RR onto CHT

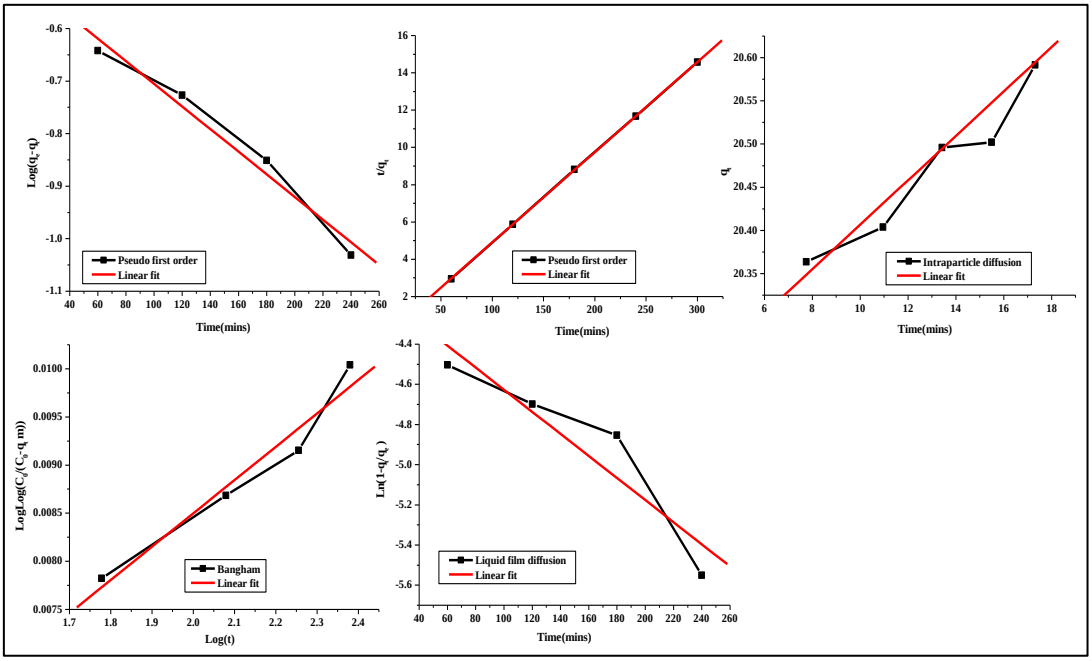

Operating parameters: 180 rpm, 100 ppm of dye, 0.05 g adsorbent, time 300 min, temperature 30^0C, optimum pH

Figure 4.43 c Linear fit of Kinetics for RH onto CHT

Table4.15 Kinetics

Kinetics	**HT**			**CHT**		
	RB	RR	RH	RB	RR	**RH**
Pseudo first order						
q_e (exp)	21.97	23.85	20.59	50.95	49.11	37.52
q_e(min^{-1}),	30.544	9.154	2.275	5.247	6.744	9.987
K_1	0.0066	0.032	0.0007	0.007	0.005	0.014
r^2	0.9790	0.998	0.976	0.977	0.964	0.998
SD	0.0253	0.0295	0.004	0.041	0.085	0.029
Pseudo second order						
q_e k_2(g/mgmin),	18.76	21.45	20.64	49.751	53.966	37.93
K_2	9.07E-01	$1.576*10^{-3}$	0.006	3.27E-05	0.0201	0.014
r^2	1	0.9951	0.999	0.994	0.999	1
SD	1.79E-04	0.0422	0.060	0.019	0.024	0.009
Intraparticle diffusion						
K_{ip}($mg.gmin^{-0.5}$)	1.4625	1.4278	0.1399	0.0257	0.048	0.098
r^2	0.988	0.9934	0.9850	0.984	0.979	0.981
SD	6.84E-01	0.5482	0.0507	0.019	0.043	0.077
Bangham						
K_m($mL.g^{-1}.L^{-1}$)	7.541	14.077	11.989	0.090	0.690	0.9920
A	0.121	0.046	0.023	0.003	0.011	0.023
r^2	0.989	0.989	0.998	0.976	0.965	0.990
SD	0.006	0.001	4.42E-04	2.45E-04	0.001	0.001
Liquid film diffusion						
K_{fd}	0.0075	0.0173	0.003	0.005	0.008	0.014
r^2	0.9884	0.9875	0.977	0.933	0.970	0.998
SD	0.0547	0.1311	0.041	0.199	0.159	0.067

Thermodynamic studies

The thermodynamic parameters (Table 4.16) which could throw more light on the nature of sorption process were determined from the experimental data obtained at various temperatures. Negative values of ΔG indicated that the adsorption process was favorable and spontaneous in nature. The positive value of enthalpy change (ΔH) confirmed the endothermic nature of the adsorption process. Positive values of ΔS suggested good affinity of the dye moeity toward the adsorbent and increased randomness at the solid-solution interface during the fixation of the dye molecule on the active site of the adsorbent.

Table 4.16 Thermodynamic parameters

Thermodynamic parameters					
ΔG(KJ/mol)					
	303K	**313K**	**323K**	**333K**	**343K**
	HT				
RB	-21.345	-23.432	-25.721	-25.987	-26.213
RR	-28.674	-29.326	-30.214	-32.543	-34.456
RH	-29.234	-30.246	-32.548	-33.412	-33.786
	CHT				
RB	-23.425	-23.876	-25.823	-26.212	-27.187
RR	-29.236	-30.287	-31.657	-32.9843	-33.654
RH	-29.987	-31.432	-33.021	-34.138	-34.276
	HT		**CHT**		
	ΔH(KJ/mol)	ΔS(J/molK)	ΔH(KJ/mol)	ΔS(J/molK)	
RB	2.14E-05	23.654	4.60E-05	42.654	
RR	2.45E-05	27.876	5.76E-05	47.876	
RH	2.75E-05	29.231	6.32E-05	63.231	

4.4.7. Dye adsorption studies of binary dye systems

The competitive adsorption of mixture of dyes with respect to HT and CHT were investigated with respect to extended Langmuir equation, the Jain and Snoeyink modified extended Langmuir model and the P-factor. Figure 4.44 (a, b & c) and 4.45 (a, b & c) shows the linear fit for isotherms of RB+RR, RB+RH and RB+RR onto HT and CHT. Table 4.17 shows the K_l and a_L for binary systems.

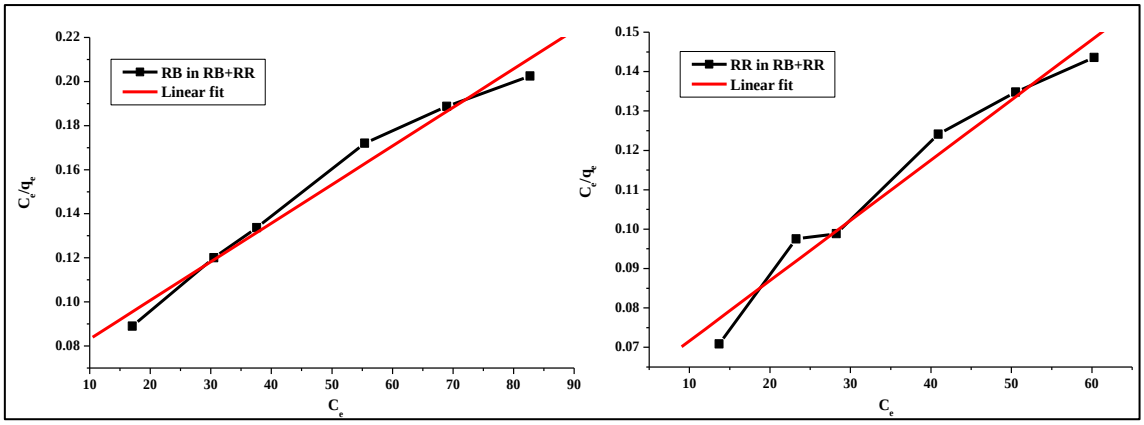

Operating parameters: 180 rpm, 100 ppm of dye, 0.05 g adsorbent, time 210 min, temperature 30^0C, optimum pH

Figure 4.43 a Linear fit of isotherm for RB and RR in (RB+RR) onto HT

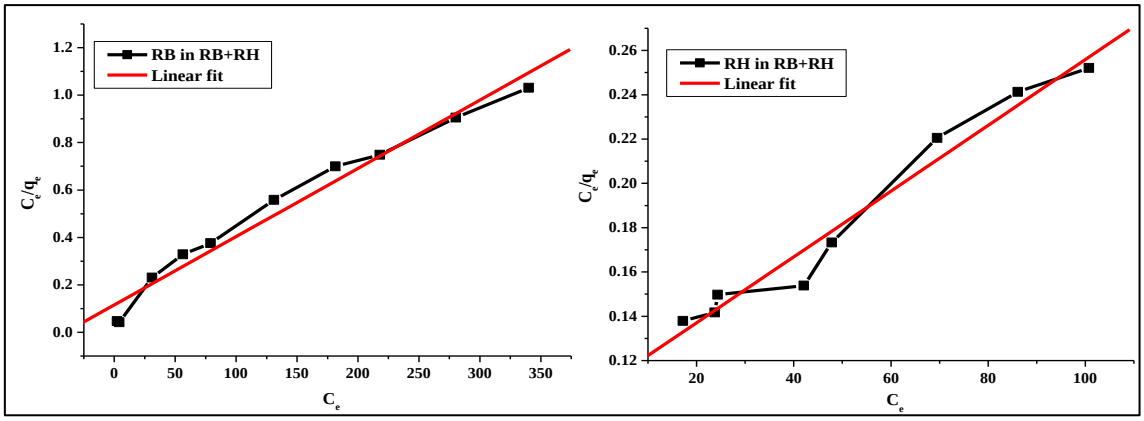

Operating parameters: 180 rpm, 100 ppm of dye, 0.05 g adsorbent, time 210 min, temperature 30^0C, optimum pH

Figure 4.43b Linear fit of isotherm for RB and RH in (RB+RH) onto HT

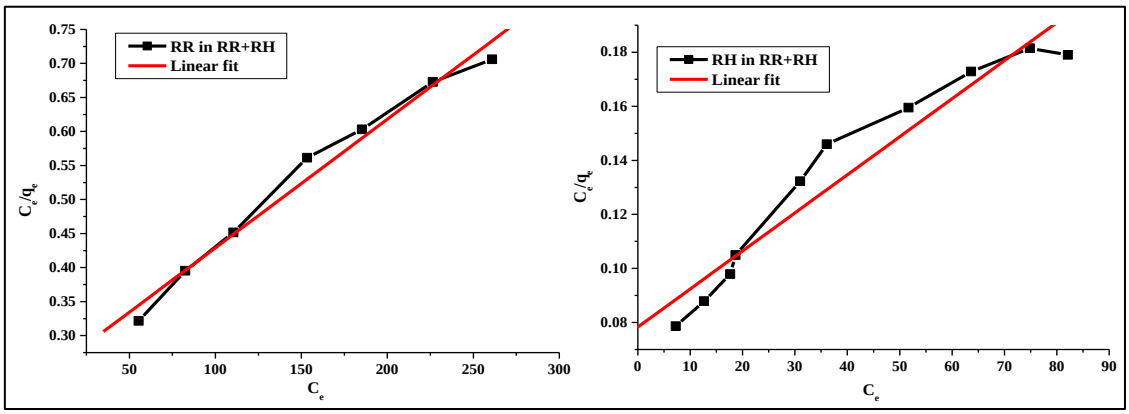

Operating parameters: 180 rpm, 100 ppm of dye, 0.05 g adsorbent, time 210 min, temperature 30^0C, optimum pH

Figure 4.43 c. Linear fit of isotherm for RR and RH in (RR+RH) onto HT

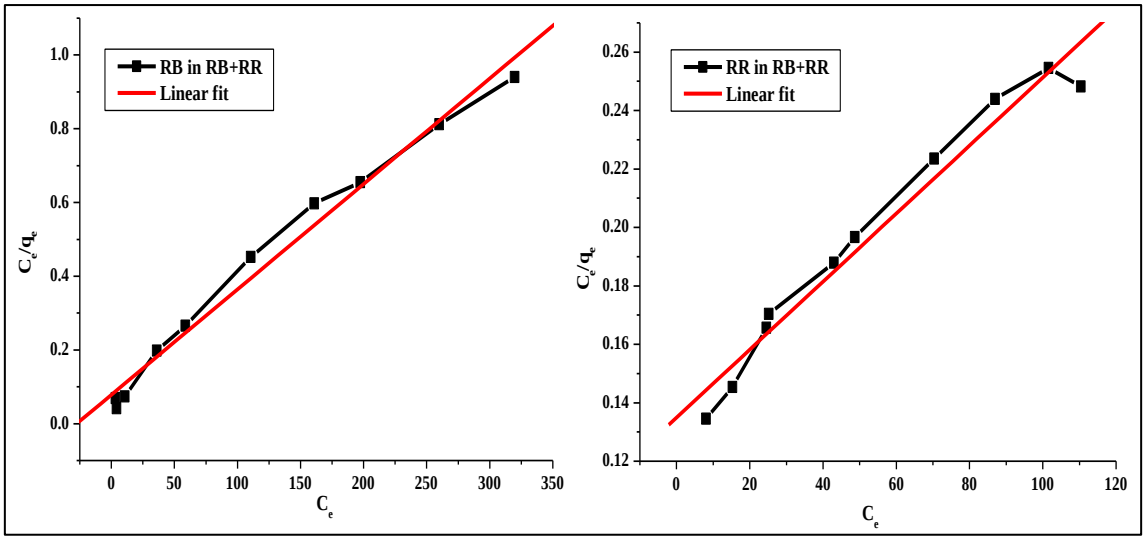

Operating parameters: 180 rpm, 100 ppm of dye, 0.05 g adsorbent, time 210 min, temperature 30^0C, optimum pH

Figure 4.44a. Linear fit of isotherm for RB and RR in (RB+RR) onto CHT

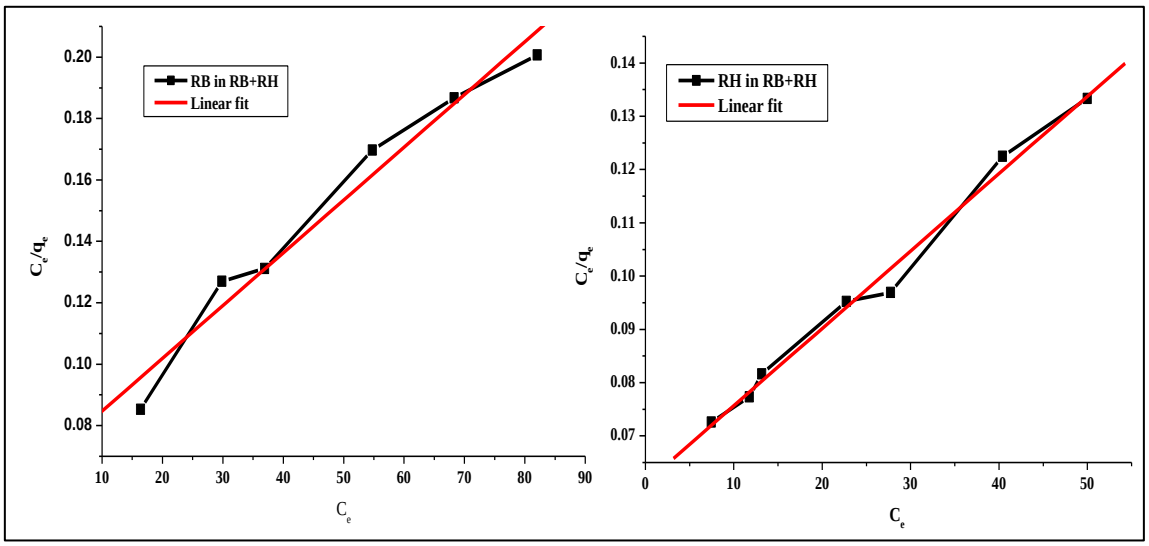

Operating parameters: 180 rpm, 100 ppm of dye, 0.05 g adsorbent, time 210 min, temperature 30^0C, optimum pH

Figure 4.44b. Linear fit of isotherm for RB and RH in (RB+RH) onto CHT

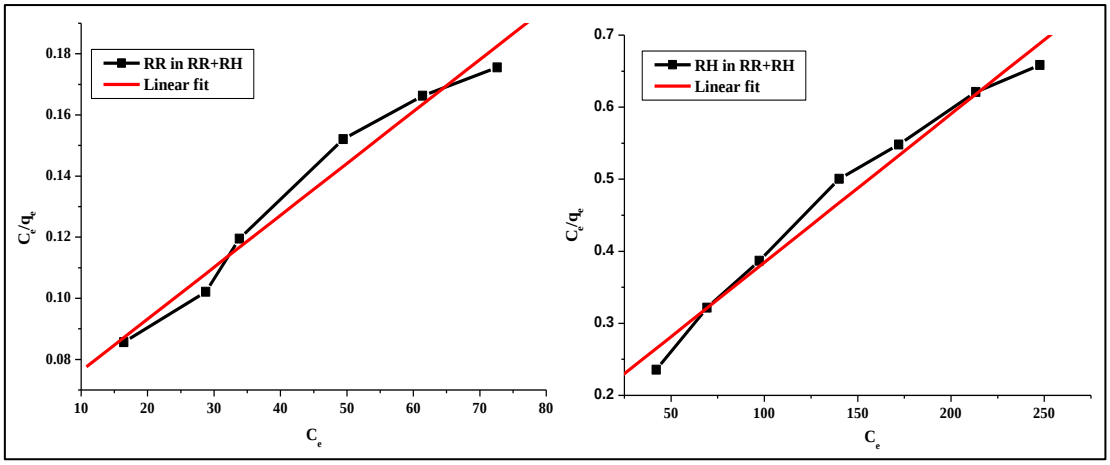

Operating parameters: 180 rpm,100 ppm of dye, 0.05 g adsorbent, time 210 min, temperature 30^0C, optimum pH

Figure 4.44c. Linear fit of isotherm for RR and RH in (RR+RH) onto CHT

Table 4. 17 Langmuir isotherm constants for binary systems

Langmuir isotherm constants for binary systems								
	Binary component system ((RR+RB)							
	HT				**CHT**			
RB+RR								
	K_l	a_l	q_m	r^2	K_l	a_l	q_m	r^2
RB	8.695	0.025	347.22	0.986	14.808	0.043	318.75	0.992
RR	8.518	0.022	371.47	0.983	7.412	0.017	423.72	0.983
RR+RH								
RR	4.168	0.012	371.14	0.990	14.808	0.043	338.75	0.983
RH	14.37	0.036	390.62	0.982	16.355	0.040	408.16	0.995
RB+RH								
RB	10.230	0.028	363.63	0.983	5.601	0.016	337.83	0.989
RH	17.752	0.044	395.25	0.982	16.877	0.045	370.37	0.986

HT			Q_m	% of dye adsorbed without competitive adsorption
	RB+ RR	RB	265	81.05
		RR	216	19.87
	RR + RH	RR	387	40.60
		RH	181	60.34
	RB+RH	RB	287	60.97
		RH	175	40.23
CHT			Q_e	
	RB+ RR	RB	387	71.31
		RR	276	29.87
	RR + RH	RR	376	70.47
		RH	265	29.53.
		RB	376	49.45
		RH	186	50.57

It was observed that the equilibrium uptake of the dyes in binary systems were lower than that of single system. The extended Langmuir could predict the adsorption of binary mixtures well for equal concentration of dyes in binary mixtures, as the qm values for the dyes in single component systems were reasonably closer. There was no interaction between anionic and cationic dyes as well. The adsorption capacities were reduced to a small extent (~<20%) as compared to single component systems due to competitive adsorption. The application of the Jain and Snoeyink model allowed estimating the contribution of competition in the biosorption process. As seen from the table for the binary mixtures greater amount of RB adsorbed without competition in the presence of RR and RH while RH adsorbed preferentially without competition over RR. On the other hand using CHT 70% of RB adsorbed without competition over RR, RB and RH adsorbed 50% without competition in their binary mixture and RR adsorbed 70% without competition over RH.

P factor model was also used to simulate the competitive sorption behaviour of mixture of dyes in bi-solute system. In all the three mixture of dyes the value of P was greater than one confirming that sorption was hindered by the presence of competing dye in the binary mixture.

Sorption kinetics of binary system

The sorption kinetics of binary system was fitted to pseudo first order, pseudo second order and intra particle diffusion models. The adsorption kinetics was well explained by pseudo second order model for all the systems onto HT and CHT. Fig. 4.45 (a, b& c) and 4.46 (a, b& c) shows the linear fit for kinetics for binary systems.

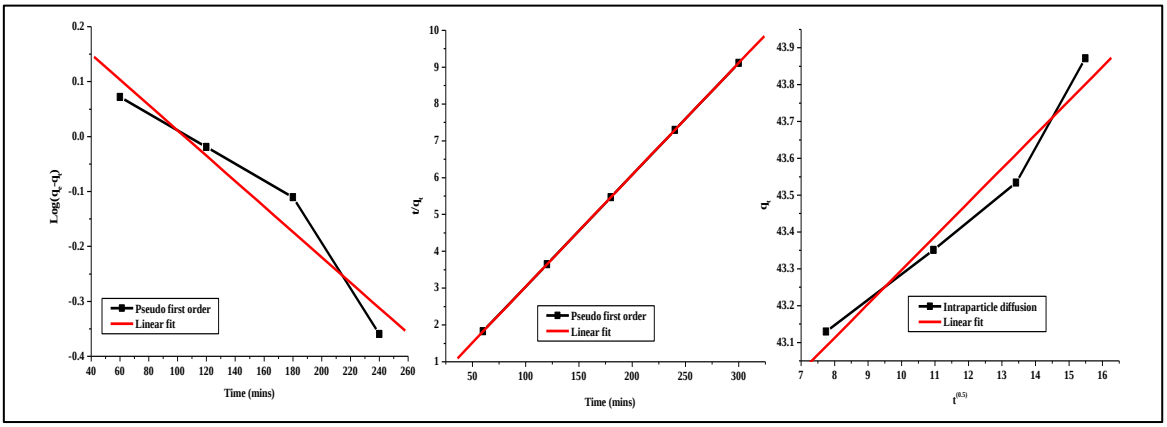

Operating parameters: 180 rpm, 100 ppm of dye, 0.05 g adsorbent, time 300min, temp 30^0C, optimum pH

Figure 4.45a Linear fit of Kinetics for RB and RR in (RB+RR) onto HT

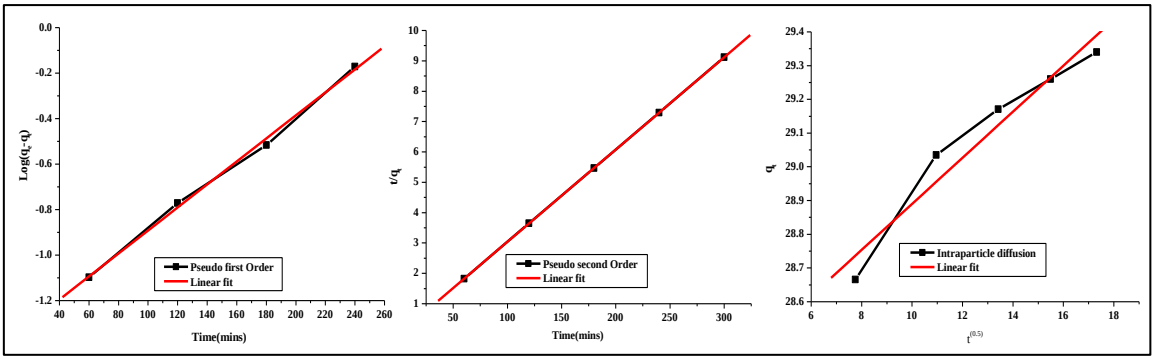

Operating parameters: 180 rpm, 100 ppm of dye, 0.05gadsorbent, time 300 min, temp 30^0C, optimum pH

Figure 4.45b Linear fit of Kinetics for RB and RR in (RB+RH) onto HT

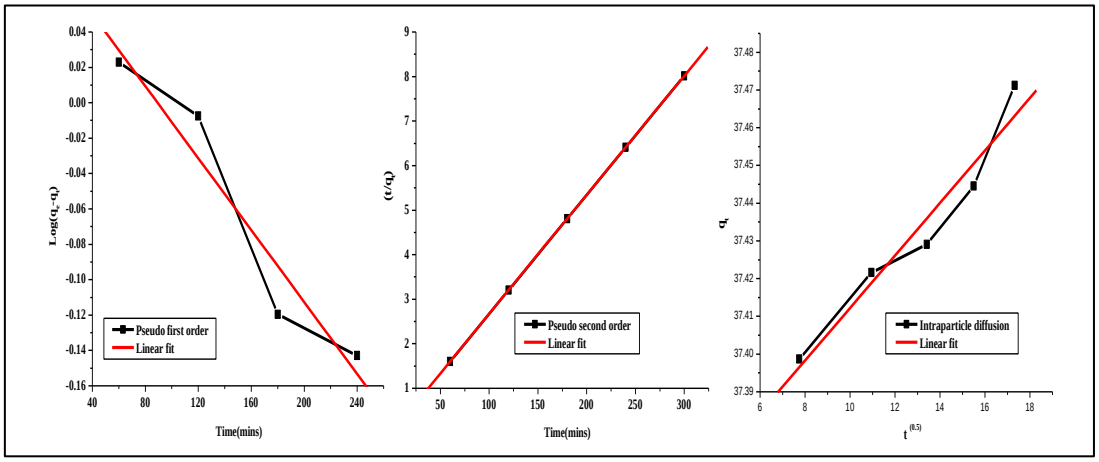

Operating parameters: 180 rpm, 100 ppm of dye, 0.05 g adsorbent, time 300 min, temp 30^0C, optimum pH

Figure 4.45c Linear fit of Kinetics for RR and RH in (RR+RH) onto HT

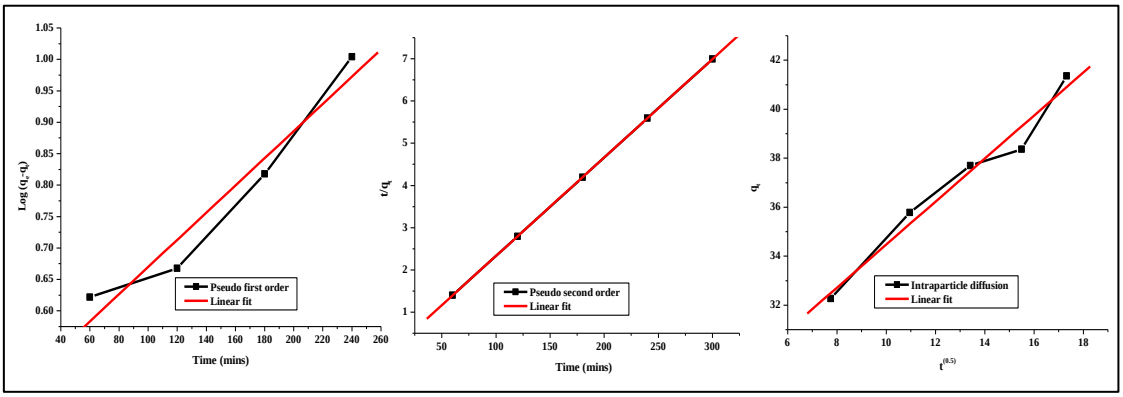

Operating parameters: 180 rpm, 100 ppm of dye, 0.05 g adsorbent, time 300min, temp 30^0C, optimum pH

Figure 4.46a. Linear fit of Kinetics for RB and RR in (RB+RR) onto CHT

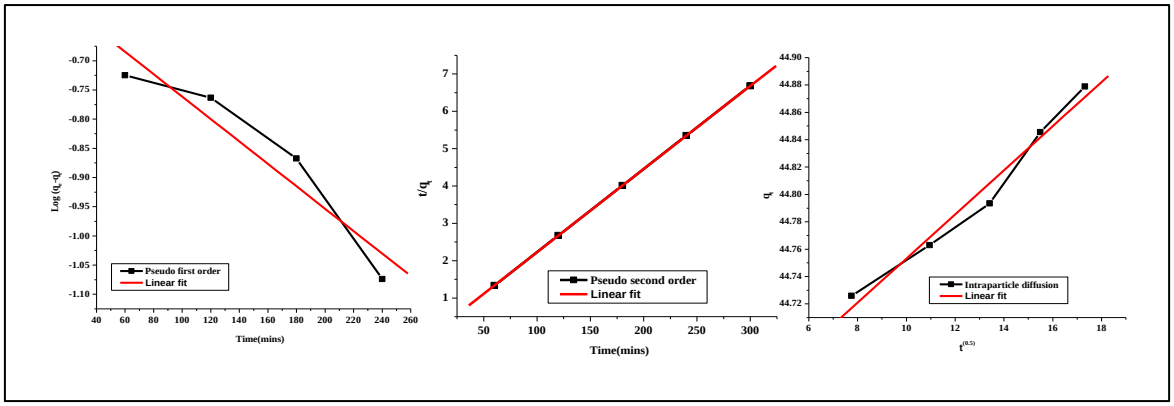

Operating parameters: 180 rpm, 100 ppm of dye, 0.05 g adsorbent, time 300 min, temp 30^0C, optimum pH

Figure 4.46b Linear fit of Kinetics for RB and RH in (RB+RH) onto CHT

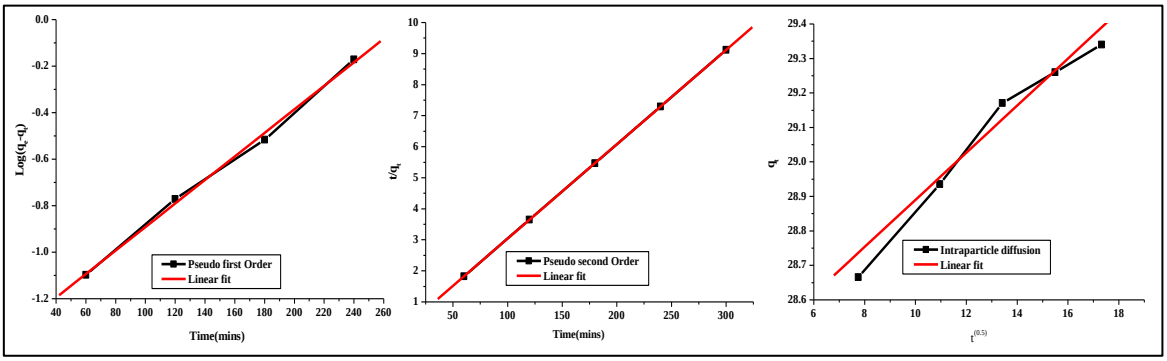

Operating parameters: 180 rpm, 100 ppm of dye, 0.05 g adsorbent, time 300 min, temp 30^0C, optimum pH

Figure 4.46c Linear fit of Kinetics for RR and RH in (RR+RH) onto CHT

Table 4.18 Kinetics for binary mixture of dyes

Kinetics	HT			CHT		
	RB+RR	**RB+RH**	**RR+RH**	**RB+RR**	**RB+RH**	**RR+RH**
Pseudo first order						
q_e **(exp)**	42.68	44.60	37.54	42.35	44.30	48.65
q_e	7.263	5.745	1.231	2.841	2.216	3.269
K_1	1.17E-02	1.17E-03	2.35E-03	4.97 E-03	6.17 E-03	4.42 E-03
r^2	0.998	0.9632	0.962	0.998	0.954	0.962
SD	0.026	0.037	0.027	0.026	0.037	0.027
Pseudo second order						
q_e k_2(g/mgmin),	36.905	39.93	31.76	42.90	43.91	47.87
K_2	2.26E-03	1.10E-03	1.10E-03	6.20 E-03	1.11 E-03	8.98 E-03
r^2	1	1	1	1	1	0.99
SD	0.092	0.021	0.016	3.12 E-03	3.16 E-03	0.016
Intraparticle diffusion						
K_{ip} K_{ip}(mg.gmin$^{-0.5}$)	0.068	0.091	0.037	0.878	0.091	0.037
r^2	0.983	0.976	0.988	0.984	0.976	0.988
SD	0.396	0.082	0.0189	0.679	0.082	0.0181

The rate of adsorption of the three dyes in binary mixtures for HT and CHT was slower than the individual adsorption of each dye in individual dye systems as expected. The experimental data was well fitted by the pseudo-second order model with high correlation coefficient values (R^2> 0.99), and the theoretical uptakes showed good agreement with experimental values. It is also seen that the pseudo-first order model cannot fit the experimental data accurately. Thus it can be concluded that the adsorption of all the three dyes onto HT and CHT obeys the pseudo second order kinetic model even in binary systems.

4.4.8 Conclusion

Chitosan-hydrotalcite composites can prove to be an efficient adsorbent for removal of cationic and anionic dyes from water. The X-ray diffraction pattern shows that the hydrotalcite structure was reconstructed after the adsorption of dyes. Adsorption isotherms were found to correlate well with the Langmuir models. Negative values of ΔG indicated that the adsorption process was favorable and spontaneous in nature. The positive value of enthalpy change (ΔH) confirmed the endothermic nature of the adsorption process. Positive values of ΔS suggested good affinity of the dye moiety with the hydrotalcite composite. The adsorption capacity of the composite for both anionic and cationic dyes suggesting this material to be an attractive adsorbent for treatment of dye waste waters.

Adsorption property of Rhodamine 6G onto Chitosan-g-(N-Vinyl Pyrrolidone) / Montmorillonite composite

4.5 Introduction

Chitosan's performance as an adsorbent has been improved by many researchers using cross-linking reagents. Cross-linking agents not only stabilize chitosan in acid solutions but also enhance its mechanical properties [111] Different crosslinkers such as glutaraldehyde (GLU) or ethylene glycol diglycidyl ether (EGDE) were employed to produce covalently crosslinked materials from gels to beads or particles for the removal of the dyes [112, 113].

However, the dye adsorption capacities and uptake efficiency significantly decreased due to the decrease of availability of amine functions for the complexation with dyes as well as the decrease of the accessibility to internal sites of the materials which could be explained by the loss in flexibility of chitosan chain resulting from the crosslinking [114, 115].

The synthesis of new hybrid polymer materials of chitosan has become a rapid expanding field in the area of polymer science using different techniques. The introduction of a second component, a hydrophobic or hydrophilic polymer into the hydrogels to form the so-called interpenetrating networks (IPNs) was the main breakthrough in this direction. Poly (hydroxyethylmethacrylate) (pHEMA) possesses high mechanical strength, resistance to many chemicals and microbial degradation. The combination of the useful properties of the synthetic pHEMA and natural chitosan as an IPN could introduce a composite matrix in many applications. In addition, the preparation of IPN from these polymers is a simple method and the presence of hydroxyl and amino groups on the IPN offers easy attachment sites for a variety of dye-ligands [116].

Wang et al. grafted acrylic acid onto chitosan filled with attapulgite for adsorption of methylene blue dye from water [117]. Lee et al., synthesized semi IPN hydrogels of acrylic acid and MBA in presence of chitosan [118]. Wang et al. reported chitosan grafted acrylic acid / attapulgite composite gel for fast removal of methylene blue from water [119]. Chen et al. developed a novel semi-IPN of chitosan and polymethacrylic acid using formaldehyde as a crosslinker [120]. The hydrogel showed high swelling with excellent pH sensitivity in the range of pH 1.40–4.50 [121]. Several semi and full IPN type hydrogels were prepared by varying initiator and crosslinker concentration and also monomer to chitosan mass ratio. These hydrogels were characterized and used for removal of methyl violet and Congo red dye from water. Genc et al synthesised a novel metal-chelating membrane, Procion Green H-4G immobilized pHEMA /chitosan composite membranes (also called interpenetrating network membranes) [122]

Thus Semi-interpenetrating polymer network (semi-IPN) technology is a simple and feasible route to fabricate polysaccharide-based hydrogels, in which hydrophilic polysaccharide chain penetrates into another crosslinked polymeric network without any chemical bonds between them [123]. The polysaccharide-based semi-IPN hydrogels have been extensively investigated in biomedical application fields due to their nontoxicity, biodegradability and biocompatibility [124-126]. It is demonstrated that the formation of semi-IPN structure can conserve the characteristics of each polymeric network and the interlocked structure in the crosslinked networks enhances the stability of the materials, thereby ensuring the mechanical strength [127, 128]. These semi-IPN hydrogels often possess porous network structure and allow solute diffusion through the hydrogel structure, and the polyelectrolytic polysaccharides in the crosslinked network have ionic functional groups such as carboxylic acid, amine, sulfonic acid groups, which can absorb and trap ionic dyes and heavy metals [129, 130]. Semi-IPN hydrogel composites were prepared by incorporating chitosan into hydrophilic copolymerized network of PEG macromer and AA monomer and investigated as absorbents for the removal of anionic dyes from aqueous.

The amphiphilic polymer materials with selective adsorption has been attracting much attention because it can be widely used in the applications such as water treatment [131-134], smart separation [135, 136],temporally controlled release of drug [137, 138] and sensor [139, 140]. For example, the recovery of valuable chemicals in the treatment of industrial wastewater can be realized by these polymer materials with the unique ability of selective adsorption [141-148].The selective adsorption of guest molecules is generally resulted from the difference in the interaction between the host polymer materials and different guest molecules. The fundamental investigation on the interaction between the host polymer materials and guest molecules reveals that the selective adsorption is usually determined by several main factors such as electrostatic interaction [149-151], hydrophobic interaction [152, 153], π–π stacking [154-157] and topology structure [158-160].

Based on these findings, a series of host polymer materials such as unimolecular micelles, nano- andmicrogels, and hydrogels with the high selectivity have been developed. Haag [161], Thayumanavan [162, 163], and wan [164] reported amphiphilic polymer as supramolecular host for transferring various guest molecules from the aqueous phaseto the organic phase with selectivity. Maskos prepared the amphiphilic poly(organosiloxane)

nanoparticles, in which the hydrophilic dyes can be loaded selectively depending on their charge and size [165].In addition to these nanomaterials, macroscale hydrogels and polymer network with selective adsorption have been also developed very recently, which are very potential in practical separation. Molina fabricated the urease−poly (ethylene oxide) hybrid matrix and found that it can adsorb selectively and separate anionic orange II from its mixture with cationic methylene blue (MB) in water [166]. A novel nanoporous polymer network prepared from smectic liquid crystals, which possesses the charge and size-selective adsorption to the hydrophilic dyes was reported by Broer et al [167]. Smith developed a versatile supramolecular hydrogel which demonstrates selective adsorption of dyes with opposite charge from aqueous solution [168]. Li et al reported that the responsive microgel prepared from hyperbranched poly (ether amine) (hPEA-mGel) exhibitedthe unique selective adsorption to fluorescein dyes with the same charge and similar structure [169].

Mishra et al have grafted different vinyl monomers onto chitosan and investigated some of their properties to make it more useful in order to increase its possible industrial applications. The selection of CS and PVP as polymers for synthesizing hydrogels rests upon the fact that they are water soluble, biodegradable and biocompatible, and have been extensively employed in biotechnical and biomedical fields. By grafting method used, not only its stability can be improved but also its physicochemical properties can be increased because of the additional properties of monomer are superimposed onto polymeric backbone of chitosan. Duan et al, grafted N-vinyl-2-pyrrolidone onto the backbone of chitosan with the objective of increasing the applications of chitosan. N-vinyl-2-pyrrolidone, which is hydrophilic and non-toxic monomer, has various industrial applications (Duan, 1993; Gaenger&Florig, 2007; Suzuki, Fukuda & Yoneto, 1993). It has been used as a main component of temporary skin covers or wound dressing (Nho & Park, 2002) and also wrapping material (O'Connell et al. 2001) of single-walled carbon nanotubes (SWNTs). Prompted by the applications of chitosan and N-vinyl-2-pyrrolidone are unreported graft copolymer viz. chitosan-g-N-vinyl-2-pyrrolidonewas prepared by employing potassium bromate/ silver nitrate redox system. For optimization of grafting conditions, the effect of potassium bromate, silver, hydrogen ion, chitosan and N-vinyl-2-pyrrolidone concentration along with the time and temperature has been investigated [171-222].

However, since the products are mainly in the gel-form [223, 224], they are not beneficial for waste water treatment applications. In recent years, the preparation of organic–inorganic composite hydrogels have attracted a great deal of attention due to their low production cost, higher mechanical resistance [225-227]and have been used to adsorb dyes [228] So, an attempt has been made to synthesize a graft copolymer of chitosan and N-vinyl-2-pyrrolidone (VP) and use it to form a series of composites with montmorillonite. The thermal, morphological characteristics and the swelling properties of the prepared composites were investigated and their potential for adsorption of RB-21, RR-141 and Rh6G as model dyes as well as their binary mixtures from aqueous solutions was explored

4.5.1 Materials and methods

Chitosan (CTS, 87.6% deacetylated and molecular weight 5.5 x 10^5 g/mol**)** and Montmorillonite (MMT) and Vinyl pyrrolidone (VP) used in this study were purchased from Sigma-Aldrich. Methylene bisacrylamide (MBA) was purchased from National chemicals and Ammonium persulphate from SISCO Research Pvt Ltd.

4.5.2 Synthesis of Chitosan-g-poly (vinyl 2-pyrollidine)/montmorillonite hydrogel composites

Five different hydrogel composites (H-1, H-0.8, H-0.6, H-0.4, and H-0.2) were prepared using CTS, VP and different percentages of MMT (1%, 0.8%, 0.6%, 0.4% & 0.2%) by a previously reported method [229, 230]. The hydrogel composites were prepared by taking 1% chitosan solution in 1% acetic acid in a three necked flask and purging with nitrogen for 30 min to remove dissolved oxygen. This was followed by the addition of 0.1 g of ammonium persulphate to the chitosan solution and heating to 600C. After an interval of 10 minutes a solution containing 5mL VP, 0.5 g of MBA and different amounts of montmorillonite (MMT) was added and further heated at 600C for 3 hr. The resultant product was neutralized with sodium hydroxide and then dehydrated with methanol. The samples were dried in an oven at 70^0C to constant weight.

4.6 Results and discussions

Figure 4.47 shows the IR spectra of IR Spectra of a) CTS b) MMT c) H-1 d) H-0.8 e) H-0.6 f) H-0.4 g) H-0.2 and Figure 4.48 shows the of IR Spectra of dye loaded adsorbents H-0.2(RB), H-0.2(RR), H-0.2(RR).

4.6.1 FT-IR spectroscopy

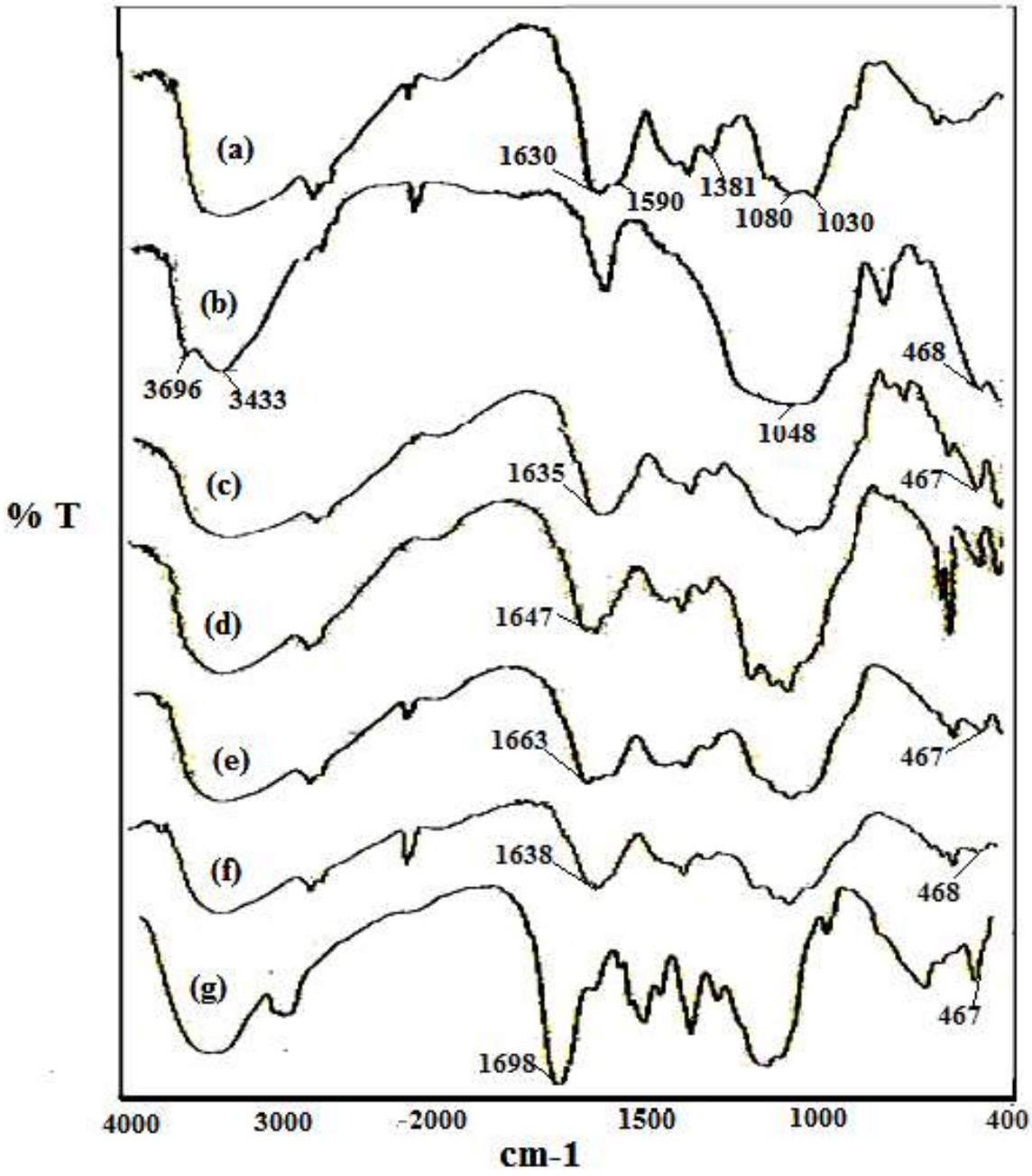

Figure 4.47 IR Spectra of a) CTS b) MMT c) H-1 d) H-0.8 e) H-0.6 f) H-0.4 g) H-0.2

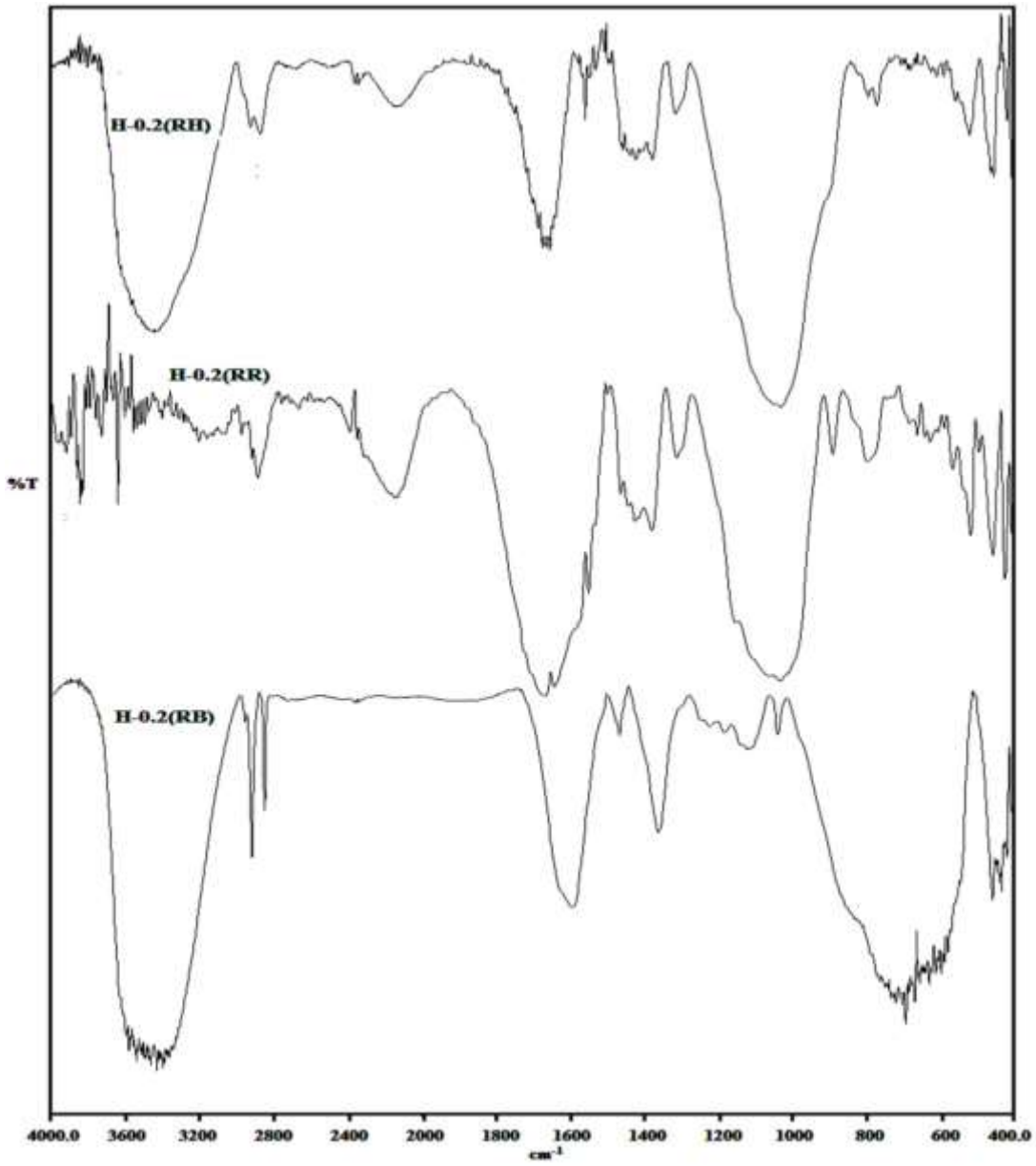

Figure 4.48 IR Spectra of dye loaded adsorbentsH-0.2(RB), H-0.2(RR) and H-0.2(RH)

In the IR spectra of of a) CTS b) MMT c) H-1 d) H-0.8 e) H-0.6 f) H-0.4 g) H-0.2, the absorption bands at 1630, 1590, 1381, 1080 and 1030 cm-1 are attributed to C=O stretching of amide I, NH of amide III(combination of NH deformation and the -CN stretching vibration), C3-OH and C6-OH of chitosan respectively. The bands at 1590 and 1381cm-1 have disappeared in the hydrogel which implies that both NH2 and OH groups of chitosan are involved in grafting. The absorption band at 3433 cm-1 in the hydrogel is due to OH groups of layered alumina silicates. The bands at 1048 and 468 cm-1 correspond to Si-O-Si stretching and Si-O deformation in clay and hydrogel composites. Absorption bands at 3496, 3696 cm-1 due to –OH of MMT disappeared in H-1 to H-0.2 indicating the participation of –

OH groups in the formation of hydrogel composite. The band at ~468 cm-1 in the hydrogel composite samples and clay correspond to Si-O deformation which shows that tetrahedral sheet of clay is involved in the hydrogel composite. A similar observation has been reported by Junping Zhang.et.al [113].

4.6.2 SEM Micrographs

Figure 4.49 shows that the surface morphology of the hydrogel composite. The morphology has changed with decreasing amount of clay. The montmorillonite makes the structure more open, porous and layered. The hydrogel composites H-0.4 and H-0.6 is sponge like (flocculated-intercalated) with small pore size morphology. The hydrogel with low percentage of clay i.e H-0.2 shows a more porous structure with interconnected pores (exfoliated-intercalated) of larger diameters making them vulnerable for absorbance of moisture or dyes. Macropores are effective solvent reservoirs, and the diffusion rate and permeability of small compounds in hydrogels with open cell structure are higher [231].

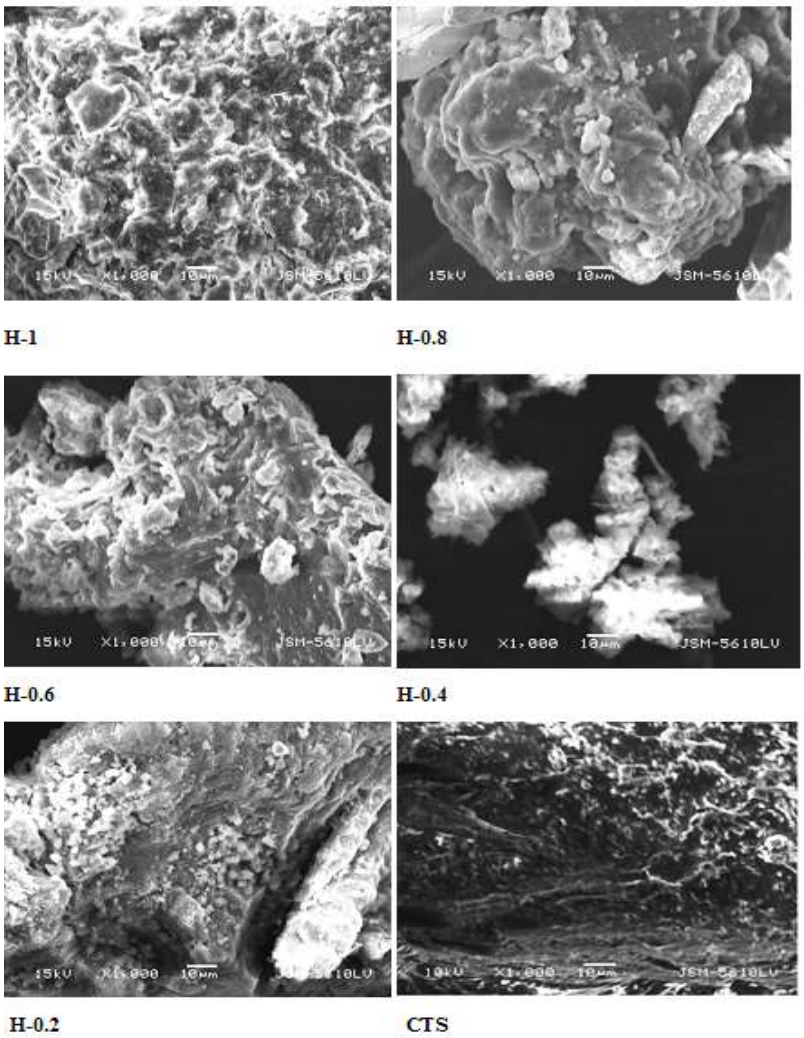

Figure 4.49 SEM Micrographs of a) H-1 b) H-0.8 c) H-0.6 d) H-0.4 e) H-0.2 f) CTS

4.6.3 X-Ray diffraction studies

Figure 4.50 shows the X-ray diffraction patterns of CTS, MMT and the hydrogel composites**.** It can be seen that chitosan exhibits two reflection peaks at 12°A and 20°A, which were assigned to crystal forms I and II, respectively [232]. The crystalline peak at 20°A disappeared in the hydrogel composites, which could be attributed to the weakening of hydrogen bonding between the amino groups and hydroxyl groups in the chitosan molecules. The hydrogel composites showed lowering and widening of the characteristic peaks of clay, implying a decrease in regular pattern of clay structure ,a partial destruction of the structure and hence exfoliation of MMT. The typical diffraction peak of MMT at 9^0A is shifted to ~12^0A on grafting with CTS in H-1 and H -0.8.This peak disappeared on further decrease in the clay content. A sharp characteristic peak is observed in H-1 at 13°A indicating the formation of a crystalline structure. The crosslinking degree of the hydrogel composite is known to depend on its crystallinity, the lower the crystallinity of the samples, the more easily the hydrogel composites swell. Figure 3.51 shows the X-ray diffraction patterns of dye loaded samples (H-0.2-(RB), H-0.2(RR), H-0.2(RH)). After loading of dyes

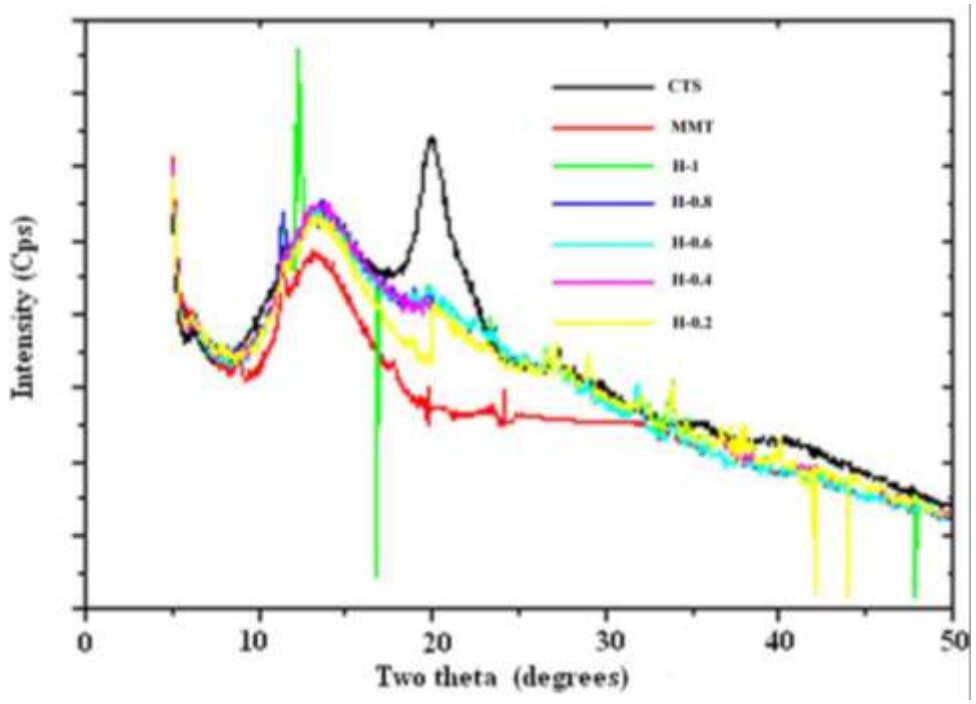

Figure 4.50 XRD patterns of a) CTS b) MMT c) H-1 d) H-0.8 e) H-0.6 f) H-0.4 g) H-0.2

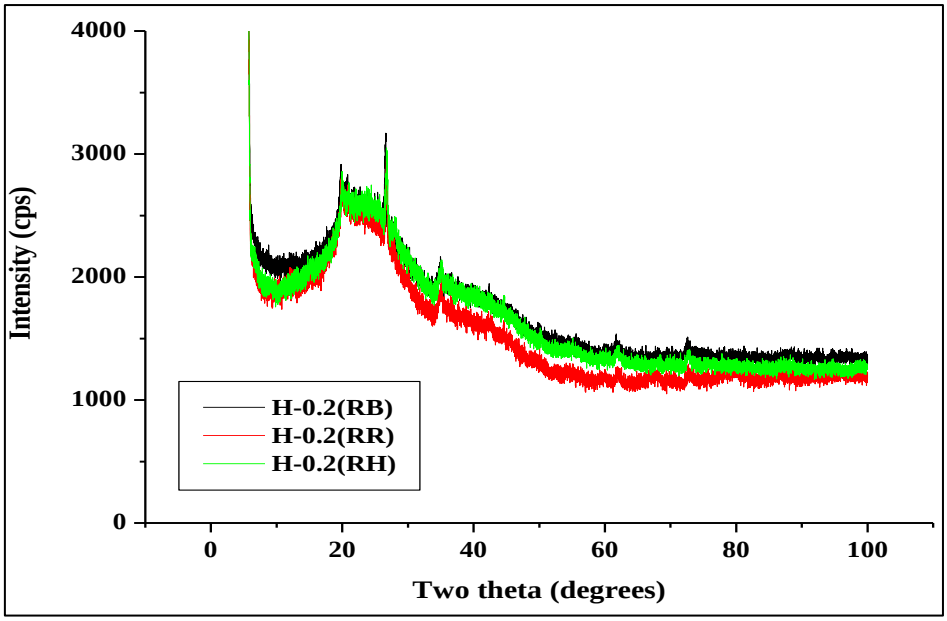

Figure 4.51 XRD patterns of dye loaded adsorbents H-0.2(RB),H-0.2(RR) and H-0.2(RH)

4.6.4 Thermogravimetric analysis

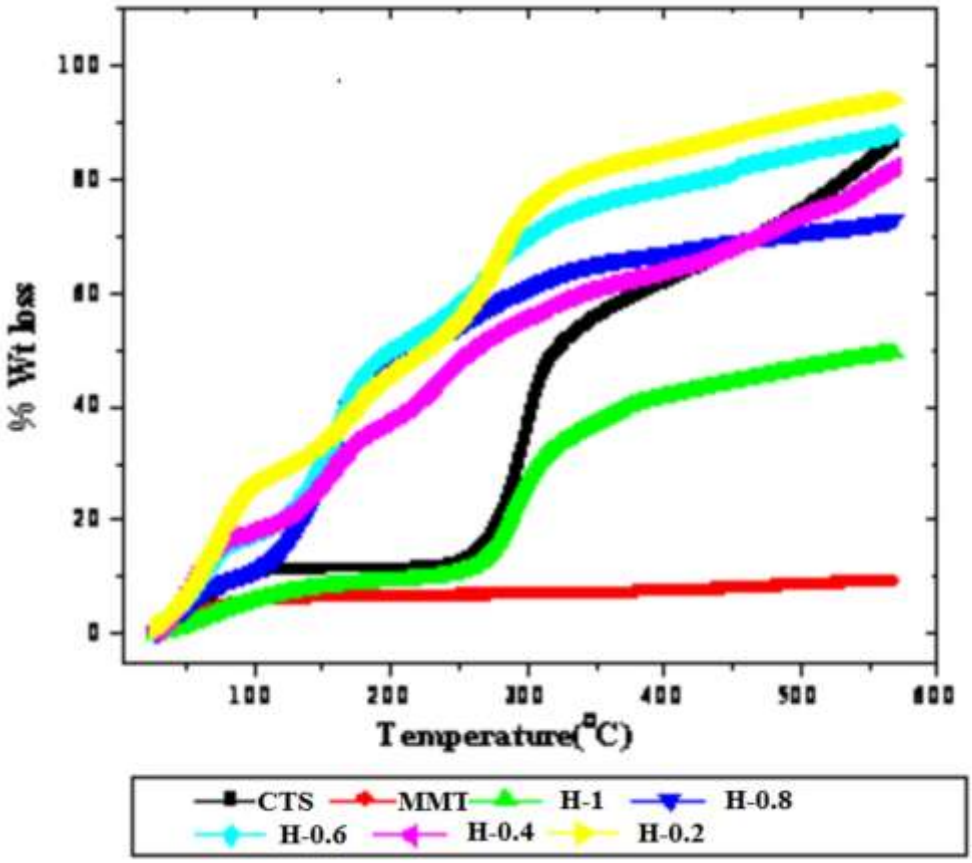

Figure 4.52 TGA Graphs of a) CTS b) MMT c) H-1 d) H-0.8 e) H-0.6 f) H -0.4 g) H-0.2

Figure 4.52 shows the thermo gravimetric analysis (TGA) results of the CTS, MMT and the hydrogel composites. The hydrogel composites decompose gradually at temperatures higher than 40^0C. The degradation process of the composites proceeds in three stages for H-0.8 to H-0.2, while the decomposition proceeds in two stages for H-1 and CTS. The first stage could be presumably due to random split of glycosidic bond and second stage due to oxidative decomposition of the residues. The TGA curve of H-1 showed high end residue as compared to chitosan and other hydrogel composites indicating that 1% clay affected the stability of the composite most and the structure was more ordered.

4.6.5 DSC analysis

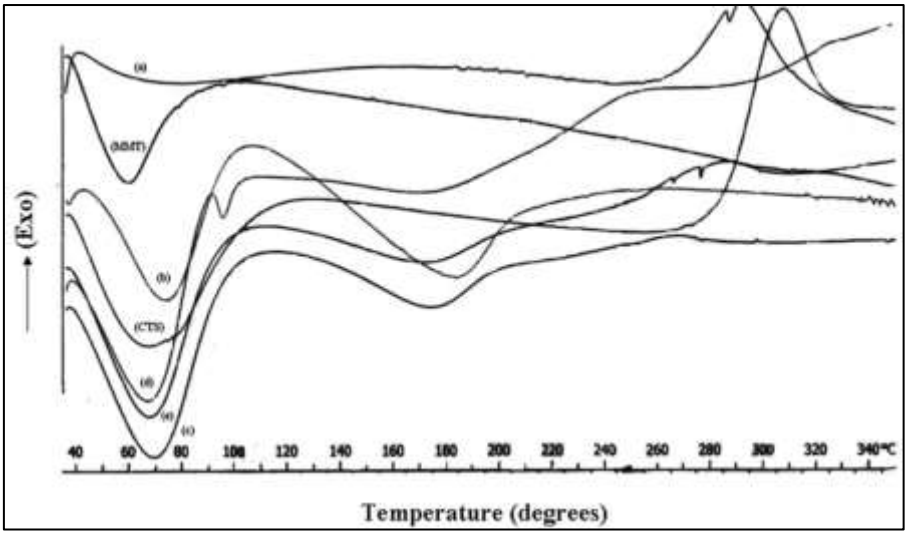

Figure 4.53DSC Scans of CTS, MMT, and dry hydrogel composites a) H-1 b) H-0.8 c) H-0.6 d) H-0.4 e) H-0.2.

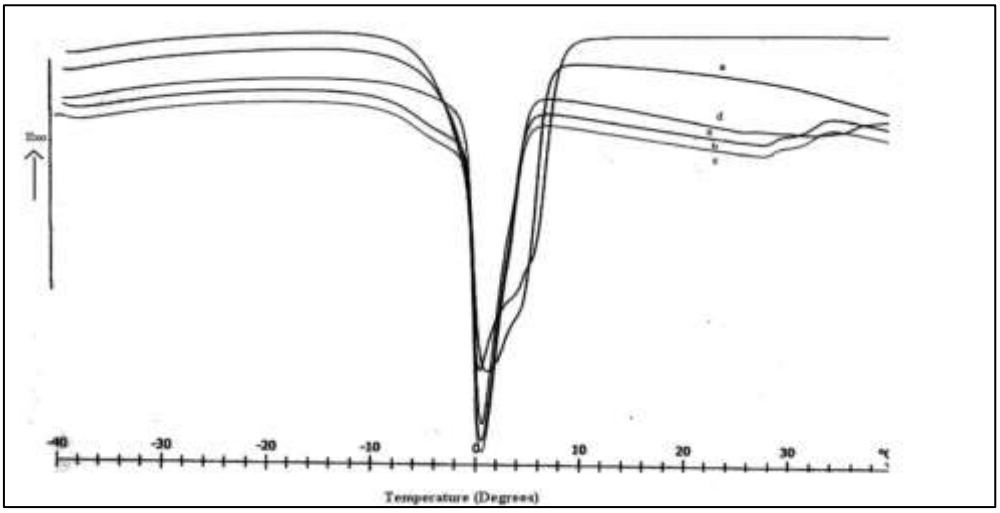

Figure 4.54 DSC Scans of swollen hydrogel composites a) H-1 b) H-0.8 c) H-0.6 d) H-0.4 and e) H-0.

The DSC heating scans of the dry hydrogel composites are shown in Figure 4.53 The broad endothermic peak observed around 75-78^{0}C for chitosan could be due to water evaporation [233]. A thermal decomposition temperature higher than 250°C is also observed. The presence of only one transition implies a high degree of miscibility and intermolecular interactions between the components of the hydrogel composites. Table 19 show that the Tg of different hydrogel composites. The higher Tg value 302^{0}C of H-1 indicates higher crosslinking density and crystallinity compared to other hydrogel composites (H-0.8 to H-0.2). The endotherm at 293^{0}C, 184^{0}C, 173^{0}C, 178^{0}C and 178^{0}C can be attributed to the evaporation of water linked to the chitosan and/or PVP and clay by different kinds of physical bonds (H-bonds, electrostatic interactions). The broadening of the peak in H - 0.8 to H - 0.2 in the temperature range 172-184°C, may reflect a micro heterogeneity of the phase domains [234]. Exothermic peaks result from degradation of polymers which is seen in H-1. The different states of water in swollen hydrogel composites were studied by DSC as it is well-known that the biocompatibility of hydrogels, diffusion of water and molecules not only depends on the equilibrium water content but also on the state of water in the hydrogels [235]. Figure3.54 shows the DSC curves of swollen hydrogel composites obtained from -40 °C to 40 °C. The water in the hydrogel is classified as frozen free water, frozen bound water, and non-frozen water [236, 237]. Since different heating and cooling cycles can cause the evaporation of water from the hydrogel composite and condensation inside the sample pan [238], the results of the first heating runs were used to calculate relative content of frozen water (W_f) and non-frozen water (Wn_f). The total water content Wc, W_f and Wn_f are listed in Table 1. From Table 4.19 we can observe that the content of frozen water was highest for H-1 which could be due to greater free volume. The non-frozen water or bound water is highest when the hydrogel composite has lower percent clay (H-0.2) indicating a strong interaction with water. It is lesser in H-1 and H-0.4 and again increases in H-0.8. This indicates that the amount of bound water depends not only on the concentration of polar groups (amino) in the hydrogel composite but also on other factors such as total water content of the hydrogel or interaction with hydrophobic moieties.

Table 4.19: Water state of hydrogel composites calculated by DSC analysis

Sample code	Total water Content(Wc)	Non-frozen water (Wnf)	Frozen water (Wf)	Tg (^{0}C)
H-1	2.055	1.07	0.98	302.1
H-0.8	2.31	1.73	0.58	180.1
H-0.6	1.9	1.225	0.675	182.3
H-0.4	1.57	0.922	0.648	188.6
H-0.2	3.87	3.39	0.48	188.8

4.6.6 Swelling studies

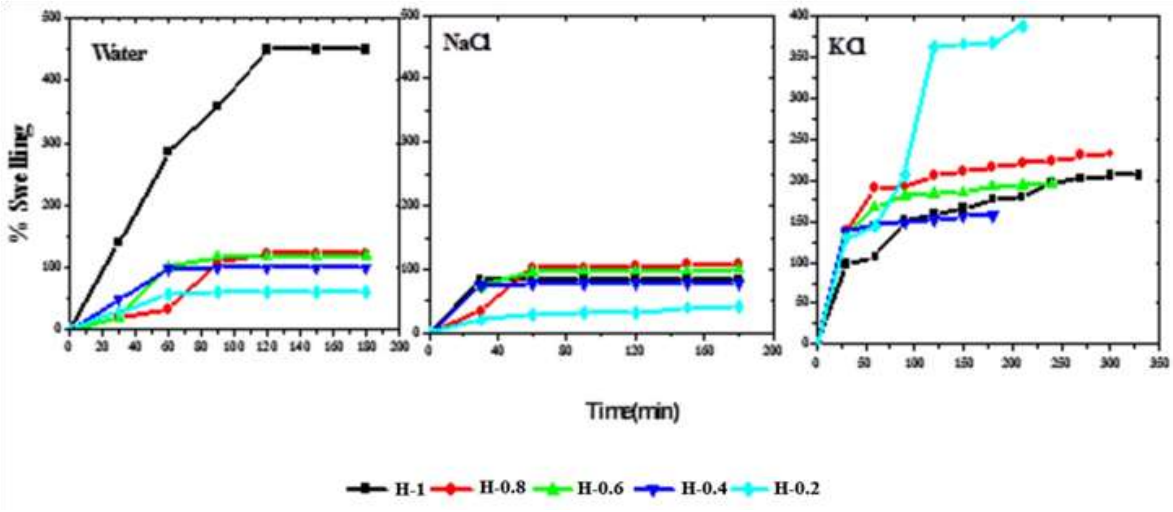

Figure 4.55 Swelling Kinetics of hydrogel composites in Water, NaCl and KCl

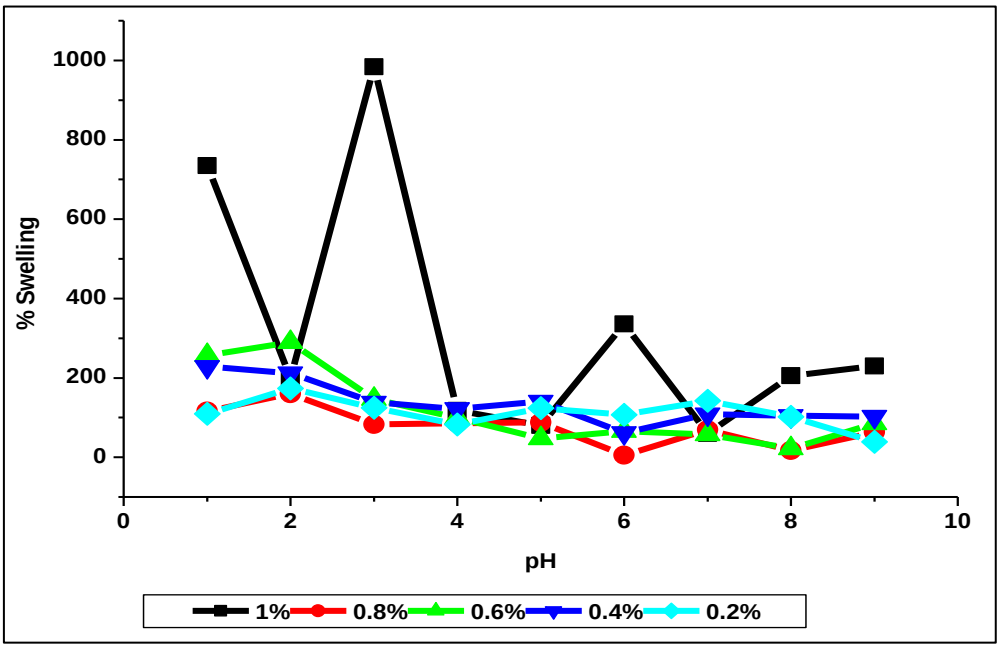

Figure 4.56 Swelling Kinetics of hydrogel composites in phosphate buffers

The effect of swelling of the hydrogel composites in water, phosphate buffers and in electrolytes was studied. The percentage swelling versus time profile in water and electrolytes is shown in Figure 4.55. Swelling in hydrogel composites occurs when water molecules get absorbed. Initially swelling is due to water molecules forming hydrogen bonds with hydrophilic groups present in the hydrogel composite. More water then penetrates around bound water to form cage like structure or clusters. Finally excess water enters freely

into the gel network resulting in more swelling. The extent of swelling is mainly dependent on the characteristics of the external medium, such as pH, charge, ionic strength and polymer nature, i.e. network elasticity, presence of hydrophilic functional groups and extent of crosslinking density.

The equilibrium water content increased with decrease in clay content. Equilibrium was achieved slowly when clay content is less (H-0.2). This may be due to increased interaction among MMT, CTS and VP, which decreases the elasticity of the polymeric chains. MMT could act as crosslinking points in the network, which caused the increase of the crosslinking density of hydrogel composite with the increase of MMT content. The greater the crosslinking density, lesser the elasticity of the polymer chains, which could restrict the penetration of water molecules into the hydrogel composite [239]. When the clay content is more, probably a part of chitosan is intercalated into the layers of MMT and hence graft polymerization is restricted. On the other hand when the clay content of the hydrogel composite is less, then chitosan intercalation into the MMT might be negligible and hence did not influence graft polymerization between chitosan and PVP resulting in higher water absorbancy.

The swelling is better in KCl medium than in NaCl and water for 1% clay in accordance with Hofmeister series [240] which is a criterion for ion effects on physicochemical properties of polymers in aqueous systems including hydrogel swelling. Similar effects were not observed for other composites. It is observed that in NaCl medium the hydrogel composite with 0.8 % clay showed more swelling and equilibrium is approached faster.

Figure 4.55 shows the swelling behaviour of the hydrogel composites in phosphate buffers. A high swelling behaviour is observed at low pH, probably due to protonation of amino groups of chitosan and the nitrogen groups of PVP. This protonation leads to polymer chain repulsion and dissociation of secondary interactions allowing more water to penetrate into the gel network. As the pH is increased, deprotonation takes place, resulting in release of counter ions and decrease in repulsion in the polymer chains. This result in reduced swelling and a decrease in the total water content of the hydrogel.

4.6.7 Dye adsorption studies of single component dye systems

The preparation of dye solutions and the batch sorption Experiments for single and binary mixture of dyes are as discussed in section 3.1.4 (chapter 3).Figure 4.57 shows the Figure. Effect of pH, temperature, concentration and adsorbent dose on % uptake of RB-21, RR-141 and RH-6G onto H-0.2

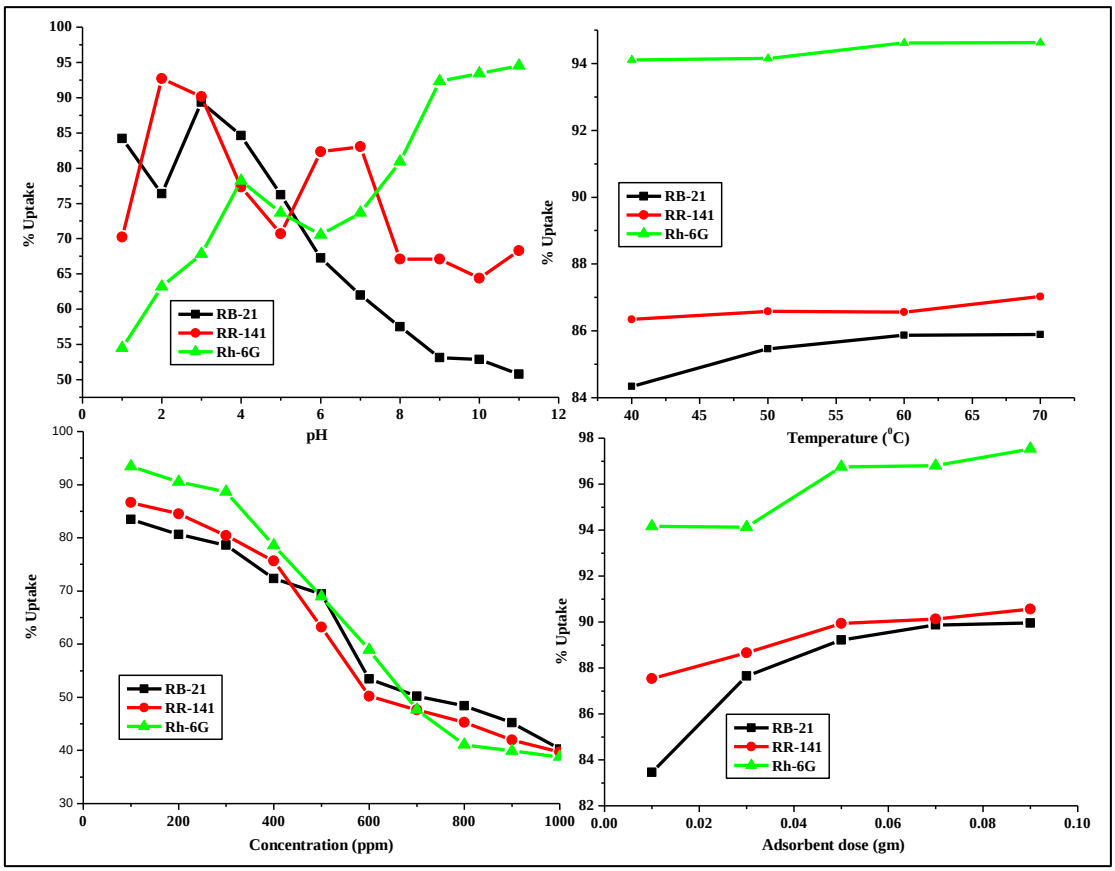

Figure 4.57 Effect of pH, temperature, concentration and adsorbent dose on % uptake of RB-21, RR-141 and RH-6G onto H-0.2

Effect of pH

The pH of the dye solution is one of the most important parameter affecting the adsorption process as it has an influence on the surface charge of the adsorbent. The effect of initial pH on the adsorption of RB-21, RR-141, Rh-6G onto H-0.2 was investigated by varying the pH of solution from 1 to 11 using 0.1N NaOH/HCl (Figure 4.57). The maximum removal was found to be at pH 2 for RB- 21, RR-141and pH 10 for Rh-6G. At acidic pH the surface charge of the hydrogel is positive and so electrostatic attraction exists between anionic dyes. As the pH increased the adsorption of cationic dye increased which could be due to the successive deprotonation of positive charged groups on the adsorbent and electrostatic attraction between negatively charged sites on the adsorbent and cationic dye.

Effect of temperature

Figure 4.58 shows the effect of temperature where a less increase in effect of uptake was observed in all the three dyes indicating the process to be endothermic, which could be due to an increase in kinetic energy of dye molecules and enhanced rate of diffusion of adsorbate.

Effect of adsorbent dose

On increasing the adsorbent dose from 0.01-0.09g the removal of dye increased and after certain amount of dose saturation limit is reached (0.05gm).

Effect of concentration

The increase in dye concentration (figure 4.59) resulted in decrease in percent uptake of the dyes suggesting that limiting number of adsorption sites are available for adsorption at higher concentration of adsorbate molecules which may be attributed to the increase in the concentration gradient and saturation of sorption sites.

Sorption isotherm

The isotherm models (Table 4.20) Freundlich, Langmuir, Temkin, and Halsey models were studied a isotherm constants for the sorption of RB-2, RR-141 and RH-6G by H-0.2 are presented in Table 4.20. Figure 4.59 (a, b & c) shows the linear fit for isotherms. The high correlation coefficient values obtained for the Langmuir model and freundlich model suggested being a best fit for the dyes. The magnitude of n indicates a measure of favorability of adsorption. In the present study, the value of n for RB-21, RR-14 and Rh-6G was less than 1 implying a favorable adsorption process over the entire range of concentration investigated. The Temkin isotherm assumes that the adsorption energy of all the molecules in the layer decreases linearly rather than logarithmically with coverage, due to adsorbent–adsorbate interactions and that the adsorption is characterized by a uniform distribution of the binding energies, up to some maximum energy. It was observed that the Temkin isotherm model did not fit well with the experimental data.

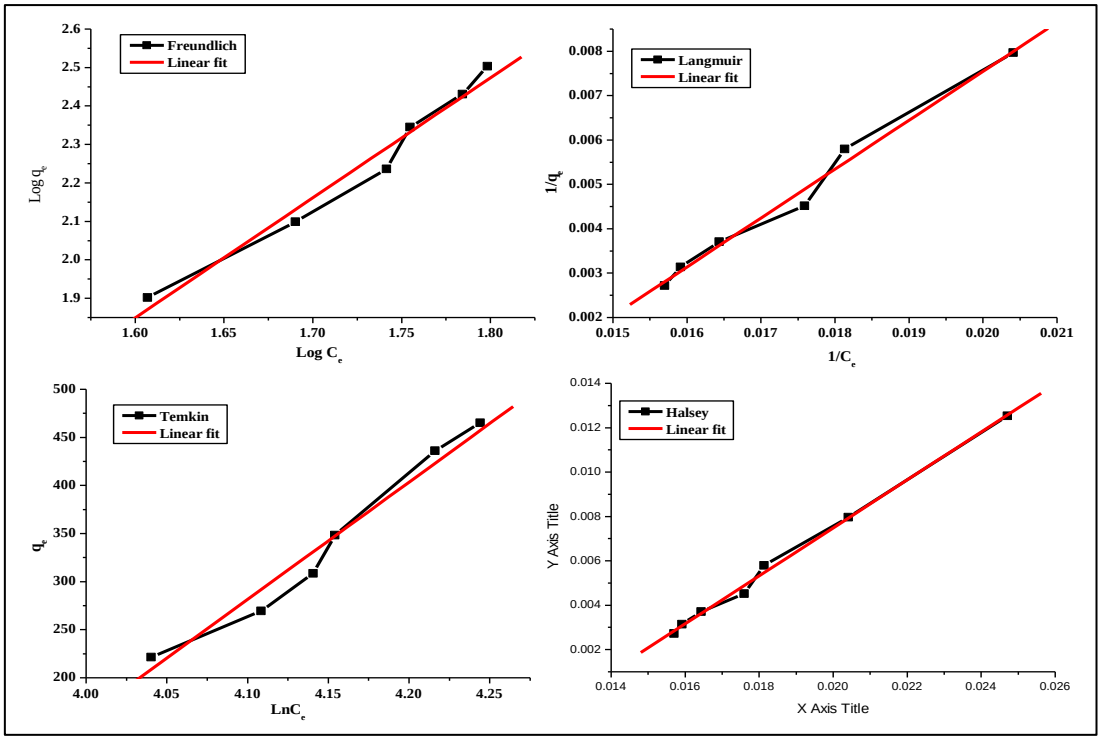

Operating parameters: 180 rpm, 100 ppm of dye, 0.05 g adsorbent, time 210 min, temperature 30^0C, optimum pH

Figure. 4.59 a Linear fit of isotherm for RB onto H-0.2

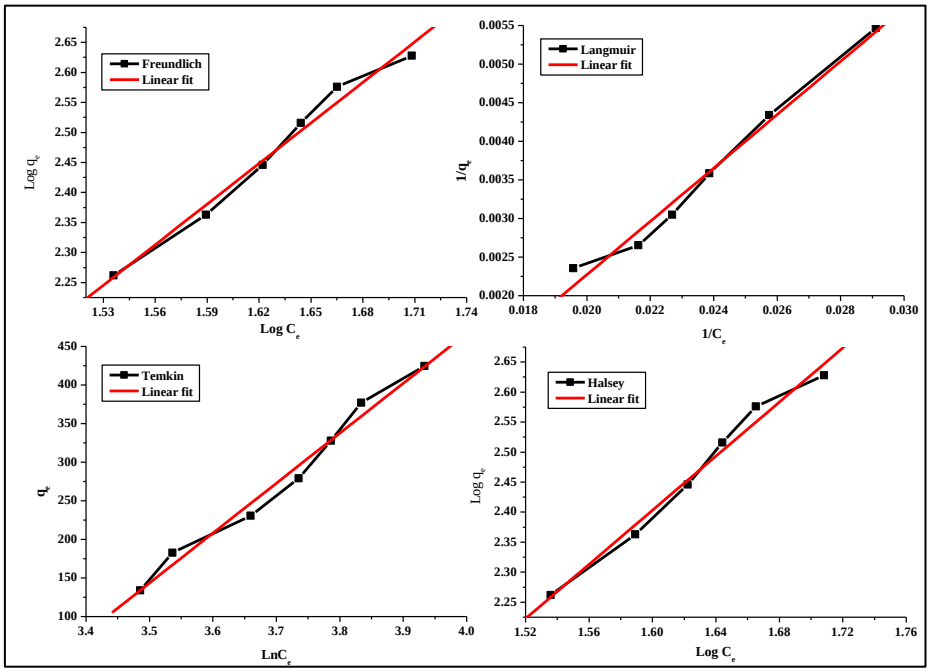

Operating parameters: 180 rpm, 100 ppm of dye, 0.05 g adsorbent, time 210 min, temperature 30^0C, optimum pH

Figure4.59b Linear fit of isotherm for RR onto H-0.2

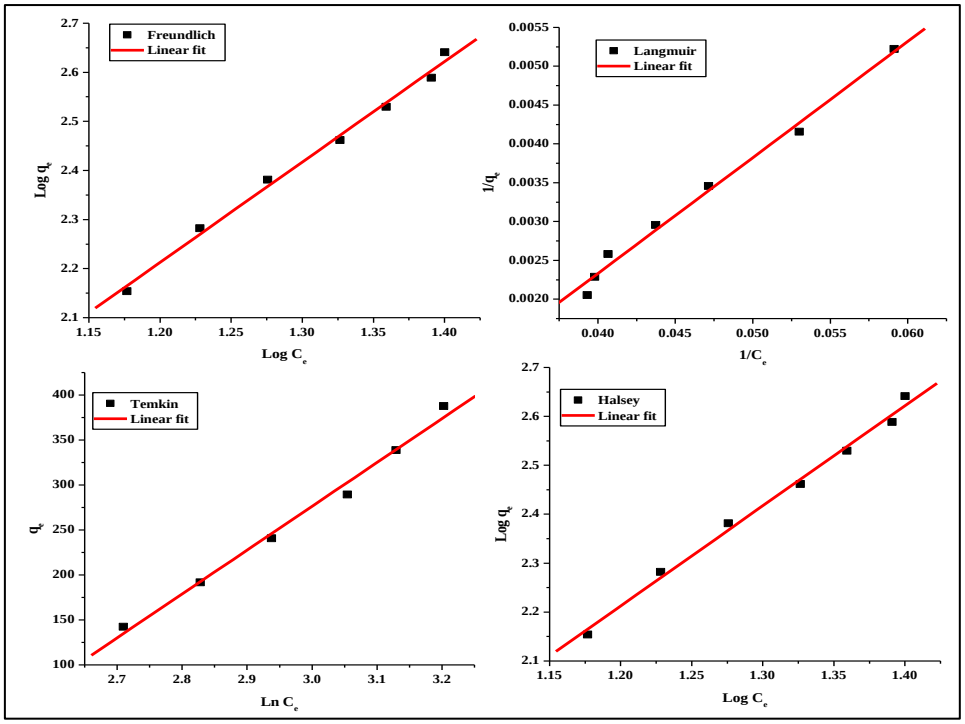

Figure 4.59 c Linear fit of isotherm for RR onto H-0.2

Table 4.20 Isotherms

Isotherms	**H-0.2**		
	RB	**RR**	**RH**
Freundlich			
q_e(exp) (mg.g^{-1})	**402**	**387**	**418**
K_f(mg.g^{-1})	6.108	7.823	12.543
N	0.546	0.213	0.425
R^2	0.987	0.985	0.99
SD	0.012	0.034	0.056
Langmuir			
q_m(mg.g^{-1})	396	352	412
K_L(L.mmol^{-1})	0.028	0.086	0.045
R^2	0.991	0.998	0.997
SD	0.015	0.016	0.021
Temkin			
β_T	324.26	543.27	385.68
K_T (L.mmol^{-1})	0.297	0.321	0.187
R2	0.999	0.997	0.999
SD	2.876	9.876	6.785
Halsey			
K_{FH}	0.098	0.076	0.023
n_{FH}	0.345	0.765	0.876
R2	0.991	0.989	0.990
SD	0.025	0.035	0.012

Sorption Kinetics

The kinetic models Pseudo First order, Pseudo Second order, Intraparticle diffusion, Bangham and Liquid film diffusion model were studied and the kinetic constants for the sorption of RB-21, RR-141 and RH-6G by H-0.2 are presented in Table 21.Fig. 4.60 (a, b & c) shows the linear fit for Kinetics of RB,RR and RH onto H-0.2. The calculated q_e value computed from pseudo second-order was much close to the experimental q_e as compared to calculated q_e for pseudo first order kinetic indicating that the pseudo second-order model was more suitable to explain adsorption of dyes onto H-0.2. Also the correlation coefficients are closer to unity for Pseudo second order kinetics than for Pseudo first order suggesting that limiting steps may be chemisorption involving valency forces through the sharing and exchange of electrons between the sorbent and substrate.

The adsorption kinetic data were thus analyzed using the intraparticle diffusion model and liquid diffusion model to elucidate the adsorption mechanism. The plots of intraparticle diffusion and liquid film diffusion models have intercepts instead of starting from origin suggesting that neither the film diffusion nor intra particle diffusion processes are the sole rate-limiting steps in the adsorption process. However, the low correlation coefficient for the liquid film diffusion model as compared to that of the intraparticle diffusion model suggested that intraparticle diffusion mainly controlled the adsorption process of dyes onto H-0.2 along with a significant contribution of film diffusion process. Also the linear coefficient values of the Bangham model suggests that the diffusion of dye molecules onto the pores of the adsorbent.

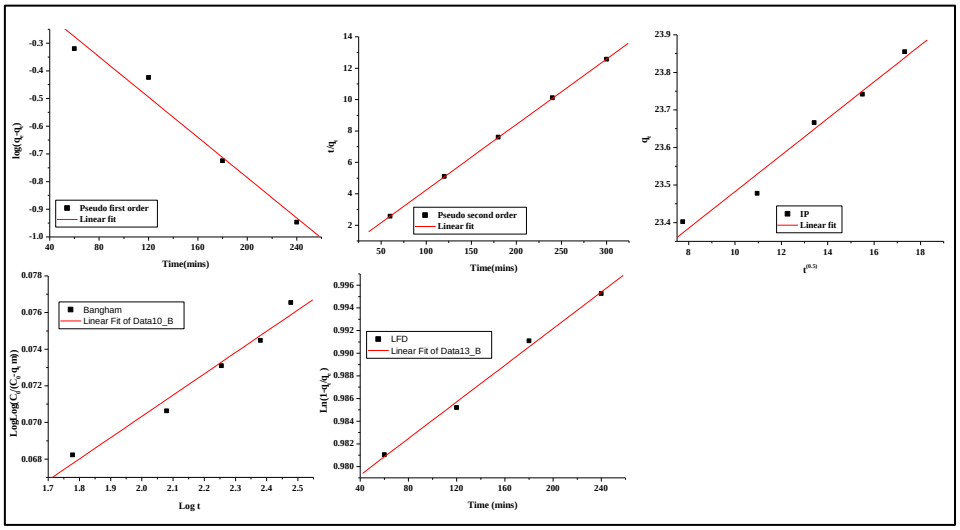

Operating parameters: 180 rpm, 100 ppmof dye, 0.05 g adsorbent, time 210 min, temperature 30^0C, optimum pH

Figure 4.60a Linear fit of Kinetics for RB onto H-0.2

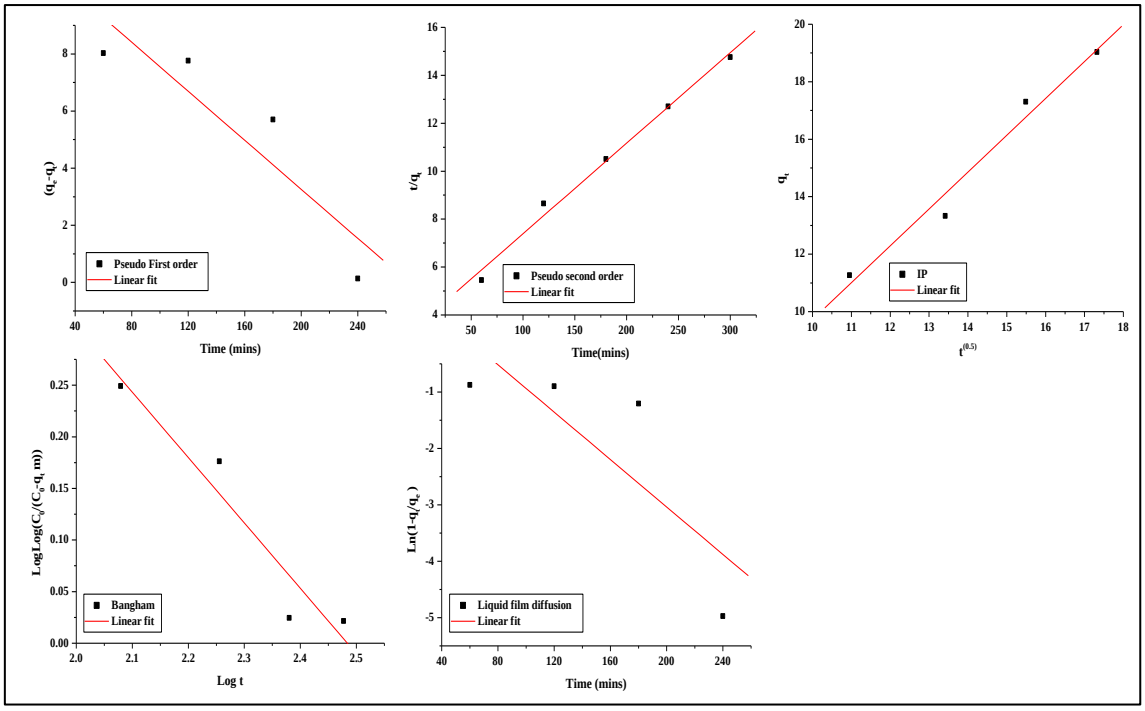

Operating parameters: 180 rpm,100 ppm of dye, 0.05g adsorbent,time210 min, temperature 30^0C, optimum pH

Figure 4.60 b Linear fit of Kinetics for RR onto H-0.2

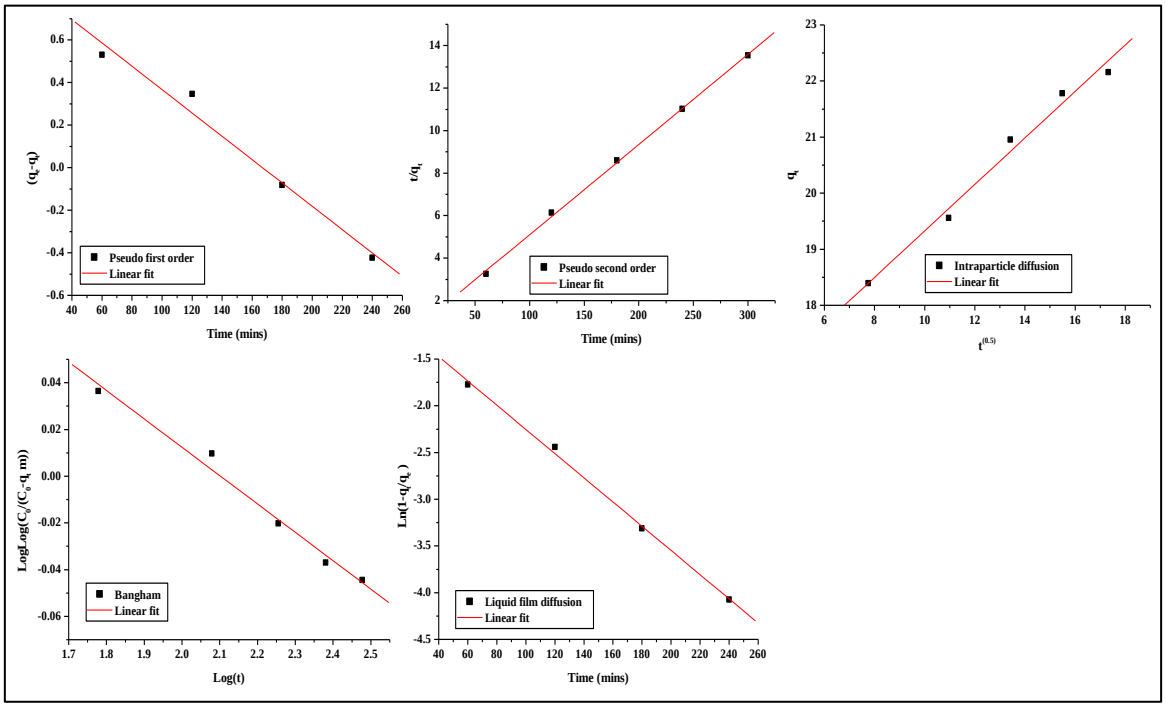

Operating parameters: 180 rpm,100 ppm of dye, 0.05g adsorbent, time 210 min, temperature 30^0C, optimum pH

Figure 4.60 c Linear fit of Kinetics for RH onto H-0.2

Table 4.21 Kinetics

Isotherms	H-0.2		
	RB	RR	RH
Pseudo first order			
q_e (exp)	44.97	43.85	46.59
q_e	19.24	18.67	12.34
Kt	0.032	0.045	0.089
r^2	0.998	0.987	0.998
SD	0.023	0.012	0.056
Pseudo second order			
q_e	42.86	41.08	45.32
Kt	0.020	0.014	0.032
r^2	0.997	0.998	0.994
SD	0.012	0.043	0.056
Intraparticle diffusion			
K_{ip}	3.276	3.4265	3.657
r^2	0.993	0.994	0.995
SD	0.043	0.021	0.056
Bangham			
K_m	12.45	15.75	21.32
A	0.221	0.146	0.123
r^2	0.979	0.979	0.997
SD	0.006	0.001	0.001
Liquid film diffusion			
K_{fd}	0.0015	0.0173	0.003
r^2	0.974	0.982	0.979
SD	0.032	0.131	0.042

4.6.7 Dye adsorption studies of binary component dye systems

The competitive adsorption of mixture of dyes with respect to H-0.2 were investigated with respect to extended Langmuir equation, the Jain and Snoeyink modified extended Langmuir model and the P-factor. Figure 4.61 (a, b & c)) shows the linear fit for isotherms of RB+RR, RB+RH and RB+RR onto H-0.2.Table 22 shows the K_l and a_L for binary systems.

P factor model was also used to simulate the competitive sorption behavior of mixture of dyes in bi-solute system. This model assumed a simplified approach to compare and correlate single-solute sorption with those of the multi-component systems by introducing a ‘‘lumped’’ capacity factor Pi. The P-factor is defined as the ratio between the monolayer capacities in

single- and multi-solute systems. In all the three mixture of dyes the higher (P>1) value of P (P>1) indicating the predominant sorption of RB over RR, RB over RH and RR over RB in single and binary system.

Also it was observed that the adsorption capacity of single component in the binary mixture is less on comparison with its existence as an individual dye itself which can be explained due to the less availability of the active sites for the second dye to get adsorbed.

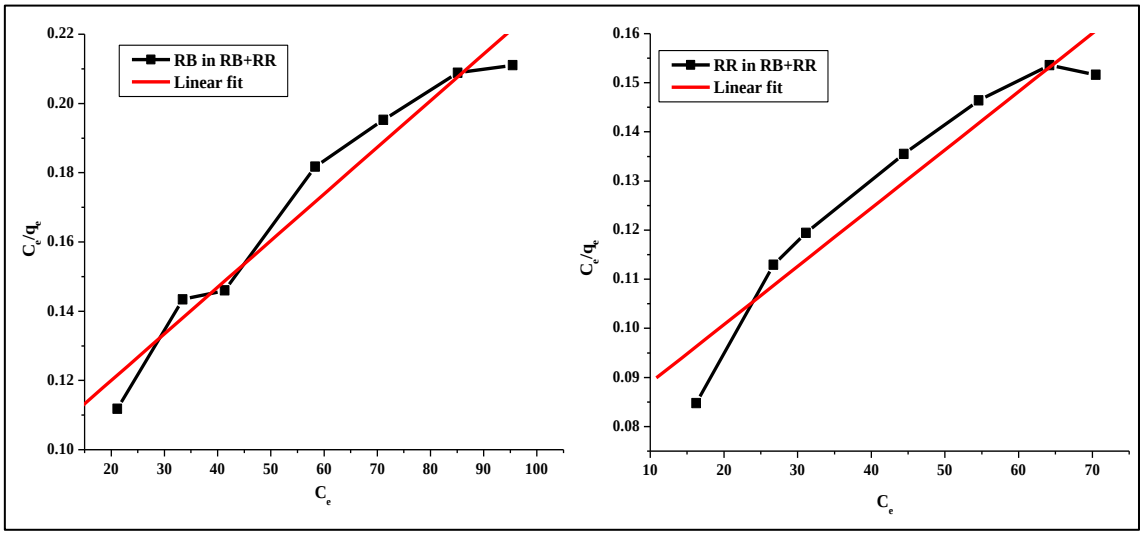

Operating parameters: 180 rpm, 100 ppm of dye, 0.05 g adsorbent, time 210 min, temperature 30^0C, optimum pH

Figure 4.67a Linear fit of isotherm for RB and RR in (RB+RR) onto H-0.2

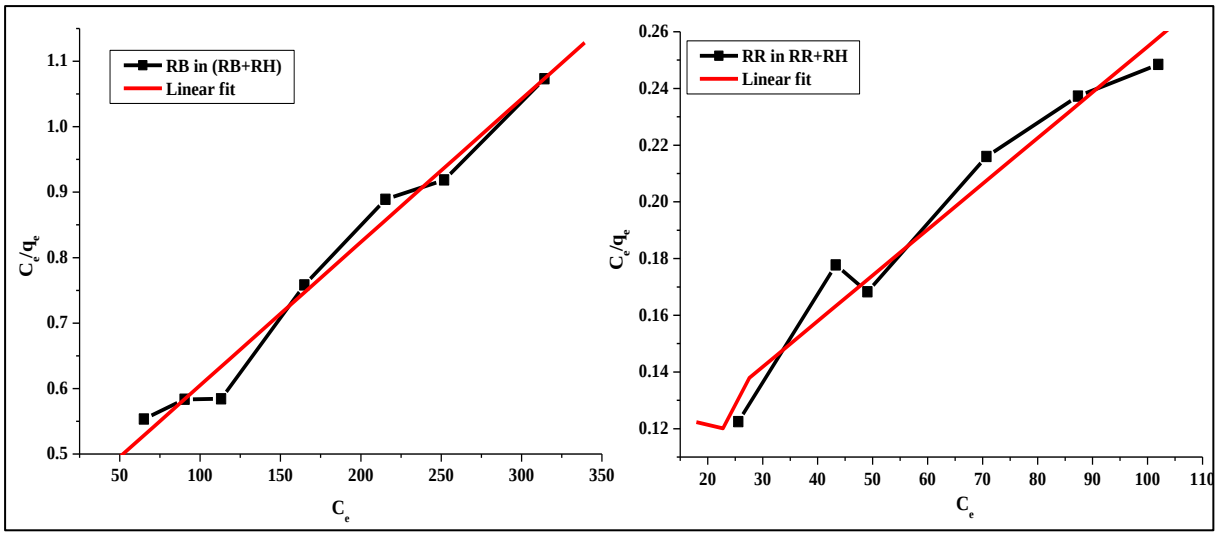

Operating parameters: 180 rpm, 100 ppm of dye, 0.05 g adsorbent, time210 min, temperature 30^0C, optimum pH

Figure 4.67b Linear fit of isotherm for RB and RH in (RB+RR) onto H-0.2

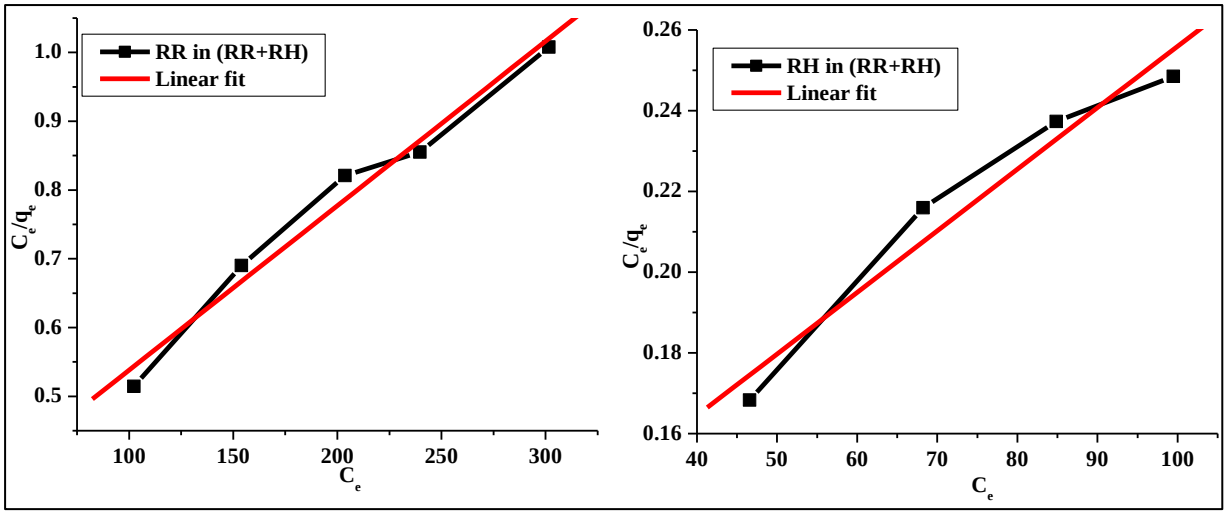

Operating parameters: 180 rpm, 100 ppm of dye, 0.05g adsorbent, time 210 min, temperature 30^0C, optimum pH

Figure 4.67 c Linear fit of isotherm for RR and RH in (RR+RH) onto H-0.2

Table 4.22Langmuir isotherm constants for binary systems

Langmuir isotherm constants for binary systems				
Binary component system ((RR+RB)				
H-0.2				
RB+RR				
	K_l	**a_l**	**q_m**	**r^2**
RB	8.695	0.025	347.22	0.986
RR	12.45	0.032	362.66	0.991
RB+RH				
RB	6.321	0.026	368.23	0.989
RH	4.561	0.024	394.19	0.992
RR+RH				
RR	5.213	0.038	329.23	0.997
RH	6.217	0.042	356.98	0.999

Table 4.23 Jain Soeinyk isotherm constants for binary systems

H-0.2			Qm	% of dye adsorbed without competitive adsorption
	RB+ RR	RB	254	79.21
		RR	203	20.29
	RR + RH	RR	217	76.03
		RH	165	23.97
	RB+RH	RB	276	58.33
		RH	161	41.67

As seen from Table 4.2.3 similar to HT systems for the binary mixtures greater amount of RB adsorbed without competition in the presence of RR and RH using H-0.2 as adsorbent. However RR adsorbed preferentially without competition over RH.

Sorption kinetics of binary system

The sorption kinetics of binary system was fitted to pseudo first order, pseudo second order and intra particle diffusion models. The adsorption kinetics was well explained by pseudo second order model for all the systems onto H-0.2 Fig. 4.68 (a, b& c) shows the linear fit for kinetics for binary systems. Table 4.24 shows the Kinetic constant for binary systems

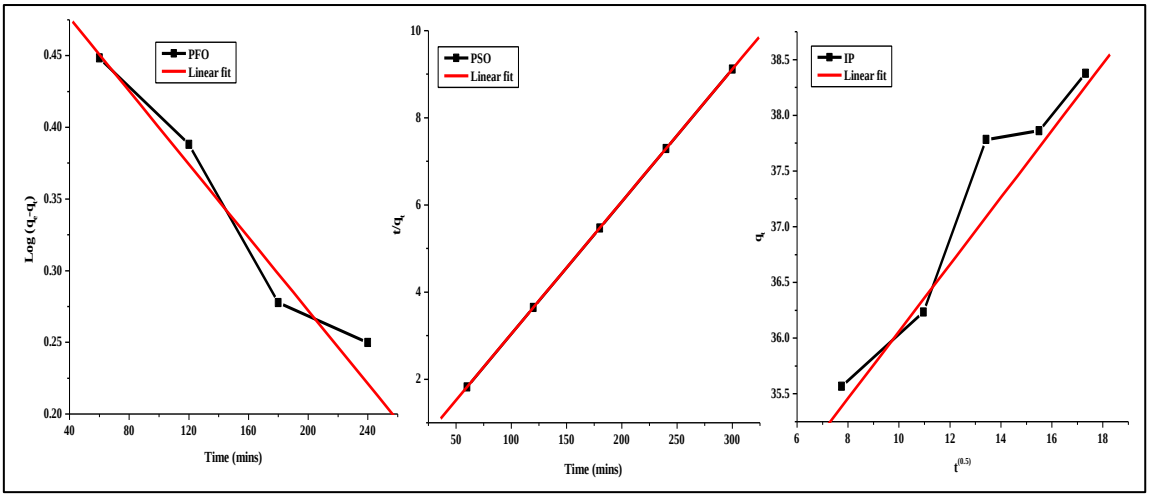

Operating parameters: 180 rpm, 100 ppm of dye, 0.05 g adsorbent, time 210 min, temperature 30^0C, optimum pH

Figure 4.68 a Linear fit of Kinetics for RB and RR in (RB+RR) onto H-0.2

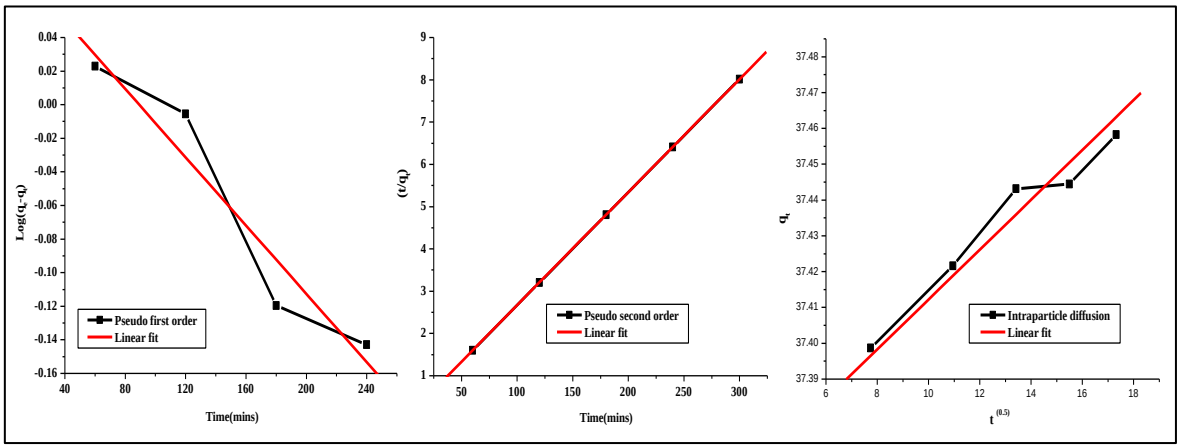

Operating parameters: 180 rpm, 100 ppm of dye, 0.05 g adsorbent, time 210 min, temperature 30^0C, optimum pH

Figure 4.68b Linear fit of Kinetics for RB and R H in (RB+RH) onto H-0.2

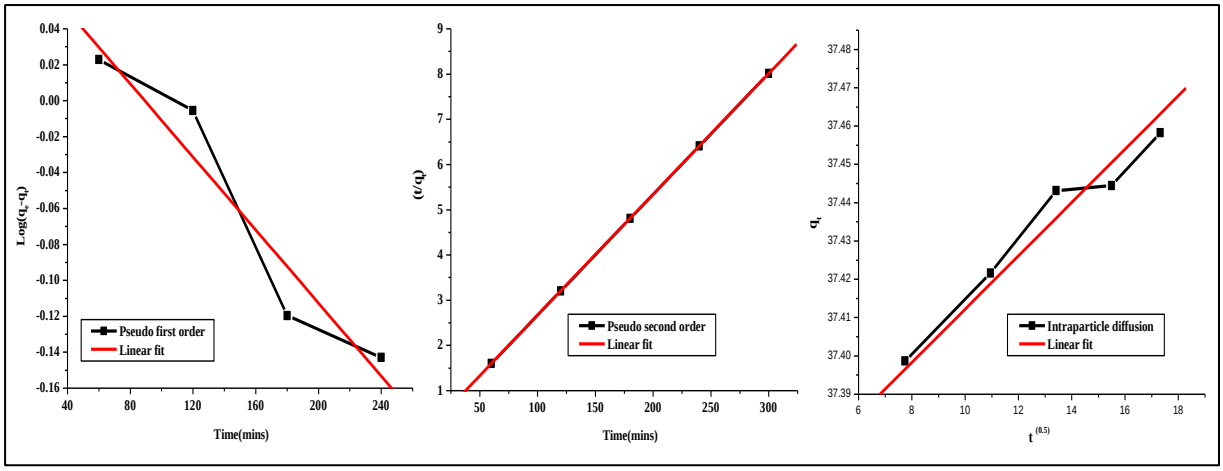

Operating parameters: 180 rpm, 100 ppm of dye, 0.05 g adsorbent, time 210 min, temperature 30^0C, optimum pH

Figure 4.68c Linear fit of Kinetics for RR and R H in (RB+RH) onto H-0.2

Table 4.24 Kinetic constants for binary systems

Kinetic constants for binary systems			
Binary component system ((RR+RB)			
H-0.2			
	RB+RR	**RB+RH**	**RR+RH**
q_e (exp)	39.67	37.32	42.64
q_e	8.345	4.213	7.897
K_1	0.013	0.098	0.019
r^2	0.988	0.991	0.986
Sd	0.0023	0.0076	0.0012
Pseudo second order			
q_e	37.98	35.32	40.54
K_1	1.21E-03	1.76E-03	1.86E-03
r^2	1	1	1
SD	0.062	0.012	0.098
Intraparticle diffusion			
K_{ip}	0.325	0.054	0.127
r^2	0.986	0.998	0.987
SD	0.021	0.001	0.002

4.6.9 Conclusion

A series of hydrogel composites were synthesized by intercalative polymerization. The different states of water in equilibrium swollen hydrogel composites were demonstrated by DSC. Swelling kinetics was investigated in aqueous, NaCl and KCl media. The effect of pH using phosphate buffers was studied and the results show that swelling was maximum in acidic pH conditions. It was observed that the hydrogel composite with low percentage of clay swelled more in water and was so chosen for dye adsorption studies. Batch adsorption experiments revealed that H-0.2 has good adsorption capacity for individual and binary mixture of dyes. Equilibrium adsorption isotherm data indicated a good fit to the Freundlich and Langmuir isotherm model and the adsorption process was heterogeneous. The adsorption process followed a pseudo-second-order rate model better than a pseudo-first-order rate model both in single and binary component systems. RB adsorbed to a greater extent without competitive adsorption over RR-141 and Rh-6G, while RB-21 adsorbed to a greater extent without competitive adsorption over Rh-6G.

The hydrogel composite can be used for environmental clean-up applications, drug delivery and other biomedical applications.

References:

[1] B. Stephen, C.P. Chiu, G.H. Ho, J. Yang, B.H. Chen, *J.Hazard. Mater*. 137 (**2006**) 226.

[2] X.Y. Yang, B. Al-Duri, *Chem. Eng. J*. 83 (**2001**) 15.

[3] G. McKay, *Chem. Eng. J*. 27 (**1983**) 187.

[4] F. Rozada, L.F. Calvo, A.I. Garcia, J. Martin-Villacorta, M. Otero, *Bioresour. Technol*. 87 (**2003**) 221.

[5] B.S. Inbaraj, C.P. Chiu, G.H. Ho, J. Yang, B.H. Chen, *Bioresour. Technol*. 99 (**2008**) 1026.

[6] B.S. Inbaraj, J.T. Chien, G.H. Hob, J. Yang, B.H. Chen, *Biochem. Eng. J.* 31 (**2006**) 204.

[7] S.M.O. Brito, H.M.C. Andrade, L.F. Soares, R.P. Azevedo, *J. Hazard. Mater.* 174 (**2010**) 84.

[8] Zh. Zhang, S. Xia, X. Wang, A. Yang, B. Xu, L. Chen, Zh. Zhu, J. Zhao, N. Jaffrezic Renault, D. Leonard, *J. Hazard. Mater.* 163(**2009**) 279.

[9] M.S. Chiou, H.Y. Li, *J. Hazard. Mater.* B93 (**2002**) 233.

[10] F. Wu, R. Tseng, R. Juang, *Water Res.* 35 (**2001**) 613.

[11] I. Uzun, *Dyes Pigments* 70 (**2006**) 76.

[12] R.G. Harris, J.D. Wells, B.B. Johnson, *Colloids Surf. A: Physicochem. Eng. Aspects* 180 (**2001**) 131.

[13] V. Meshko, L. Markovska, M. Mincheva, A.E. Rodrigues, *Water Res.* 35 (**2001**) 3357.

[14] A. Gurses, S. Karaca, C. Dogar, R. Bayrak, M. Acikyildiz, M. Yalcin, *J. ColloidInterface Sci.* 269 (**2004**) 310.

[15] M. Dogan, Y. Ozdemir, M. Alkan, *Dyes Pigments* 75 (**2007**) 701–713.

[16] A.S. Ozcan, B. Erdem, A. Ozcan, *Colloids Surf. A: Physicochem. Eng. Aspects* 266 (**2005**) 73.

[17] V. Vimonsesa, Sh. Lei, B. Jina, Ch.W.K. Chowd, Ch. Saintb, *Chem. Eng. J.* 148 (**2009**) 354–364.

[18] O. Ozdemir, B. Armagan, M. Turan, M.S. Celik, *Dyes Pigments* 62 (**2004**) 49.

[19] M. Darder, M. Colilla, E. Ruiz-Hitzky, *Appl. Clay Sci.* 28 (**2005**) 199.

[20] J.-H. An, S. Dultz, *Appl. Clay Sci.* 36 (**2007**) 256.

[21] Sh. Hua, H. Yang, W. Wang, A. Wang, *Appl. Clay Sci.* 50 (**2010**) 112.

[22] S. Kittinaovarat, P. Kansomwan, N. Jiratumnukul, *Appl. Clay Sci.* 48 (**2010**) 87.

[23] P. Monvisade, P. Siriphannon, *Appl. Clay Sci.* 42 (**2009**) 427.

[24] C. Aguzzi, P. Capra, C. Bonferoni, P. Cerezo, I. Salcedo, R. Sánchez, C. Caramella, C. Viseras, *Appl. Clay Sci.* 50 (**2010**) 106.

[25] M. Darder, M. Colilla, E. Ruiz-Hitzky, *Appl. Clay Sci.* 28 (**2005**) 199.

[26] J.-H. An, S. Dultz, *Clay Miner.* 42 (**2007**) 329.

[27] J.-H. An, S. Dultz *Appl. Clay Sci.* 36 (**2007**) 256.

[28] N. Bleiman, Y.G. Mishael, *J. Hazard. Mater.* 183 (**2010**) 590.

[29] M. Darder, M. Colilla, E. Ruiz-Hitzky, *Appl. Clay Sci.* 28 (**2005**) 199.

[30] R. Celis, M.C. Hermosín, L. Cox, J. Cornejo, *Environ. Sci. Technol.* 33 (**1999**) 1200.

[31] V. Addorisio, S. Esposito, F. Sannino, *J. Agric. Food Chem.* 58 (**2010**) 5011.

[32] S.A. Boyd, S. Shaobai, J.F. Lee, M.M. *Clays Clay Miner.* 36 (**1988**) 125.

[33] F. Bruna, R. Celis, I. Pavlovic, C. Barriga, J. Cornejo, M.A. Ulibarri, *J. Hazard. Mater*. 168 (**2009**) 1476.

[34] L. Cardoso, J.B. Valim, J. *Phys. Chem. Solids* 67 (**2006**) 987.

[35] M.J. Carrizosa, M.J. Calderón, M.C. Hermosín, J. Cornejo, *Sci. Total Environ.* 247 (**2000**) 285.

[36] R. Celis, W.C. Koskinen, A.M. Cecchi, G.A. Bresnahan, M.J. Carrisoza, M.A. Ulibarri, I. Pavlovic, M.C. Hermosín, *J. Environ. Sci. Health Part B* 34 (**1999**) 929.

[37] M.C. Hermosín, J. Cornejo, *Chemosphere* 24 (**1992**) 1493.

[38] M.C. Hermosín, J. Cornejo, *J. Environ. Qual.* 22 (**1993**) 325.

[39] Zhao, W.F. Jaynes, G.F. Vance, *Chemosphere* 33 (**1996**) 2089.

[40] L. Cox, M.C. Hermosín, R. Celis, J. Cornejo, *Water Res.* 31 (**1997**) 1309.

[41] M.C. Hermosín, J.L. Pérez-Rodríguez, Clay Miner. 29 (**1981**) 143.

[42] G. Lagaly, *Appl. Clay Sci.* 18 (**2001**) 205.

[43] J. Cornejo, R. Celis, I. Pavlovic, M.A. Ulibarri, *Clay Miner.* 43 (**2008**) 155.

[44] R. Prost, B. Yaron, *Soil Sci.* 166 (**2001**) 880.

[45] A. Radian, Y.G. Mishael, *Environ. Sci. Technol.* 42 (**2008**) 1511.

[46] T. Undabeytia, Y.G. Mishael, S. Nir, B. Papahadjopoulos-Sternberg, B. Rubin, E. Morillo, C. Maqueda, *Environ. Sci. Technol.* 37 (**2003**)4475.

[47] M. Auta, B. H. Hameed, *Chem Eng J* 237 (**2014**) 352.

[48] H.M.F. Freundlich, *J. Phys. Chem.* 57 (**1906**) 385.

[49] K.Y. Foo, B.H. Hameed, *Chem. Eng. J.*156 (**2010**) 2.

[50] M.I. Tempkin, V. Pyzhev, *Acta Phys. Chim. USSR* 12 (**1940**) 327.

[51] G. Halsey. *J. Chem. Phys.*, 16 (**1948**) 931.

[52] S. Lagergren, *Kungliga Svenska Vetenskapsakademiens. Handlingar*, 24 (**1898**) 1.

[53] Y.S. Ho, G. McKay, *Process Safety and Environmental Protection*, 76 (**1998**) 332.

[54] W.J. Weber Jr., J.C. Morris. *J. Sanitary Eng. Div. Proceed. Am. Soc. Civil* Eng 89 (**1963)** 31.

[55] W.J. Weber, J.C.S. Morris, Proceedings of International Conference on Water Pollution Symposium. Oxford **1962**, *2*, 231.

[56] C. Aharoni, S. Sideman, E. Hoffer, Adsorption of phosphate ions by colloid ioncoated alumina, *J. Chem. Technol. & Biotechnol.*,29 (**1979**) 404.

[57] G.E. Boyd, A.W. Adamson, L.S. Myers. *J. Am. Chem. Soc*. 69 (**1947**) 2836.

[58] L. Wang, J. Zhang, A. Wang, Fast removal of methylene blue from aqueous solution by adsorption onto chitosan-g-poly[acrylic acid] / attapulgite composite, Desalination. 266 (**2011**) 33.

[59] R.J. Samuels, J. Polym. Sci., Part A: Polym. Chem. 19 (**1981**) 1081.

[60] K. Ogawa, T. Yui, M. Miya, *Biosci., Biotechnol., Biochem.* 56 (**1992**) 858.

[61] M. Jain, V. Garg and K. Kadirvelu, *J. Hazard. Mater.*162 (**2009**) 365.

[62] E. Demirbas, M. Z. Nas. *Desalination* 243(**2009**) 8.

[63] T. Sismanoglu, Y. Kismir, S. Karakus ,*J. Hazard. Mater.*184 (**2010**) 164.

[64] M. Faraji, Y. Yamini, E. Tahmasebi, A. Saleh, F. Nourmohammadian, *J. Iran. Chem. Soc.* 7 (**2010**) 130.

[65] J. D. J. D. S. Neta, G. C. Moreira, C. J. D. Silva, C. Reis, E. L. Reis. *Desalination* 281 (**2011**) 55.

[66] E. Voudrias, K. Fytianos, E. Bozani, *Glob Nest: the Int. J*. (**2002**) 75.

[67] S. Pankaj, G. Shikha, T. Rajesh, *The Can. J. Chem. Eng.* 92 (**2014**) 41.

[68] R. Dolphen, N. Sakkayawong, P. Thiravetyan, W. Nakbanpote, *J. Hazard. Mat.* 145 (**2007**) 250.

[69] L. Sunantha, *Res. Journal of Appl. Sci.* 6 (**2011**) 15.

[70] C. Singhakant, K. Tipprasertsin, D. Inthorn, *Environment Asia* 3 (**2010**) 90.

[71] E. L. Foletto, G. C. Collazzo, M. A. Mazutti, S. L. Jahn, *Separ. Sci.Technol.* 46 (**2011**) 2510.

[72] Pankaj, T. Bhawna, G. Shikha, P. Prem Kishore, *J. Applicable Chem.* 1 (**2012**) 505.

[73] K. Shen, M.A. Gondal, Journal of Saudi Chemical Society, In Press (**2013**) doi:10.1016/j.jscs.2013.11.005.

[74] S. Sadhasivam, S. Savitha, K. Swaminathan, *J. Environ. Manage.* 85 (**2007**) 155.

[75] G.Sreelatha, P.Padmaja, *J.Environ.prot.Sci*, 2 (**2008**) 63.

[76] H. Ren, D. D. Kulkarni, R. Kodiyath, W.Xu, I.Choi, V. V. Tsukruk, *Appl. Mater. Interfaces* 6 (**2014**) 2459.

[77] K. C. Maheria, U.V.Chudasama, *Ind. Eng. Chem. Res.* 46 (**2007**) 6852.

[78] J. Das, D. Das, K.M. Parida, *J. Colloid. Interf. Sci.*301 (**2006**) 569.

[79] S.V. Prasanna, P.V. Kamath, *Solid State Sci.* 10 (**2008**) 260.

[80] M.R. Kang, H.M. Lim, S.C. Lee, S.H. Lee, K.J. Kim, *Adv. Technol. Mater. Mater. Process J.* 6 (**2004**) 218.

[81] C.D. Hoyo, *Appl. Clay Sci.* 36 (**2007**) 103.

[82] I.M. Ahmed, M.S. Gasser, *Appl. Surf. Sci.* 259 (**2012**) 650.

[83] F.B.D. Saiah, B.L. Su, N. Bettahar, *J. Hazard. Mater.* 165 (**2009**) 206.

[84] R. Extremera, I. Pavlovic, M.R. Pe´ rez, C. Barriga, *Chem. Eng. J.* 213 (**2012**) 392.

[85] A.R. Auxilio, P.C. Audrews, P.C. Junk, L. Spiccia, D. Neumann, W. Raverty, N. Vanderhoek, *Polyhedron* 26 (**2007**) 3479.

[86] M. Bouraada, M. Lafjah, M.S. Ouali, L.C. de Menorval, *J. Hazard. Mater.* 153 (**2008**) 911.

[87] B. Wang, H. Zhang, D.G. Evans, X. Duan, *Mater. Chem. Phys.* 92 (**2005**) 190.

[88] Y. You, H. Zhao, G.F. Vance, *Colloid Surf.* 205 (**2002**) 161.

[89] F. Bruna, I. Pavlovic, C. Barriga, J. Cornejo, M.A. Ulibarri, *Appl. Clay Sci.* 33 (**2006**) 116.

[90] F. Bruna, I. Pavlovic, R. Celis, C. Barriga, J. Cornejo, M.A. Ulibarri, *Appl. Clay Sci.* 42 (**2008**) 194.

[91] F. Bruna, R. Celis, M. Real, J. Cornejo, *J. Hazard. Mater.* 225–226 (**2012**) 74.

[92] G. Akc¸ay, K. Yurdakoc¸, *Acta hydrochim. hydrobiol.* 28 (**2000**) 300.

[93] Z. Rawajfih, N. Nsour, *J. Colloid Interf. Sci.* 298 (**2006**) 39.

[94] R. Celis, W.C. Koskinen, M.C. Hermosin, M.A. Ulibarri, J. Cornejo, *Soil Sci. Am. J.* 64 (**2000**) 36.

[95] F. Bruna, I. Pavlovic, C. Barriga, J. Cornejo, M.A. Ulibarri, *Appl. Clay Sci.* 33 (**2006**) 116.

[96] M.J. Carrizosa,W.C. Koskinen, M.C. Hermosin, *Soil Sci. Soc. Am. J.* 68 (**2004**) 1863.

[97] E. Klumpp, C. Contreras-Ortega, P. Klahre, F.J. Tino, S. Yapar, C. Portillo, S. Stegen, F. Queirolo, M.J. Schwuger, *Colloids Surf. A: Physicochem. Eng. Aspects* 230 (**2004**) 111.

[98] N. Viwanathan, S. Meenakshi, *app. clay sci.* 48 (**2010**) 607.

[99] H. Tagaya, A. Ogata, T. Kuwahara, S. Ogata, M. Karasu, J. Kodakawa, K. Chiba, *Microporous Mater.* 7 (**1996**) 151.

[100] U. Costantino, N. Coletti, M. Nocchetti, G.G. Aloisi, F. Elisei, *Langmuir*15 (**1999**) 4454.

[101] V. Melanova, L. Benes, V. Zima, J. Svoboda, *J. Incl. Phenom. Macrocycl. Chem.* 51 (**2005**) 97.

[102] J. Orthman, H.Y. Zhu, G.Q. Lu, *Sep. Purif. Technol.* 31 (**2003**) 53.

[103] Z. Mao-Xu, L. Yan-Ping, X. Mei, X. Hui-Zhen, *J. Hazard. Mater.* 120 (**2005**) 163.

[104] J. Das, D. Das, K. M. Parida, J. Colloid Interface Sci. 301 (**2006**) 569.

[105] S. Mariam Sumari, Y. Yamin, H. Zaini, *The Malaysian J. Anal. Sci.* 13 (**2009**) 120.

[106] Y.S. Al-Degs, M.I. El-Barghouthi, A.A. Issa, M.A. Khraisheh, G.M. Walker,Water Res. 40 (**2006**) 2645.

[107] L. Jianwei, Z. Yanhui, Z. Zhiliang, *Coll. Surf. A: Physicochem, Eng. Aspects* 3849 (**2011**) 9.

[108] K.K.H Choy, J.F. Porter, J.F.G. McKay, Chem. Eng. J. 103 (**2004**) 133.

[109] M. S. Chiou,Carbohyd. Poly. 83 (**2011**) 1446.

[110] M. S. Chiou,H. Y. Li, *Chemosphere* 50 (**2003**) 1095.

[111] M. S. Chiou, H. Y. Li, *J Hazard Mater* 93 (**2002**)233.

[112] R. S. Juang, F.C. Wu, R. L. Tseng, *Adv Environ Res* 6 (**2002**) 171.

[113] Y. Shimizu, A. Taga, H. Yamaoka,*Adsorpt Sci Technol* 21 (**2003**) 439.

[114] A. Shiosaki, M. Goto, T. Hirose, *J. Chromatogr.* 679 (**1994**) 1.

[115] X., Zheng, Y. Wang, *J. Hazard. Mater.*168 (**2009**) 970.

[116] J. W. Lee, S. Y. Kim, S. S. Kim, Y. M. Lee, K. H. Y. Lee, and S. J. Kim, 73 (**1999**) 113.

[117] Li Wang, J. Zhang, A. Wang, *Desalination* 266 (**2011**) 33.

[118] S. Chen, M. Liu, S. Jin, and Y. Chen, J. Appl. Polym. Sc 98 (**2005**) 1720.

[119] A. Khan, M. Othman, K. Razak, H. Akil, . *J. Poly. Res.* 20 (**2013**) 273.

[120] Ö. Genç, *Carbohydr. Polym.* 104 (**2014**) 8.

[121] Ö. Genç, *J. Hazard. Mater.*B97 (**2003**) 111.

[122] G. Q. Zhang, L. S. Zha, M. H. Zhou, J. H. Ma,B. R. Liang, *J Appl Polym Sci* 97 (**2005**) 1931.

[123] M.L. Zhai, Y. Q. Zhang, J. Ren, M. Yi, H. F. Ha, J. F. Kennedy *Carbohyd Polym* 58 (**2004**) 35.

[124] B. L. Guo, Q. Y. Gao, *Carbohyd Res* 342 (**2007**) 2416.

[125] J. T. Zhang, S. X. Cheng, R. X. Zhuo. *Colloid Polym Sci* 281 (**2003**) 580.

[126] S. P. Zhao, D. Ma, L. M. Zhang, *Macromol Biosci* 6 (**2006**) 445.

[127] Yi JZ, Ma YQ, Zhang LM. *Bioresour Technol* 99 (**2008**) 5362.

[128] Gad YH. *Radiat. Phys Chem* 77 (**2008**) 1101.

[129] M. Henmi, K. Nakatsuji, T. Ichikawa, H. Tomioka, T. Sakamoto, M. Yoshio, T. Kato, *Adv. Mater.*, 24 (**2012**) 2238..

[130] F. Pu, X. Liu, B. Xu, J. Ren, X. Qu, Langmuir 30 (**2014**)14597

[131] M. A. Shannon, P. W. Bohn, M. Elimelech, J. G. Georgiadis, B. J. Marinasaaa, A. M. Mayes, *Nature* 452 (**2008**) 301.

[132] V. Bekiari, P. Lianos, *Chem. Mater.* 18 (**2006**) 4142.

[133] M.-H. Park, C. Subramani, S. Rana, V. M. Rotello, *Adv. Mater.* 24 (**2012**) 5862.

[134] R. Wang, B. Yu, X. Jiang, J. Yin, *Adv.Funct. Mater.* 22 (**2012**) 2606.

[135] S. Schmidt, P. A. L. Fernandes, B. G. De Geest, M. Delcea, A. G. Skirtach, H. Möhwald, A. Fery, *Adv. Funct. Mater.* 21 (**2011**) 1411.

[136] S. Ganta, H. Devalapally, A. Shahiwala, M. A. Amiji, *J. Controlled Release* 126 (**2008**) 187.

[137] J. N. Wilson, Y. Wang, J. J. Lavigne, U. H. F. Bunz, *Chem. Commun.* 14 (**2003**) 1626.

[138] B. S. Sandanaraj, R. Demont, S. Thayumanavan, *J. Am. Chem. Soc.* 129 (**2007**) 3506.

[139] K. Ariga, A. Vinu, M. Miyahara, J. P. Hill, T. Mori, *J. Am. Chem. Soc.* 129 (**2007**) 11022.

[140] Y.-H. Kim, B. Lee, K.-H. Choo, S.-J. Choi, *Microporous Mesoporous Mater.* 138 (**2011**) 184.

[141] Y. Liu, Z. Liu, J. Gao, J. Dai, J. Han, Y. Wang, J. Xie, Y. Yan, *J. Hazard. Mater.* 186 (**2011**) 197.

[142] H. Yan, J. Dai, Z. Yang, H. Yang, R. Cheng, *Chem. Eng. J.* 174 (**2011**) 586.

[143] S. Deng, R. Wang, H. Xu, X. Jiang, J. Yin, *J. Mater. Chem.* 22 (**2012**) 10055.

[144] B. Li, X. Jiang, J. Yin, *J. Mater. Chem.* 22 (**2012**) 17976.

[145] S. Deng, H. Xu, X. Jiang, J. Yin, *Macromolecules* 46 (**2013**) 2399.

[146] G. Fu, Z. Su, X. Jiang, J. Yin, *Polym. Chem.* 5 (**2014**) 2027.

[147] Y. Chen, Z. Shen, L. Pastor-Pérez, H. Frey, S.-E. Stiriba, *Macromolecules* 38 (2004) 227.

[148] S. Basu, D. R. Vutukuri, S. Thayumanavan, *J. Am. Chem. Soc.* 127 (**2005**) 16794.

[149] D. Wan, G. Wang, H. Pu, M. Jin, *Macromolecules* 42 (**2009**) 6448.

[150] Haag, R. *Small* 9 (**2013**) 894.

[151] A. Sunder, M. Krämer, Hanselmann, R, Mülhaupt, R. Frey, *Angew. Chem., Int. Ed.* 38 (**1999**) 3552.

[152] H. Türk, A. Shukla, P. C. Alves Rodrigues, H. Rehage, R. Haag, *Chem.Eur. J.* 13 (**2007**) 4187.

[153] B. Trappmann, K. Ludwig, M. R. Radowski, A. Shukla, A. Mohr, H. Rehage,; C. Böttcher, R. A Haag, *J. Am. Chem. Soc.* 132 (**2010**) 11119.

[154] R. Tyagi, S. Malhotra, A. F. Thünemann, A. Sedighi, M. Weber, A. Schäfer, R. Haag, *J. Phys. Chem. C* 117 (**2013**) 12307.

[155] Z. Guo, Y. Feng, D. Zhu, S. He, H. Liu, X. Shi, J. Sun, M. Qu, *Adv. Funct. Mater.* 23 (**2013**) 5010.

[156] S.-E. Stiriba, H. Kautz, H. Frey, *J. Am. Chem. Soc.* 124 (**2002**) 9698.

[157] S. Xu, Y. Luo, R. Haag, *Macromol. Biosci.* 7 (**2007**) 968.

[158] E. Burakowska, J. R. Quinn, S. C. Zimmerman, R. Haag, *J. Am. Chem. Soc.* 131 (**2009**) 10574.

[159] M. Krämer, M. Kopaczynska, S. KrauseR. , Haag, *J. Polym. Sci., Polym. Chem.* 45 (**2007**) 2287.

[160] A. Gomez-Escudero, M. A. Azagarsamy, N. Theddu, R. W. Vachet, S. Thayumanavan, *J. Am. Chem. Soc.* 130 (**2008**) 11156.

[161] D. C. González, E. N. Savariar, S. Thayumanavan, *J. Am. Chem. Soc.* 131 (**2009**) 7708.

[162] D. Wan, H. Pu, M. Jin, *Macromolecules* 43 (**2010**) 3809.

[163] N. Jungmann, M. Schmidt, J. Ebenhoch, J. Weis, M. Maskos, *Angew. Chem., Int. Ed.* 42 (**2003**) 1714.

[164] E. F. Molina, R. L. T. Parreira, E. H. De Faria, H. W. P. de Carvalho, G. F. Caramori, D. F. Coimbra, E. J. Nassar, K. J. Ciuffi, *Langmuir* 30 (**2014**) 3857.

[165] H. P. C. van Kuringen, G. M. Eikelboom, I. K. Shishmanova, D. J. Broer, A. P. H. J. Schenning, *Adv. Funct. Mater.*24 -(**2014)** 5022.

[166] B. O. OkesolaD. K., Smith, *Chem. Commun.* 49 (**2013**) 11164.

[167] B. Li, X. Jiang, J. Yin, *J. Mater. Chem.* 22 (**2012**) 17976.

[168] Mishra et al., Carbohydrate Polymers 80 (**2010**) 790.

[169] J. Bassett, R. C. Denney, G. H. Jeffery, J. Mendham, *Vogel's textbook of quantitative inorganic analysis (4th ed.).* (**1978**) London 370.

[170] J. Berger, M. Reist, J. M. Mayer, O. Felt, R. Gurny, Euro. J. Pharm. Biopharm. 57 (**2004**), 35.

[171] J. Bratby, *Coagulation and flocculation, Cambridge* (1980) UK.

[172] A. Dedinaite, J. Iruthayaraj, N. Gorochovceva, R. Makuska, P. M. Claesson, *Prog. Colloid Polym. Sci.* 132 (**2006**) 124.

[173] S. A. Dergunov, I. K. Nam, T. P. Maimakov, Z. S. Nurkeeva, E. M., Shaikhutdinov, G. A. Mun, *J. Appl. Polym. Sci.* 110 (**2008**) 558.

[174] S. R. Deshmukh, R. P. Singh, P. N. Chaturvedi, *J. Appl. Polym. Sci.* (**1985**) 4013.

[175] D. C. Duan, Pressure-sensitive adhesives, U.S. Patent 5225473 (**1993**).

[176] P. K. Dutta, S. Tripathi, G. K. Mehrotra, J. Dutta, *Food Chemistry* 114 (**2009**) 1173.

[177] H. A. A. EL-Rehim, E. S. A. Hegazy, A. M. Ali, . *J. Appl. Polym. Sci.* 76 (**2000**) 125.

[178] K. F. El-Tahlawy, M., El-Rafie, Safaa., A. S. Aly, Carbohydr. Polym.66 (**2006**) 176.

[179] T. A. Erciyes, M. Erim, B. Hazer, Y. Yagci, *Angew. Makromol. Chem.*, 200 (**1992**) 163.

[180] G. F. Fanta, *Block and graft copolymerization*. In R. J. Ceresa (Ed.). 1(**2007**) New York 1.

[181] Gregory, J. *Hair treatment composition containing a combination of three different film-forming hair-fixing polymers.* U.S. Patent, 7279153. (**1983**).

[182] K. C. Gupta, M. N. V. Ravi Kumar, *Polym. Int.*, 49 (**2000**) 141.

[183] R. Hejaji, M. Amiji, *J. Controlled Release* 89 (**2003**) 151.

[184] D. Hua, W. Deng, J. Tang, J. Cheng, X. Zhu, *Int. J. Biol. Macromol.*, 43 (**2008**) 43.

[185] G. Huacai, P. Wan, L. Dengke, *Carbohydr. Polym.* 66 (**2006**) 372.

[186] S. M. Hudson, C. Smith, *Biopolymers from renewable resources* (**1998**) New York. 115

[187] K. Inou,, Y. Baba, K. Yoshizuka,. *Bull. Chem. Soc. Jpn.* 66 (**1993**) 2915.

[188] R. Jayakumar, M. Prabahara, R. L. Reis, J. F. Mano, *Carbohydr. Polym.* 62 (**2005**) 142.

[189] D. W. Jenkins, S. M. Hudson, *Macromolecules* 35 (**2002**) 3413.

[190] D. W. Jenkins, M. Samuel, S. M. Hudson, Chem. Rev. 101 (**2001**) 3245.

[191] W. F. Lee, Y. J. Chen, *J. Appl. Polym. Sci.* 82 (**2001**) 2487.

[192] J. Lehto, K. Vaaramaa, E. Vesterinen, H. Tenhu, *J. Appl. Polym. Sci.* 68 (**1998**)355.

[193] L. Liu, X. Xu, S. Guo, W. Han, *Carbohydr. Polym.* 75 (**2009**) 401.

[194] G. Y. Liu, Y. L. Zhai, X. L. Wang, W. T. Wang, Y. B. Pan, X. T. Dong, *Carbohydr. Polym.*, 74 (**2008**) 862.

[195] F. L. Mi, Y. C. Tan, H. F. Liang, H. W. Sung, *Biomaterials* 23 (**2002**) 181.

[196] D. K. Mishra, J. Tripathy, K. Behari, *Carbohydr. Polym.*71 (**2008**) 524.

[197] D. K. Mishra, J. Tripathy, M. M. Mishra, K. Behari, *J. Appl. Polym. Sci.*, 110 (2008) 3455.

[198] D. K. Mishra, J. Tripathy, A. Srivastava, M. M. Mishra, K. Behari, *Carbohydr. Polym*. 74 (**2008**) 632.

[199] D. K. Mishra, J. Tripathy, A. Srivastava. P. K. Pandey, K. Behari, *J. Appl. Polym. Sci.*, 113 (**2009**) 2429. .

[200] Q. Mu, Y. Fang, *Carbohydr. Polym*., 72 (**2009**) 308.

[201] R. A. A. Muzzarelli, *Native, industrial and fossil chitin. In P. Jollès & R. A. A. Muzzarelli (Eds)* (**1999**) Switzerland

[202] Y. C. Nho, K. R. Park, *J. Appl. Polym. Sci.* 85 (**2002**) 1787.

[203] M. J. O'Connell, P. Boul, L. M. Ericson, C. Huffman, Y. Wang, E. Haroz, *Chem. Phys. Lett.* 342 (**2001**), 265.

[204] E. Onsoyen Q. Skaugrud, *J. Chem. Technol. Biotechnol.*, 49 (**1990**) 395.

[205] H. Park, K. Park, D. Kim, Preparation and swelling behavior of chitosan based superporous hydrogels for gastric retention application. J. Biomed. Mater. Res. A., 76 (**2006**) 144.

[206] S. B. Park, J. O. YouH. Y., Park, S. J. Haam, W. S. Kim, *Biomaterials* 22 (**2001**) 323.

[207] A. Pourjavadi, G. R. Mahdavinia, *Turkish Journal of Chemistry* 30 (**2006**) 595.

[208] A. Pourjavadi, G. R. Mahdavinia, M. J. Zohuriaan-Mehr, H. Omidian, *J. Appl. Polym. Sci.* 88 (**2003**) 2048–2054.

[209] M. N. V. Ravi Kumar, React. Funct. Polym. 46 (**2000**) 1.

[210] B. L. Rivas, H. A. Maturana, M. J. Molina, M. R. Gomez-Anton, I. F. Pierola, *J. Appl. Polym. Sci*, 67 (**1998**) 1109.

[211] P. X. ShengY. P., Ting, J. P. Chen, L. Hong, *J. Colloid Interface Sci* 275 (**2004**) 131.

[212] J. Singh, P. K. Dutta, J. Dutta, A. J. Hunt, D. J. Macquarrie, J. H. Clark, *Carbohydr. Polym.*76 (**2009**) 188.

[213] T. Suzuki, M. Fukuda, K. Yoneto, .*Pharmaceutical preparation for percutaneous absorption*, E.P. 0529123 (**1993**).

[214] K. Takayama, M. Hirata, Y. Machida, T. Masada, T. Sannan, T. Nagai, *Chem. Pharm. Bull.*, 38 (**1990**) 1993.

[215] S. Tripathi, G. K. Mehrotra,, P. K. Dutta, *E-Polymers* 93 (**2008**) 1.

[216] S. Tripathi, G. K. Mehrotra, C. K. M. Tripathi, B. Banerjee, A. K. Joshi, P. K. Dutta, *Asian Chitin Journal* 4 (**2008**) 29.

[217] J. Tripathy, D. K. MishraK. , Behari, *Carbohydrate Polymers* 75 (**2009**) 604.

[218] J. Tripathy, D. K. Mishra, M. Yadav, K. Behari, *Carbohydr. Polym.*, 79 (**2010**) 40.

[219] Y. N. WangL. , Cui, T. K. Xu, *Wool Textile Journal* 5 (**2008**) 18–20.

[220] C. C. Wang, C. H. Su, C. C, Chen, *J. Biomed. Mater. Res.* A, 84 (**2008**) 1006.

[221] P. Wongpanit, N. Sanchavanakit, P. Supaphol, S. Tokura, R. Rujiravanit, *Macromolecular Bioscience* 5 (**2005**) 1001.

[222] Y. Xiang, J. Si, Q. Zhang, Y. Liu, H. Guo, J. Polym. Sci., Part A: Polym. Chem 47 (**2009**) 925.

[223] H. X. Xu, Y. H. Yan, T. Wan, S. P. Li, *Journal of Wuhan University of Technology* 29 (**2007**) 51.

[224] L. Yinghai, L. Zhenghao, Z. Yanzhe, D. Kuilin, *Pure Appl. Chem.* A39 (**2002**) 129.

[225] A. Li, A.Q. Wang, *Eur. Polym. J.* 41(**2005**) 1630.

[226] J.H. Wu, Y.L. Wei, H.M. Lin, S.B.Lin, *Polymer*44(**2003**) 6513.

[227] S. Thambiannan, R. Rajendran, M. Lima Rose, *Clean– Soil, Air, Water.* 41(**2013**) 797.

[228] O. Bengi, B. Ayça A. Işıl, G. Gamze, *Clean– Soil, Air, Water* 39(**2011**) 1001.

[229] Z. Junping, W. Li, W. Aiqin, *Ind. Eng. Chem. Res.*46 (**2007**) 2497.

[230] Y.EI. Mouzdahir, A. Elmchaouri, R. Mahboub, A. Gil, S.A. Korili, *Desalination* 250(**2010**) 335-338.

[231] Y. Liu, Y. Zheng, A. Wang, *J. Environ. Sci.* 22(**2010**) 486.

[232] Y.T. Xie, A.Q.Wang, *J of Polym Res* 16 (**2009**) 143.

[233] C. Lin, I. Gitsov, *Macromol.* 43(**2010**) 3256.

[234] R.J. Samuels, Solid, *J Polym Sci. Polym Phys.* 19 (**1981**) 1081.

[235] F.S. Kittur, K.V. Harish Prashanth, K. UdayaSankar, R.N. Tharanathan, *Carbohydr. Polym.*.49(**2002**) 185.

[236] G. David, C. Bogdan Simionescu, A. *Biomacromol.* 91(**2008**)1678.

[237] T. Goda, J. Watanabe, M. Takai, K. Ishihara, *Polymer* 47 (**2006**)1390.

[238] A. Higuchi, J. Komiyama, T.Iijima, *Polym. Bull.* 11(**1984**)203.

[239] W. Chunyan, Y. Bazhang, K. Bernard, H. Julie, M. Francis, M. Yvone, *Biomacromolecules*. 9(**2008**), 561.

[240] W.E. Roorda, J.A. Bouwstra, M.A.D.Vries, H.E. Junginger, *Biomaterials* 9 (**1988**) 494.